Fall 12-18-2020

Long-Acting Nanoformulated Antivirals for the Treatment and Prevention of HIV-1 and HBV infections

Dhruvkumar M. Soni Dr.
University of Nebraska Medical Center

Recommended Citation

Long-Acting Nanoformulated Antivirals for the Treatment and Prevention of HIV-1

and HBV infections

by

Dhruvkumar Soni

A Dissertation

Presented to the Faculty of the University of Nebraska Medical Center Graduate

College in Partial Fulfillment of the Requirements

for the Degree of Doctor of Philosophy

Pharmaceutical Sciences Graduate Program

Under the Supervision of Professors Dr. Benson J. Edagwa

and

Dr. Howard E. Gendelman

University of Nebraska Medical Center

Omaha, Nebraska

December, 2020

Supervisory Committee:

Dr. Howard E. Gendelman, M.D.

Dr. Benson J. Edagwa, Ph.D.

Dr. JoEllyn McMillan, Ph.D

Dr. Jered Garrison, Ph.D.

Dr. Daryl J. Murry, Pharm D.

Long-Acting Nanoformulated Antivirals for the Treatment and Prevention of HIV-1 and HBV infections

Dhruvkumar Soni, Ph. D.

University of Nebraska Medical Center, 2020

Supervisors: Professors Benson J. Edagwa, Ph. D.

and

Howard E. Gendelman, M.D.

While antiretroviral therapy (ART) has revolutionized treatment and prevention of human immunodeficiency virus type one (HIV-1) infection, regimen adherence, viral mutations, drug toxicities, stigma and pill fatigue are limitations. These have led to the development of long acting (LA) ART. These include, but are not limited to, implantable devices, new chemical entities, prodrug modifications and nanoformulations. To these ends, this thesis focues on the transformation of nucleoside reverse transcriptase inhibitors (NRTIs) into LA parenterals, While elusive, data from our laboratories demonstrated that modifications to the PROdrug and nucleoTide technology (ProTide) enables improvements in drug apparent half-life and tissue and cell drug penetrance. Specifically, we now show that this modified ProTide approach could be applied successfully to emtricitabine (FTC) amongst other hydrophilic compounds to generate LA formulations. This advance can be seen as a principal part of commonly accepted antiretroviral and other antiviral treatment regimens.

Table of Contents

List of Figures and Tables

List of Abbreviations

ABC; abacavir

ALB; albumin

ART; antiretroviral therapy

ARV; antiretroviral drugs

BD; biodistribution

CAB; cabotegravir

cART; combination ART

CFM; chloroform

CEM; cellosaurus cell line

DCM; dichloromethane

DLS; dynamic light scattering

DSPG; distearoylphosphatidylglycerol

DTG; dolutegravir

EC_{50}; half maximal effective concentration

EFV; efavirenz

ELISA; enzyme-linked immunosorbent assay

FA; folic acid

FTC; emtricitabine

FTP; FTC triphosphates

3TC; lamivudine

FT-IR; fourier transform infrared spectroscopy

HBV; hepatitis B

HBsAg; hepatitis B surface antigen

HCV; hepatitis C virus

HIV-1; human immunodeficiency virus one

I.M.; intramuscular

INSTI; integrase strand transfer inhibitor

LA; long-acting

LASER ART; long-acting slow-release antiretroviral therapy

LC-MS; liquid chromatography-mass spectrometry

LoD; limit of detection

LPV; lopinavir

M2FTC; first generation FTC ProTide,

M4FTC; second generation FTC ProTide,

M1NIT; prodrug of tizoxanide

M1TFV, M2TFV; TFV ProTides.

M23TC; 3TC ProTide

MCSF; macrophage-colony stimulating factor

MDM; monocyte-derived macrophages

MOI; multiplicity of infection

MS; mass spectrometry

MS/MS; tandem mass spectrometry

MTT; 3-(4,5-dimethylthiazol-2-yl)-2,5-diphenyltetrazolium bromide

NM2FTC; nanoformulated emtricitabine ProTide (M2FTC)

NM4FTC; nanoformulated second generation emtricitabine ProTide (M4FTC),

NMR; nuclear magnetic resonance

NRTI; nucleoside reverse transcriptase inhibitor

NNRTI; non-nucleoside reverse transcriptase inhibitor

NSG; non-obese diabetic severe combined immunodeficiency-*2rgc*[null]

P407; poloxamer 407

PBL; peripheral blood lymphocyte

PD; pharmacodynamics

PDI; polydispersity index

PFA; paraformaldehyde

PLWH; people living with HIV

PK; pharmacokinetics

ProTide; prodrug nucleotide

RT; reverse transcriptase

RPV; rilpivirine

RPV LA; rilpivirine long-acting

TAF; tenofovir alafenamide

$TCID_{50}$; tissue culture of infective dose 50

TDF; tenofovir disoproxil fumarate

TEM; transmission electron microscopy

THF; tetrahydrofuran

TFV; tenofovir

UPLC; ultra-performance liquid chromatography

XRD; x-ray diffraction

WB; western blot

Acknowledgements

It was my dream to work in Dr. Howard Gendelman's lab since I joined UNMC in 2015. However, my destiny brought me to Dr. Gendelman's lab later. The happiest moment was my selection as graduate student with Drs. Benson Edagwa and Howard Gendelman as my mentors in PhD graduate program. I felt extremely blessed for this great opportunity I received and would cherish it for my lifetime.

I sincerely want to thank my mentors Drs. Edagwa and Gendelman for their continued support, encouragement, and the sense of security I received throughout my tenure as graduate student in this reputed lab. My mentors instilled upon me the qualities of determination, hard work, positive aggressiveness, and productivity. I want to thank them for their patience during my learning phase by providing me enough time to grow and nurture my professional and interpersonal skills. In addition to professional support received multiple times being a PhD student of this great lab, I was inspired and motivated by mentors' caring and passionate demeanor. Drs. Gendelman and Edagwa provided great support in all my aspirations I thought would lead me to be a productive student. I was never stopped from exploring new ideas and from building collaborations within the lab with the eventual reward of which I have as many co-authored manuscripts and review articles in high impact journals. This was achieved because of overwhelming cooperation from other members of the lab especially Dr. Bhavesh Kevadiya and his colleagues. In addition to my mentors' strong motivation and support towards doing great, I always maintained the attitude of doing great by doing good. This attitude was further fueled by mentors' encouragement towards working hard and serving good.

It was my honor to have worked for my PhD degree and dissertation under my mentor's prestigious guidance and I subconsciously thanked every moment I had with

them for their guidance, support, motivation, determination, love and a sense of purpose I felt during my interaction with them. Even during their busiest schedules and commitments, I was been given priority so that we (as student) never witness a delay in our progress. I could never be thankful enough to my mentors for their gesture. In addition to providing all the securities a graduate student would need to be successful such as an inspiring project and mentorship, availability of resources and a great work environment, my mentors taught me the importance being courageous, keep going and moving forward attitude which would constitute my prime assets towards every bit of success I would accomplish from now on. One of the reasons I could work hard was seeing their passion for research and thus living up to their expectation was my the most important motivation. I will always be grateful and indebted to my mentors for my scientific and personal prowess achieved during graduate education. Thank you.

I would like to sincerely thank my parents. Their prayers and words of positivity kept me moving forward towards achieving higher goals. I want to thank them for being my best friends and cheer leaders during my not so good times. I owe them for everything I could achieve till date.

My heartfelt thanks to my supervisory committee members Drs. JoEllyn McMillan, Jered Garrison, Daryl Murry for their valuable comments, guidance, support and availability during my research progress updates and committee meetings. I would like to sincerely thank Dr. Ram Mahato for appointing me into the Pharmaceutical Science Graduate Program and giving me this opportunity to be a part of University of Nebraska Medical Center. I would like to thank Dr. Mahato for taking care of their laboratory's and departmental students and supporting them in their professional career and growth. I would like to sincerely thank Drs. Jered Garrison and Dong Wang for the lab rotation opportunities and sharing their research expertise and guidance during my rotations.

viii

Chapter 1

Introduction

1.1 Human Immunodeficiency Virus (HIV)

1.1.1 Structure and Lifecycle of HIV

Acquired Immunodeficiency syndrome (AIDS) is caused by HIV infection with associated host immune system destruction leading to the clinical disease [1, 2]. HIV (**Figure 1.1**) belongs to the group lentivirus, retroviridae family and orthoretrovirinae subfamily. There are two types of HIV (HIV-1 and HIV-2) that are known to cause viral immunopathogenesis and AIDS [3], however, HIV-2 has lower pathogenicity and transmissivity. The simian immunodeficiency virus, SIV affecting non-human primates also belongs to lentivirus genus [4]. Thus, HIV-1 forms major target of therapeutics with the goal of treating and curing HIV-1/AIDS [5]. HIV-1 has two identical single stranded (ss) RNA molecules of approximately 9.8 kilobase pairs flanked by two long terminal repeats (LTRs) responsible for encoding different HIV proteins i.e. gag, pol, vif, vpr, vpu, enc, tat, rev, nef, and antisense protein (ASP) [6] commanding viral infectability and intracellular replication processes [7, 8]. The viral ssRNA undergoes reverse transcription to form HIV proviral genome (proviral DNA) which then gets integrated into host genome with the help of integrase enzyme.

Key to Terms

HIV capsid: HIV's core that contains HIV RNA

HIV envelope: Outer surface of HIV

HIV enzymes: Proteins that carry out steps in the HIV life cycle

HIV glycoproteins: Protein "spikes" embedded in the HIV envelope

HIV RNA: HIV's genetic material
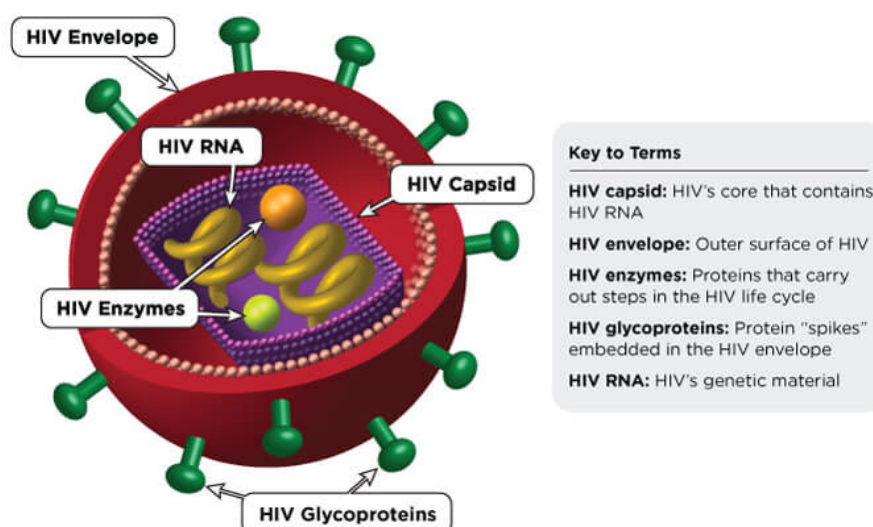
Figure 1.1 *Structure of HIV [9]*

Intravenous injection, sexual intercourse, and mother-to-child (vertical transmission) are physical routes through which HIV-1 spreads in human hosts [10, 11]. Once infected, HIV patients undergo three stages of diseases. First is acute infection, second chronic infection and third clinical disease, the AIDS [12]. Initially, HIV-1 infects CD4+ T cells that express the CD4 receptor (lymphocytes, monocytes, dendritic cells, microglial, perivascular macrophages in the central nervous system and histiocytes). This occurs through its surface glycoprotein (gp)120 binding to CD4+ receptor whereas CCR5 and CXCR4 co-receptors aid in virus binding and cellular internalization as co-receptors [13]. The lifecycle of HIV-1 infection in target host cells is been represented in **Figure 1.2**.
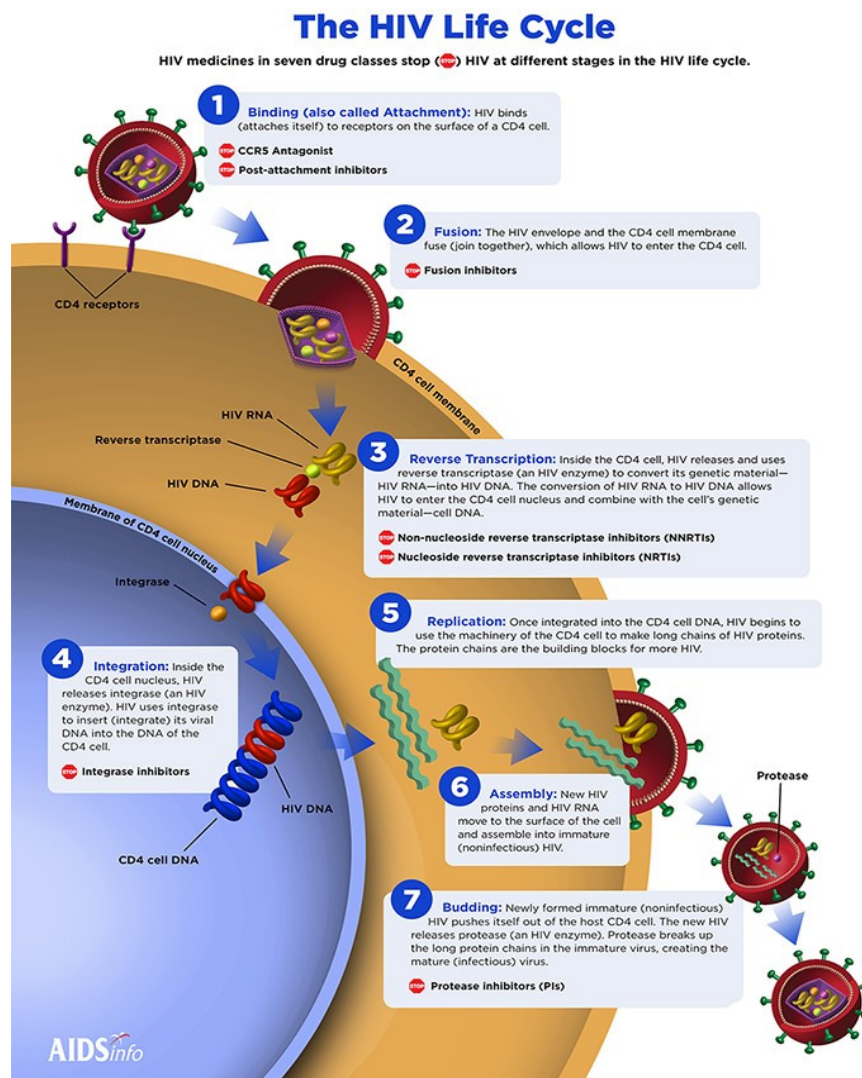
Figure 1.2 *Different stages in the lifecycle of HIV infection [9]*

1.1.2 Epidemiology and Current Treatments

1.1.2.1 Global HIV Statistics

According to global HIV-1 and acquired immune deficiency syndrome (AIDS) statistics – 2020 fact sheets, UNAIDS, 26 million infected people are ART treated (by the end of June 2020). In 2019 globally, there were 38 (31.6-44.5) million people living (PLW). However, 690,000 (500,000-970,000) died due to AIDS related complications. In the same year, 1.7 (1.2-2.2) million people succumbed to new HIV-1 infections. From the

start of AIDS epidemic, 75.7 (55.9-100) million people have been infected with HIV and 32.7 (24.8-42.2) million people have lost their lives due to AIDS related complications [14, 15]. The global epidemic and global response of PLWH (in millions) in terms of WHO region are represented in **Figures 1.3 A** and **1.3 B** respectively [15]. Additionally, the distribution of new HIV infections by key populations globally in 2019 is tabulated in **Table 1.1**. The appearance of new cases of HIV and consequential deaths in 2019 relative to 2010 by WHO region is represented in **Table 1.2.** The classification of different categories of drugs [16] is represented in **Table 1.3.**
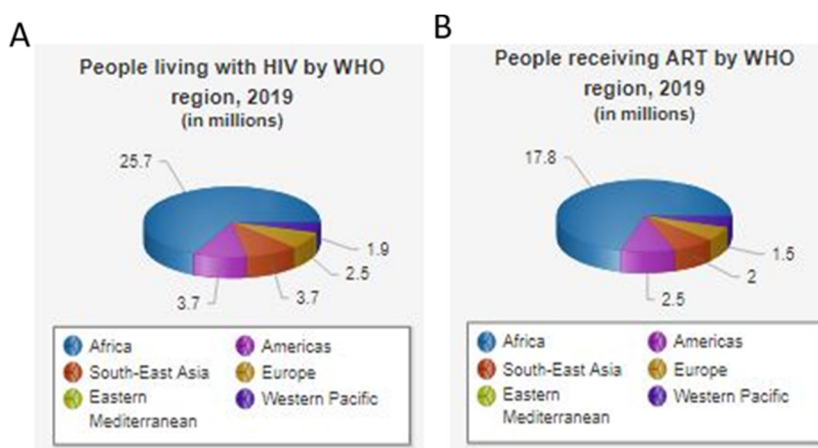
Figure 1.3 Distribution of *(A)* PLWH and *(B)* people receiving ART by WHO region in 2019.

Sr. No.	Key population	Percent distribution, 2019
1.	Sex workers	8
2.	People who inject drugs	10
3.	Gay men and other men who have sex with men	23
4.	Transgender women	2
5.	Clients of sex workers and sex partners of other key populations	19
6.	Remaining population	38

Table 1.1 Distribution of new HIV cases amongst key populations in 2019.

Sr. No. PLWH (millions)	WHO region	New Diagnosis (%) annually relative to 2010	Deaths (%) annually related to 2010
1.	African (25.7)	-35	-46
2.	Americas (3.7)	+7	-20
3.	Eastern Mediterranean region (0.42)	+47	+57
4.	European region (2.6)	+46	+14
5.	South East Asian (3.7)	-26	-30
6.	Western pacific (1.9)	+3	-36

Table 1.2 *Summary of regional HIV epidemic, 2019.*

	Category	Mechanism	Examples
1	**Entry Inhibitors**	These are classes of US FDA approved drugs which prevent HIV infection from infecting CD4+ T-cells.	**CCR5 Antagonist:** Maraviroc (Selzentry) **Fusion inhibitor:** Enfuvirtide, T-20 (Fuzeon) **Attachment inhibitor:** Ibalizumab (Trogarzo)
2	**Integrase Inhibitors**	These are group of drugs which inhibitor the process of integration of pro-viral DNA into human genome	Bictegravir, Dolutegravir (Tivicay), Elvitegravir (Viteka), Raltegravir (Isentress).
3	**Nucleoside and Nucleotide Reverse Transcriptase Inhibitors (NRTIs/NUKES)**	These are class of nucleoside/nucleotide analog drugs which inhibit the activity of HIV's reverse transcriptase enzyme.	Emtricitabine, FTC (Emtriva), Lamivudine, 3TC (Epvir), Abacavir (Ziagen), Tenofovir (TFV),

			Tenofovir alafenamide fumarate (TAF), Tenofovir disoproxil fumarate (TDF, Viread), Zidovudine (AZT, Retrovir), FTC plus TAF (Descovy), FTC + TDF (Truvada)
4	**Non - Nucleotide Reverse Transcriptase Inhibitors**	These are drugs which bind non-competitively to HIV-1 reverse transcriptase and inhibit conversion of HIV RNA to pro-viral DNA.	Rilpivirine (RPV, Edurant) Doravirine (DOR, Pifeltro) Etravirine (ETR, Intelence) Efavirenz (Sustiva) Nevirapine (Viramune)
5	**Protease inhibitors**	These drugs inhibit the viral protease enzyme	Darunavir (Prezista), Ritonavir (Boosting agent, Norvir), Saquinavir (Invirase), Atazanavir (Reyataz).
7	**Fixed dose combinations**	These constitute approved combination of two or more drugs in single tablet regimen (STR).	Atripla (Emtriva, Sustiva, Viread) Bictarvy (Descovy and Bictagravir), Cimduo (Epivir and Vilead) Complera (Emtriva, Vilead, Edurant)

			Delstrigo (Pifeltro, Epivir, Viread)
			Odefsey (Emtriva, TAF, Edurant)
			Dovato (Tivicay, Epivir)

Table 1.3 *Classes of US FDS approved anti – HIV drugs acting at different stages of infection [16].*

1.2 Hepatitis B Virus Infection

Hepatitis B viral (HBV) infection is one of the most common liver infections and a global public health threat leading to both acute and chronic disease conditions [17]. In 2015, 257 million people (chronically infected) showed positive test for hepatitis surface antigen and 887,000 people died from hepatitis B and related disorders such as hepatic cirrhosis and hepatocellular carcinoma (HCC). According to Centers for Disease Control and Prevention (CDC) Reports, the estimated number of new HBV infection has remained stable since 2015. However, in 2018 an estimated number of infections was 21, 600 slightly higher than 2018 target estimate number of 21,500. Thus, according to CDC's Division of Viral Hepatitis 2025 Strategic Plan, reduction of 16.7 % from the estimated number of new HBV infections in 2018 is needed to be attained to reach 2025 goal of 18, 000 estimated infections (Figure 1.4) [18-20].
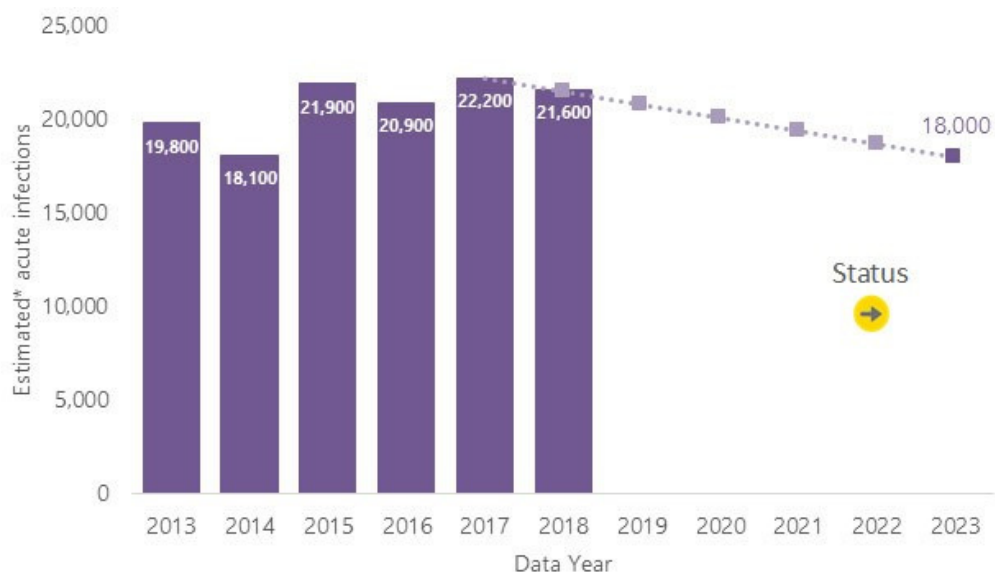
Figure 1.4 *Estimated new HBV infections*

Until 2016, 27 million people were aware of their infection condition and 4.5 million people were on treatment [21]. Additionally, according to the latest WHO reports, the proportion of children under 5 years of age which are chronically infected dropped just 1% from around 5% of pre-vaccine era [22]. The prevalence of hepatitis B infection is highest in WHO Western Pacific Region (6.2 %) and the WHO African Region (6.1%) with lowest in the WHO Region of the Americas (0.7%). Amongst the foreign-born individuals staying in the US, prevalence of HBV infection observed in individuals in 2017 is depicted in **Figure 1.5**.
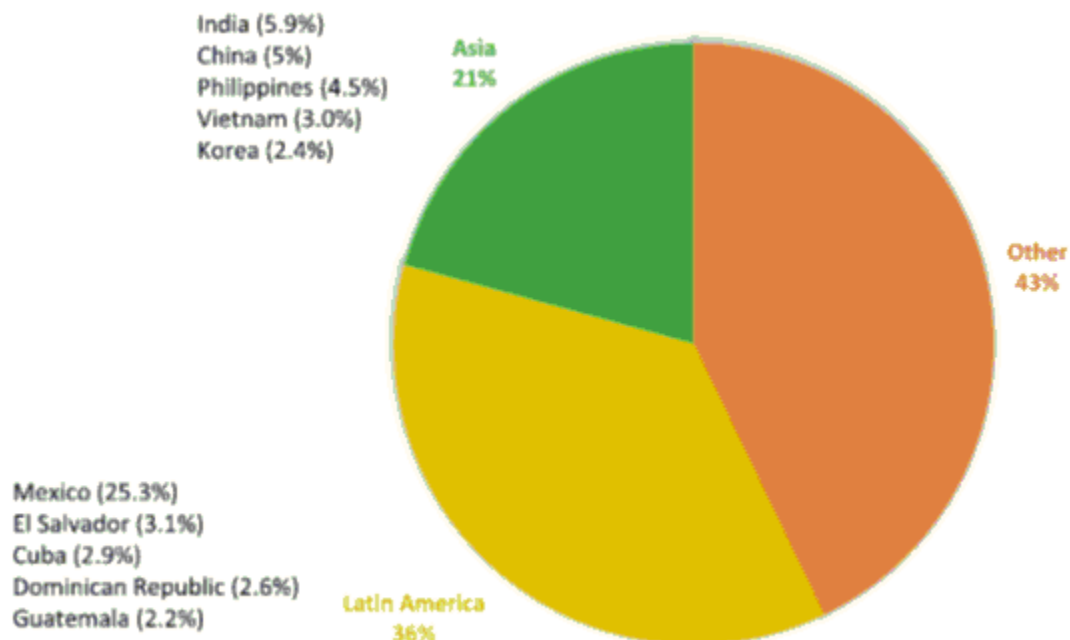
Figure 1.5 Prevalence of HBV infection in foreign born individuals living in the US in 2017

HBV infection is transmitted through perinatal route (mother to child at the birth) [23] or through horizontal transmission (exposure to the infected blood) from injected child to uninfected child in the first five years of age [24]. HBV infections can spread through needlestick injury during medical, surgical and dental procedures, tattooing, piercing, and exposure to infected body fluids [22]. Yellowing of the skin and eyes (jaundice), extreme fatigue, and dark urine are major symptoms of infection. Some acutely infected patients may develop liver failure may lead to death. However, chronically infected patients may develop liver cirrhosis or HCC over later period. Both acute and chronic HBV infections are diagnosed by the presence of antibodies against hepatitis B surface antigen (HBVsAg). Chronically infected patients are treated with anti-viral medications such as entecavir and tenofovir as oral regimen given as 1 pill per day and noted to have fewer side effects [25]. However, acutely infected patients should be provided immediate care, comfort and nutritional balance [26]. Even though there are various treatment modalities

available for controlling the chronic HBV infection, the viral persistence and need of daily pill of medication over chronic period are primarily responsible for emergence of viral resistance to these treatments [27]. Thus, there forms a great need of developing newer drugs and strategies acting against different stages of HBV infection to overcome resistance against single class of drugs [28]. Loss of hepatitis B surface antigen (HBsAg) with or without parallel loss in hepatitis B antibody (HBsAb) seroconversion and undetectable HBV DNA constitute functional cure of HBV. However, cccDNA which constitute part of HBV functional cure, should be silenced or eliminated to achieve complete cure of HBV [29].

1.2.1 HBV pathogenesis

HBV is a small DNA virus belonging to the family, Hepadnaviridae. It undergoes replication through RNA intermediate formation and then integrates into the host genome [30]. HBV is composed of partially double stranded relaxed circular DNA which upon entry into the host hepatocytes gets converted into tightly coiled covalently closed circular DNA (cccDNA) [31]. cccDNA as a part of episomal minichromosome, plays a vital role in the transcription of viral RNA and production of viral proteins [32]. The reported higher stability of cccDNA together with long half-life of hepatocytes which HBV infects constitute the prime reasons for chronic HBV infections [33]. Stable integrated cccDNA constitute latent HBV infection and any abrupt activation due to immunotherapies or chemotherapy may cause HBV rebound and worsening of disease condition [34]. Thus, continued suppression of HBV infection is highly warranted in improving clinical outcomes such as reversing the degree of fibrosis and decreasing the chances of HCC [35].

Current treatment for chronic HBV infection include immunomodulatory drugs such as interferon gamma and nucleotide analogs such as 3TC, entecavir (ETV), adefovir

dipivoxil, TDF and TAF [35], The life cycle of HBV infection and therapeutic targets against various stages of the infection is demonstrated in **Figure 1.6.**
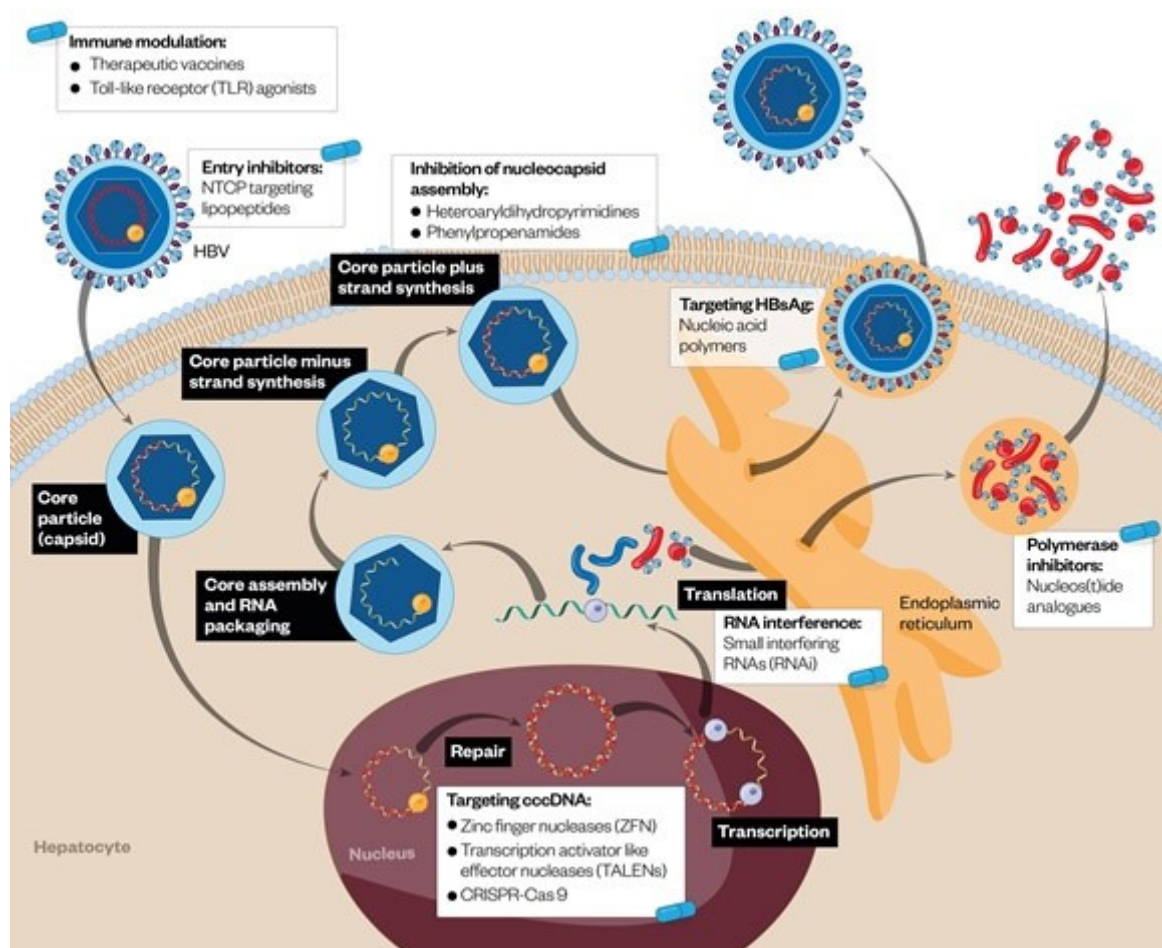
Figure 1.6 Replication cycle of HBV and various therapeutic approaches explored against each of the stage of HBV replication [36].

1.2.2 Anti – HBV Drugs directed to different Stages of the viral life cycle

1.2.2.1. Entry Inhibitors

Cellular receptor sodium taurocholate co-transporting peptide (NTCP) is widely responsible for viral entry into the hepatocytes [37]. One example of NTCP receptor inhibitor is Myrcludex which lipopeptide which is reported to block the entry of HBV into target hepatocytes. Clinical trials of Myrcludex (in combination with PEG interferon alfa

2a, tenofovir, and entecavir are either completed or active. Myrcludex, also known as Bulevirtide has shown be safe and effective in phase IIa study in which 75% of the patients reported to have one log reduction in HBV DNA after 12 weeks of treatment with Myrcludex B [38] [39]. Cyclosporin A, Ezetimibe are other examples of entry inhibitors approved for HBV treatment [40].

1.2.2.2. Capsid/viral assembly Inhibitors

Capsid/ viral assembly inhibitors act as anti – HBV agents by destabilizing the viral nucleocapsid and blocking the process of RNA packaging thereby generating empty capsids with no genetic material encapsulation. For example, AT-130 is a phenylpropenamide which stimulates premature initiation of viral assembly and capsid formation thereby generating capsids which are empty and non-infectious [41]. Similarly, BAY 41-4109 is an heteroaryldihydropyrimidine compound which interferes with capsid formation and misdirects viral assembly process thereby lowering the stability of normal capsid formation [42].

1.2.2.3. Silencing/eliminating cccDNA

Recently, a high capacity adenoviral vector which lacks almost all the DNA viral sequences termed high capacity adenoviral (HCAdV) or helper-dependent adenoviral vector (HDAdV) [43, 44] was designed to encode multiplexed CRISPR/Cas9 nuclease system/ a transcription activator like effector nucleases (TALENS) directed against HBV genome [45]. Since, covalently closed circular DNA (cccDNA) persists chronically in the HBV infected cells, its elimination is need of the day towards successful HBV treatment [46]. In the study developed by Schiwon et. al., combination of gRNA expression cassettes along with Cas9 expression cassettes in one HCAdV resulted in significant decrease in HBV antigen production and yielded mutations in HBV genome and degradation of HBV cccDNA thereby demonstrating successful HCAdV delivery and anti-

viral efficacy [45]. In another study, the authors carefully designed and selected target gRNA sequences based on conserved HBV genomic sequences and minimum homology to human genome [47]. The target gRNAs designed against the core, polymerase, and X-open reading frames (ORFs) in HBV genome were explored after their co-transfection of HepG2 cell line with HBV expression plasmid. However, single guide RNA (sgRNA) 17 and 21 demonstrated consistent reduction in pre-genomic HBV RNA and HBsAg production. Interestingly, hydrodynamic injection of CRISPR gRNA21/Cas9 expressing plasmid in HBV mouse model showed higher suppression in HBV expression as evidenced by decrease in HBVsAg and four-fold decrease in viremia on day 4 after plasmid administration. Similar reports of developing novel CRISPR/Cas9 therapeutics targeting HBV-S and X genes demonstrated better anti-HBV activity in-vitro and in M-TgHBV mouse model after hydrodynamic injection was noted as evidenced by decreased serum HBsAg and hepatic HBcAg levels [48, 49].

1.2.2.4. Halting HBsAg secretion

High circulating levels of HBsAg is reported to inhibit host dendritic cells induced cytokine production. It further leads to T-cells exhaustion and the attainment of immunosuppressive stage. In efforts to lower HBsAg and serum HBV DNA, nucleic acid polymers were developed and tested in HBV infected patients in preliminary study. Unfortunately, patients in this study experienced viral bound. Further evaluations of inhibitors of HBsAg release are under clinical trials testing [50] [51].

1.2.2.5. mRNA silencing

Developing small interference RNA (siRNA) target against viral mRNA could lead to prevention of viral protein translation. In pre-clinical mouse model, siRNA was reported to reduce HBsAg and HBeAg levels [52]. In phase II a clinical trial of stable

siRNA candidate, ARC 520 when administered in patients who were on entecavir regimen, demonstrated 22% reduction in HBsAg levels compared to baseline [53].

1.2.2.6. Immune modulatory agents and vaccines

Several strategies augmenting host immune response to achieve HBV functional cure are been developed [54] [55]. Varied vaccine delivery approaches to stimulate host immune response are been explored under clinical evaluations which include vaccines based on HBV envelop proteins, T-cells epitopes, HBsAg and HBcAg, tarmogens, and DNA based vaccines [56, 57]. Since, toll-like receptors (TLR) play viral role in HBV suppression, novel molecules like GS 9620, a TLR agonist, demonstrated suppression of HBV DNA accompanied with reduction in HBsAg and HBeAg levels in chimpanzee infection model [58].

1.2.2.7. Thiazolides

Thiazolide compounds, in addition to their anti-infectives properties have been reported to have broad spectrum anti-viral activity [28, 59]. NTZ represents first thiazolide compound indicated for *cryptosporidium parvum* infections. Its anti-viral activity was serendipitous discovery when patients with AIDS (HBV or HCV co-infections) were treated for cryptosporidial infections leading to diarrhea [60]. NTZ was approved by US FDA in 2002 as anti-protozoal for *cryptosporidium parvum* infections and marketed as Alinia™ by Romark Laboratories Ltd (Tampa, Florida, USA) [61]. However, NTZ was reported to have broad spectrum activity against different types of viruses, protozoa, anaerobic bacteria, and helminths [62]. NTZ and its active metabolite - tizoxanide (TIZ) was reported to have anti – HBV activity in-vitro by inhibiting HBV DNA and HBV core antigens HBVsAg and HBVeAg [63]. Recently, NTZ was found to inhibit viral transcription and viral product levels by inhibiting the interaction of HBV regulatory protein HBX with the host protein DDB1 and through restoration of Smc5/6 expression levels. Even though

nucleotide analogs are efficacious in inhibiting viral replication, they fail to affect viral protein transcription from episomal viral covalently closed circular DNA (cccDNA). Thus, by inhibiting the protein – protein interaction, NTZ therapy could provide new means of achieving functional HBV cure (**Figure 1.7**) [64].
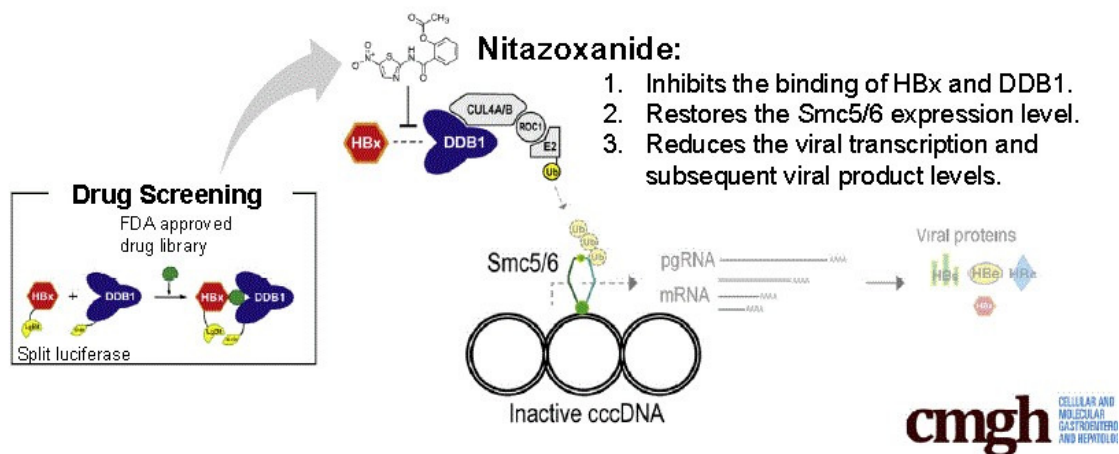
Figure 1.7 *Mechanism of action of nitazoxanide in HBV infection model of primary human hepatocytes [64].*

Additionally, NTZ was found to be involved in intra-cellular protein kinase activation by double stranded RNA (PKR) which mimics interferon induced cellular antiviral activity [65]. Thus, synergistic effects were observed from TIZ, an active metabolite of NTZ against HCV infection in 1a and 1b derived replicon cells and 2a cell culture models when combined with interferon or ribavirin [63].

An interventional clinical trial study evaluating the efficacy of NTZ (300 mg) compared to placebo in patients with HBeAg negative chronic hepatitis B infection, is recently recruiting participants as of January 23rd, 2020. A total of 48 participants will be randomized in 1:1:1:1 groups with 12 participants in each group to study the effect of NTZ compared to placebo and mean change of quantitative HBeAg levels from baseline to 12 weeks will be monitored as primary outcome measure of the study [66]. Previous trials carried out in March 2005 and April 2007 demonstrated NTZ efficacy in 9 subjects which

were treatment naïve and HBVeAg positive and HBV DNA quantitated in serum. NTZ (500 mg) when administered orally twice daily was effective in reducing HBV DNA below the level of detection in 89% of the patients after 4 – 20 weeks of treatment with NTZ. 33 % (3/9) of patients became HBsAg negative (2/3 after 8 weeks and 1/3 after 48 weeks) and 2 subjects which were HBeAg positive became HBeAg negative after 4-16 weeks of treatment [67, 68].

1.3 Nucleosides analogs

1.3.1 FTC

FTC belongs to nucleoside analog class of reverse transcriptase (RT) inhibitors (NRTIs), having cytosine backbone. Chemically, FTC is 5-Flouro-1-[2R, 5S)-2-(hydroxymethyl)-[1,3]oxathiolane-5-yl] cytosine and similar in structure to lamivudine (3TC) [133] [134]. FTC undergoes intracellular activation to FTC triphosphates (FTC TP/FTP) by phosphokinases like other NRTIs. FTP acts as pseudonucleotide and prevents integrated proviral DNA transcription by inhibiting 3'-5' phosphodiester bond formation between 5' nucleotide triphosphates of viral DNA chain and the drug thereby causing cessation of DNA transcription and inhibition of reverse transcriptase activity [135] with eventual lowering of plasma viral loads and improvement of CD4+ T-cell counts [134]. FTC is eliminated through renal excretion [133]. FTC is often employed in combination with other ART for the treatment of HIV-1, HIV-2, HBV and HCV infections [133][136][137]. Even though FTC is not approved for HBV indication, it is been recommended as an important backbone of fully suppressive anti-retroviral regimen along with TAF/TDF for the treatment of patients with HIV and HBV co-infections [138-140]. FTC belongs to category B which does not show teratogenicity and congenital abnormalities. For pregnant women with concurrent HIV infection, an ART regimen

consisting of FTC/abacavir/3TC and tenofovir should be started as early as possible to avoid the risk of HIV transmission to the newborn child [137]. Additionally, FTC, in combination with tenofovir (TFV) constitute an important component of PrEP medications for HIV infection approved by USFDA i.e. Truvada (FTC/TDF 200/300 mg) and Descovy (FTC/TAF 200/25 mg). A 2015 PROUD study which was an open labelled randomized controlled trial executed at 13 sites in England, UK to test the effectiveness of daily oral PrEP regimen of FTC/TFV showed 86 % reduction in the incidence of HIV infection in gay, bisexual, and other men who had sex with men (MSM) [19]. FTC is also indicated for post-exposure prophylaxis (PEP) after HIV infection as combination with second NRTI (TAF/TDF) and a drug from different category [142]. Combination regimen for PrEP treatment of HIV infection should be initiated within 72 hours and continued for 28 days. Administration of FTC is not associated with serious side effects. However, skin discoloration was observed in some patient populations [133]. Headache, fatigue, fever, arthralgia, anxiety, insomnia, and depression are some of side reactions associated with FTC which are common amongst NRTI class of drugs [143].

1.3.2 TFV

Tenofovir alafenamide fumarate (TAF) belongs to acyclic nucleotide diester analog of adenosine monophosphate which is administered in prodrug forms i.e. as tenofovir disoproxil fumarate (TDF) and TAF by oral route [107]. Development of prodrugs of tenofovir reflect of nucleoside reverse transcriptase inhibitors (NRTIs) has beneficial effects as it enhances their pharmacokinetics (PK) and biodistribution (BD) to reservoir sites of latency infection i.e. lymphoid tissue and the brain [108]. Its active intracellular metabolite – tenofovir diphosphate is responsible for viral suppression during both HIV and HBV infections. TDF was approved by the U.S. Food and Drug Administration (FDA) for HIV-1 and HBV indication in 2001 and 2008 respectively and soon became the backbone for treatment of these infections [109][110][111]. However, TAF was found to

be superior to TDF in terms of number of patients treated with TAF showing smaller mean serum creatinine increases, less proteinuria, and smaller decreases in spine and hip bone mineral densities [112][113]. Thus, TAF was then approved by FDA in 2015. TAF, a tenofovir ProTide was reported to have improved plasma stability due to phosphoramidate bond compared to TDF having phosphonate bond linkage in its structure [114]. Additionally, TAF showed better intracellular accumulation and activation to its diphosphate active metabolite thereby demonstrating 10-fold higher potency in mononuclear cells (lymphocytes) which are primary sites of HIV infection [115][116]. On Feb 7th, 2018, the US FDA approved Bictegravir as a triple combination medication to be marketed as Bictarvy having Bictegravir 50 mg/FTC 200 mg/TAF 25 mg as active constituents. Bictegravir is indicated for treatment of HIV infection in patients which are naïve to the treatment or as a replacement therapy in patients who are virologically suppressed (HIV-1 RNA<50 copies/mL) with no history of treatment failure or prior resistance to any of the component of bictarvy [69].

1.4 Non-nucleoside reverse transcriptase inhibitors (NNRTIs) for HIV infection

Another highly potent NNRTI molecule doravirine (DOR) developed by Merck [70] is available as single drug (Pifeltro[TM]) as combination formulation of single tablet regimen (STR) along with 3TC and TDF (Delstrigo[TM]) indicated for both treatment naïve patients and patients which are virologically suppressed [70]. A phase IIb study is currently active evaluating the safety, tolerability, anti-retroviral efficacy and PKs of islatravir (ISL) in combination with DOR and 3TC in treatment naïve HIV-1 infected patients [71]. Participants randomly assigned to receive 3 days of ISL i.e. 0.25, 0.75, 2.25 mg in combination with DOR and 3TC or DOR/3TC/TDF. At 48 weeks, 77.4-89.7% of patients receiving different doses of ISL showed viral suppression compared to 83.9% of

patients receiving DOR/3TC/TDF. Recently, a phase III randomized, double blind clinical trial study for the evaluation of efficacy and safety of DOR (100 mg) / ISL (0.75 mg) in treatment naïve patients with HIV-1 infection, sponsored by Merck Sharp and Dohm is currently recruiting participants [72] with primary hypothesis that DOR/ISL is non-inferior to BIC/FTC/TAF treatments based on percentage of participants with HIV RNA <50 copies/mL at week 48. Additionally, a novel investigational inhibitor of HIV-1 capsid i.e. GS-6207 having activity against broad range of HIV mutants showing resistance to ARVs and other maturation inhibitors have been developed and evaluated in phase I studies [73]. Clinical studies demonstrated the potent activity of GS-6207 administered subcutaneously with extended duration of action [74].

1.5 HIV Reservoir Sites of Latency

The term latency is the state of non-productive infection in subset of cells that are transcriptionally dormant but able to produce the infectious virus after stimulation (re-activation of latency) [75]. Additionally, the term reservoir is referred to cellular or anatomical location wherein the HIV resides in a latent state [76]. Even after continued suppression of HIV-1 infection in patients due to ART utilization), progeny HIV-1 virions can remain persistent in an integrated form as replication competent proviral DNA. This is present in a subset of long-lived cells constituting latent reservoir [77, 78]. However, aberrant cessation of ART causes re-activation of integrated provirus leading to rebound viremia and subsequent emergence of resistant mutant HIV strains [79, 80]. Thus, the presence of latently infected cells i.e. reservoirs constitute a major challenge in achieving functional HIV cure [80, 81]. The establishment of latent infection occurs early on during acute infection and gets executed even before the virus enters systemic circulation [82]. Thus, early initiation of treatment can reduce the size of HIV latent reservoirs and bring us close to the success in achieving functional HIV cure [79, 83].

HIV reservoir sites are broadly classified as cellular and anatomical reservoirs [84, 85]. Immune cells, specifically CD4+ T-cells constitute the primary site of HIV-1 infection and are involved in the reservoirs of HIV infection [86-88]. Due to cytopathic effects, the activated CD4+ T-cells, post HIV infection undergo cell death. Cytotoxic T cells also play a role in killing the infected CD4+ T cells [89]. However, in this process some cells revert to their resting state and then proliferate into memory cells [90]. These cells are pivotal in the establishment of cellular latency as they get infected by different extend by HIV and are in viral persistence [90-92]. Other cell type of myeloid origin includes mononuclear phagocytes (MP; monocytes, macrophages, and dendritic cells) which are highly susceptible targets for HIV transmission and are responsible for establishment of persistent reservoirs in tissues thereby controlling viral spread [93, 94]. Additionally, dendritic cells are heterogeneous subsets of antigen presenting cells and are responsible for sequestering the HIV virion and present them to T-cells thereby causing infection [95]. Astrocytes, endothelial and epithelial cells could also serve as reservoir, but it needs affirmation to prove their involvement [96].

The other sites of HIV latency are the anatomical sites of reservoirs. Lymphoid tissues such as spleen, thymus, lymph nodes and gut associated lymphoid tissues (GALT) are sites of HIV replication and form the primary anatomical sites of HIV reservoir for latency [96]. Within days of infection, the HIV disseminates from blood into the lymph nodes and infects resident CD4+ T lymphocytes and MP which then re-localize to other tissues and organs such as brain, gut, lungs, kidneys, liver, adipose, bone marrow, and genitourinary systems. The transmission of infection occurs through individual virions and through cell-cell interactions [88, 97].

1.6 Long-Acting (LA) ART

The development of next generation of agents with prolonged apparent half life is required not only for healthy individuals with high susceptibility of acquiring HIV infection and in people living with HIV-1 infection [98, 99]. Although ART has enabled HIV to become a manageable disease, it cannot eliminate the virus from the host cell genome after infection [100]. ART has been successful in reducing the mortality and morbidity associated with HIV, thereby prolong the life span of people living with HIV infection. One of the major limitations of ART is poor medication adherence in patients who need to take these medications for life. Failure to achieve medical adherence is not only devastating to the patient's life but also to the health care system [101]. This is because medical non-adherence leads to sub-optimal therapeutic levels in the treated patients with resultant emergence of mutations causing drug resistance events. These treatments then become non-effective requiring a switch to few alternative regimens causing substantial financial burden [102]. Medicinal non-adherence could originate from patient, health care provider and health care system [101]. Additionally, there is a fair amount of variability observed in the adherence – drug resistance relationship characteristics in which some cART regimes are more successful than the others based on cost, complexity, intrusiveness and accuracy of the treatments [103]. Furthermore, several other factors leading to decreased adherence to ART include societal stigma [104], race/ethnicity [105], [106], depression [107, 108], cognitive impairment [106], substance use [109] age [110, 111] and adverse effects of medications [112]. Thus, the development of adherence monitoring tool is very essential [113]. The importance of RTA was demonstrated in a study carried out amongst HIV infected adults and children in rural Uganda wherein real time wireless electronic adherence monitoring (EAM) had median adherence of 89.5 % and 92.8 % amongst adults and children, respectively. However, 99 – 100 % of adherence was observed by interactive voice response (IVR) and short message service (SMS) [114]. However, monitoring of technical components and

acceptability of patients to these technologies are major challenges which require further investigation [115].

LA therapeutics for the prevention and treatment of HIV infection plays a forefront armamentarium for the management of the disease [116]. The abilities of LA anti-retroviral therapeutics to sustain drug levels in the therapeutic window for extended duration of time constitute the major advantage over standard daily cART. Further development of highly potent LA therapeutics could result in the effective dose reduction leading to improved toxicity profile and maximize the risk to benefit ratio of the therapy. Drawing from contributions made by LA therapeutics in achieving efficacy in avoiding unexpected pregnancy [116] and psychiatric disorders [117], the application of LA system for overcoming adherence issues in HIV treatment modality would be highly beneficial to both the patients and healthcare providers [118]. Various approaches in the development of LA therapeutics are explored. These include LA injectables, LA implants, LA oral medications, and LA slow effective release (LASER) ART.

1.6.1 LA Parenteral (LAP)

LA parenteral delivery strategy has several advantages which include bypassing hepatic first pass metabolism, avoiding gastric pH induced hydrolysis and degradation thereby avoiding variability in plasma concentrations that could be evidenced after oral administration. Additionally, since these formulations show sustained release kinetics, the chances of dose dumping leading to systemic toxicity are at minimum possibility [119]. LA parenteral formulations are beneficial for patients suffering from pill aversion, swallowing dysfunctions, malabsorption, and neurological disorders wherein patients are more dependent to clinical care personnel [120]. Since societal stigma is one of the causes of patient non-adherence, LA parenteral formulations having sustained

efficacy after single administration have great potential in overcoming this stigma and improve adherence [121].

1.6.2. LA Injectables

More than 75 % of people living with HIV taking oral medications want to switch to LA therapeutics given on monthly basis compared to weekly regimen [118, 122-124]. With success seen in LA formulation for conditions such contraception [123], mental health [125] and disorders related to bones [126], LA ART is expected to improve patient adherence and lower issues related to treatment fatigue and emergence of escape mutants leading to resistance to therapy [123]. Ibalizumab, a humanized IgG4 monoclonal antibody delivered via i.v. infusion is one of the examples of FDA approved LA injectable (2018) under streamlined approval process for HIV infected patients requiring newer therapies [127]. Ibalizumab is a non-competitive inhibitor of CD4+ receptor on to which HIV binds and gain entry inside the cell. Ibalizumab when administered as 2000 mg infusion following by 800 mg i.v. infusion every 2 weeks demonstrated half log reduction in HIV RNA in 82.5 % of treated patients, and 43% of the patients had viral loads less than 50 copies/mL in phase III clinical trials enrolling 40 extensively treated adults with multi drug resistance (MDR) HIV infection. The other examples of drugs which are developed into LA formulations are rilpivirine and cabotegravir. A diarylpyrimidine derivative, rilpivirine (RPV, TMC278) is non-nucleoside reverse transcriptase inhibitor approved as a part of oral combination antiretroviral regimen by US FDA in 2011 [128, 129]. Due to RPV's inherent insolubility in aqueous media, RPV LAP was developed as its nanosuspension formulation [129]. RPV nanosuspension formulation when evaluated in phase I clinical trials in HIV negative healthy individuals showed sustained plasma RPV levels of more than 10 ng/mL over 12-26 weeks, plasma elimination half-life of 44-61 days with no grade 4 adverse effects

noted [130].   A newer generation of integrase strand transfer inhibitor (INSTI) – cabotegravir (CAB, GSK1265744) is an investigational compound currently in late-stage clinical development with structure similarity to dolutegravir (DTG) and bictegravir (BIC) and comparable potency [131].   However, BIC and DTG possess higher genetic barrier to HIV resistance compared to CAB [132].

Similarly, given the fact that cabotegravir was able to exhibit plasma drug half of 31.5 hours, 2.2 and 2.3 $\log_{10}$ reduction in HIV RNA levels over 10 days in HIV uninfected and PLW HIV after single daily oral doses in Phase I and IIa double blind studies, LA injectable nanosuspension of CAB (200 mg/mL) was developed and evaluated in phase I open labelled clinical trials. CAB LA administered I.M. in HIV uninfected individuals demonstrated sustained plasma CAB levels up to 52 weeks [133].   Several clinical trials evaluating combination of CAB LA and RPV LA for the treatment of HIV infection are ongoing.   These include LA Anti-retroviral Treatment Enabling (LATTE) phase IIb studies [134], the First LA Injectable Regimen (FLAIR) phase III non-inferiority study (NCT02938520) [135] and the ART as LA Suppression (ATLAS, NCT02951052) studies [136]. Recently, the HIV Prevention Trials Network Study (HPTN 084) to evaluate safety and efficacy of CAB LA for PrEP in HIV uninfected women reported CAB LA when administered I.M. every 8 weeks demonstrated higher efficacy and safety in preventing HIV acquisition amongst cisgender women. Data and Safety Monitoring Board (DSMB) stopped the trial early due to CAB LA's higher efficacy compared to oral Truvada regimen [137, 138].   Heath Canada, the regulatory agency for drug approvals in Canada has approved Cabenuva, a combination of CAB LA (200 mg/mL) and RPV LA (300 mg/mL) as a once monthly injectable nanosuspension formulation for patients who are virologically suppressed (HIV-1 RNA < 50 copies/mL). Cabenuva reduces doses days from 365 to 12 annually [139].

lbuvirtide, ISL, and GS-6207 (HIV-1 capsid inhibitor) are newer LA agents currently under development. Albuvirtide (320mg) when administered i.v. once weekly in combination with lopinavir/ritonavir showed reduction in HIV viral load to less in 50 copies/mL in 80% of treated patients in phase III trials compared to 66 % of treated control patients receiving second line three drug regimen containing TDF [140], NCT03272347.

Another potent antiviral drug under development by Merck is ISL (ISL, MK-8951) which belongs to a new class of compounds called nucleoside reverse transcriptase translocation inhibitor [141]. Currently, Merck in collaboration with the Melinda and Gates Foundation are in the process of initiating a Phase 3 trial (IMPOWER 22) to evaluate the efficacy of oral long acting ISL administered once monthly for PrEP treatment of women and girls at high risk of HIV-1infection in sub-Saharan Africa region [142].

1.6.2.1. LASER ART

Rapid metabolism, poor pharmacokinetics (PK) and biodistribution (BD) profiles constitute major limitation of ARV drugs [143]. However, chemical modifications and efficient encapsulation of ARV into LA formulations with desired sustained release kinetics could overcome these limitations. The term LASER ART was coined based on the need to improve ARV's inherent disadvantages. The utilization of LASER ART was achieved by chemically modifying parent active ARVs into hydrophobic and lipophilic prodrugs and their subsequent nanoformulation with resultant improvement in dissolution profiles enabling enhanced drug membrane permeability and distribution with sustained release of active drug levels in the therapeutic window to limit related systemic toxicity and development of drug resistance [144]. LA prodrugs undergo enzymatic and or chemical mediated hydrolysis to release active parent molecules over extended periods [145] [146]. These lipophilic formulations target immune cells such as CD4+ T cells and macrophages which serve as drug depots and transporters of ARVs to reservoir sites of

HIV-1 infection such as central nervous system [147]. Prior reports of drugs modified to produce LASER nanoformulations have demonstrated enhanced and sustained anti-retroviral efficacy [148].

1.6.2.2. Targeted nanotechnology (Nano) ART

ART targeted towards CD4+ T-cells and macrophages which constitute primary sites of HIV infection, has been developed and explored by attaching targeting ligands on the surface of the drug delivery carrier. To this end, folic acid (FA) mediated targeted therapeutics for monocyte-macrophage targeting [149] are being widely explored. In one of the studies, FA conjugated to poloxamer P407 surfactant was synthesized and then conjugated onto the polymer used to coat ARV drug nanoparticles. Interestingly, the folate-P407 targeted ritonavir boasted atazanavir nanosuspension demonstrated enhanced macrophage uptake, retention and sustained in-vitro anti-retroviral efficacy with minimum cytotoxicity. Following I.M. injection, the folate targeted formulation showed 5-fold increased drug levels in both plasma and tissue compartments and 100-fold improvement in drug pharmacodynamic profiles in mice models [150]. Similarly, anti-CD4+ antibody targeted liposomal formulation was developed and explored. Anti-CD4+ targeted nevirapine and saquinavir dual loaded immunoliposomes were then evaluated for cellular uptake using confocal microscopy (qualitative) and flow cytometry (quantitative) in Jurkat T-cells. Enhanced cellular uptake and suppression of viral replication was observed at a concentration of 5ng/mL for dual loaded immunoliposomes implying their efficacy in better management of HIV infection [151].

Thus, development of targeted therapeutics and their delivery through intramuscular route has achieved the ideal characteristics of LA formulation which are plasma stability, cell and tissue targetability with improved pk and pharmacodynamic profiles in both rodents and primate studies [150, 152].

1.6.3. Implantables

LA implants play very vital role in disease states in which sustained release of therapeutic agents is highly needed. These include conditions involving hormonal contraception, prostate cancer, diabetes, chronic coronary artery disease, cytomegaloviral rhinitis and HIV infections [153]. One of the important requirements for drug compatibility with implant technologies is potency [154]. Since there is a limitation in the amount of drug that could be loaded into an implant, therapeutic molecules with higher potency and lower dose are suitable for formulation into an implant drug delivery vehicle.

LA implant approaches are categorized into two types [155]:

1. *Matrix type:* Drug is dispersed in a polymeric matrix which dissociates by biodegradation thereby releasing the drug in the systemic circulation at a controlled rate

2. *Reservoir type:* Consist of a core of drug which is encased into polymeric barrier. The rate of drug release depends on the physico-chemical properties of the polymeric component.

TAF which is indicated for both HIV and HBV infections has been formulated as an LA implant using several approaches. In one of them, the drug was loaded into microperforated silicone tubing having polyvinyl pyrrolidone (PVA) coating. This was then implanted subcutaneously into beagle dogs and its PK and drug release profile was monitored [156]. A zero-order release kinetics was observed for TAF from the implant over first 30 days and intracellular drug concentration of tenofovir diphosphate observed was 11 – 31 times higher than those achieved in iPrEX study with TDF administration [157]. Elsewhere, a refillable non polymeric nanofluidic implant also called as nanochannel delivery implant, NDI was developed for delivering TAF and FTC [158]. NDI is composed of silicone nanochannel membrane two sealable, refillable silicone drug

loading ports and a titanium drug reservoir. Drug loaded device had FTC (69.1 mg) or TAF (72.9 mg) sealed within silicone. NDI has superior advantages of refillability meaning once the drug reservoir gets exhausted it could be refilled without removing the implant. Post administration in rhesus macaques, NDI showed TFV DP concentrations in PBMCs 3 days after implantation and increased up to 70 days. FTC-TP levels were detected and sustained in PBMCs from days 3 – 28 post implantations. NDI was found to be well tolerated with 33 % of the animals showed swelling/seroma around the device which was resolved within a week and 2/3 developed ulceration over 70 days. Additionally, ISL (ISV) which is a potent reverse transcriptase translocation inhibitor [159] which was formulated as non-biodegradable polymeric implant and evaluated in rats. Apparent ISV plasma half-life noted was about 100 days which inspired researchers to further develop and evaluate ISV implant in human clinical trials. Currently, phase I clinical trials of ISV is in process and initial finding showed 62 mg dose implant could achieve a sustained linear drug release with zero order kinetics with levels of ISV triphosphates which were 7 times higher than EC_{50} inhibitory concentration in wild type virus over 12 months duration [154]. Another paradigm of implant technology includes biodegradable implants. Recently, an ultra LA biodegradable implant of DTG was developed and evaluated in rhesus macaques and a humanized bone marrow liver thymus (BLT) mouse model of HIV infection. This technology was focused on in-situ subcutaneous implantation approach wherein DTG, PLGA and NMP in the ratio 0.3:1:3 was injected as liquid formulation which solidifies subcutaneously within first 48 hours and then biodegrades gradually. Subcutaneously solidifying implant of DTG was found to be well tolerated in both the animal models. Detectable DTG levels were recorded for up to 9 months in some mice and up to 140 days in non-human primates. Additionally, single administration of DTG subcutaneous implant demonstrated suppression of acute HIV replication and protection against repeated high dose vaginal HIV challenges [160].

Additionally, a subdermal implant of TAF was developed and its pharmacokinetic profile was evaluated in beagle dogs [156]. The implant designed was developed by authors inspired by their previous success on pod intravaginal ring (pod-IVR) system [161]. The subdermal implant consisted of polyvinyl alcohol (PVA) coated drug filled silicone cylinder having orthogonal delivery channels. The physicochemical properties of the coating polymer and the number and cross-sectional diameter of the cylinder determine the drug release profile from the subdermal implant (**Figure 1.8**). The TAF loaded subdermal implant showed zero order burst free sustained release over 30 days in vitro. On average, 98% of TAF was released in-vitro over 40 days period. However, in-vivo pharmacokinetic evaluation of subdermal TAF implant in beagle dogs showed statistically insignificant differences to in-vitro release documented previously. No adverse toxic events related to implant was noted during the study. TAF implant showed sustained plasma TAF/TFV levels with constant TAF/TFV molar ratio demonstrating implant stability in-vivo throughout the study. A median TFV active metabolite i.e.TFV diphosphate (TFV-DP) levels of 511.8 fmoles/10^6 was noted over 35 days which declined over 40 days. These median TFV-DP concentrations were 11-32 times higher compared to the protective TFV-DP concentration observed in iPrEX clinical trial study which was 16 – 48 fmoles/10^6 cells. The authors conclude that the subdermal implant should be further developed for once a year delivery system and when used in combination with parenteral injectable system could form an important element of highly active anti-retroviral therapy regimen. Another approach for innovative delivery of TAF is a silicone-based transdermal matrix-based (drug-in-adhesive) patch with polyisobutylene adhesives, which has been tested on dermatomed human cadaver skin and has been established to yield a permeation flux of 7 µg/cm2/h over 1 week, which extrapolates to a release rate of 8.4 mg of TAF per day. This noninvasive approach offers convenience, simplicity, has no procedural requirements and thus stands to be more user friendly.

Thus, LA strategies that could extend the biological activity from weeks to months to a year could be a major step forward in managing the HIV disease in a safe and efficient manner [118]. However, LA implants have both advantages and disadvantages as sustained release drug delivery modality. LA implants carry advantages in terms of treatment termination wherein the administered dose in implant could be halted anytime during the treatment if potential side effects were noted or the therapy was needed to be stopped due to treatment completion. Additionally, due to their sustained release kinetics, reduction in frequency of dosing could be achieved and dose dumping phenomenon could be avoided thereby lowering systemic toxicity. Furthermore, encapsulating highly potent therapeutic molecules could reduce the amount of drug needed to be release thereby rate of release could be efficiently controlled and monitored. LA implants also provide privacy during the treatment thereby overcoming issues related to societal stigma, thus improving patient adherence. LA implants are widely employed to achieve contraceptive efficacy to avoid unwanted pregnancy in low income countries [162]. For HIV treatment, formulating a single implant with two or more drug combination could be achieved or having two different implant formulations could also be developed. However, to further enhanced the efficacy of treatment, long injectable formulations of cabotegravir or rilpivirine or LA broadly neutralizing anti-bodies [163, 164] could be administered along with LA implant. However, the needed of LA implants to be inserted and removed by trained personnel in a sterile environment forms the major disadvantage towards their development.
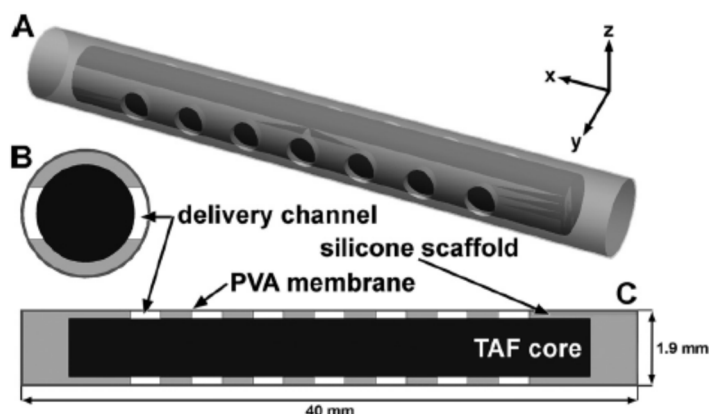
Figure 1.8 *Structural representation of TAF implant. **(A)** Three-dimensional model and **(B and C)** cross-sectional sketch of TAF implant. The TAF was loaded in black space inside PVA coated silicone scaffold [156].*

1.6.4. Broadly Neutralizing Antibodies (bnAb)

Neutralizing antibodies elucidate humoral response against specific sites on the antigen present in xenobiotic agent i.e. foreign to human body [165]. Foreign bodies could be the microorganisms responsible for bacterial, fungal, and viral infections. Even though neutralizing antibodies are effective against specific antigen with minimal genetic variation, these antibodies became less effective against complex viruses such as HIV and influenza showing broader variability in their genetic components. Recently, antibodies with their ability to neutralize microbes with wider range of genetic variability are been developed termed as bnAbs. Antibodies are known for their efficacy against bacterial and viral infections and Palivizumab monoclonal antibody was approved by the US FDA in 1998 for the prevention of respiratory syncytial infections in adults who are the risk of acquiring the infections [165]. Although a transient reduction in plasma viral loads and delayed rebound was observed after administration of first generation of bnAbs against HIV infection such as b12, 2F5, 4E10, 2G12 and KD-247, emergent of resistant viral strains was the major challenge in the bnAb pre-clinical and clinical development

[166, 167]. However, development of potent bnAbs such as 3BNC117 and VRC01 against CD4 binding cites was found to be slow down viral rebound in patients with analytical ART interruption and having low viremia compared to patients administered with ART in phase II b clinical trials [168]. Excitingly, both VRC01 and PGT121 have shown to block HIV replication in activated T-cells constituting viral reservoir in-vitro [168]. Additionally, PGT121 was found to be associated with significant depletion in proviral DNA due to its dual activity of killing latently infected cells by recruiting NK cells and latching on HIV-Env protein expressed on infected cells thereby preventing further formation of latently infected cells by inhibiting HIV release from activated reservoirs [168], [169]. bnAbs having abilities to inhibit both cell free and cell associated viral replication i.e.10-1074 and NIH 45 – 46 mAbs are effective in suppressing viraemia in-vivo compared to mAbs inhibiting cell free virus i.e.10E8 and 3BC16 [169].

Furthermore, modifications of bnAbs that could enhance their potency, prolong their biological half-life, improve Fc receptor (FcR) binding and achieve polyfunctional activity are widely been explored [170]. Selective modifications on antigen binding fragment of Fab of bnAbs have been reported to enhance both the potency and polyfunctionality of bNAbs. Additionally, several studies have shown that the modifications of Fc region of bnAbs could extend the serum IgG half-life, maintain IgG homeostasis, enhance mucosal localization, immune protection, and durability of immune protection [171, 172], [173]. For example, VRC01-LS generated from site directed mutation of VRC01 resulted in 3 fold enhancement in serum half-life in non-human primates, and caused increased persistence of antibodies at the mucosal sites thereby improving immunity (Figure 1.5) [170, 174].
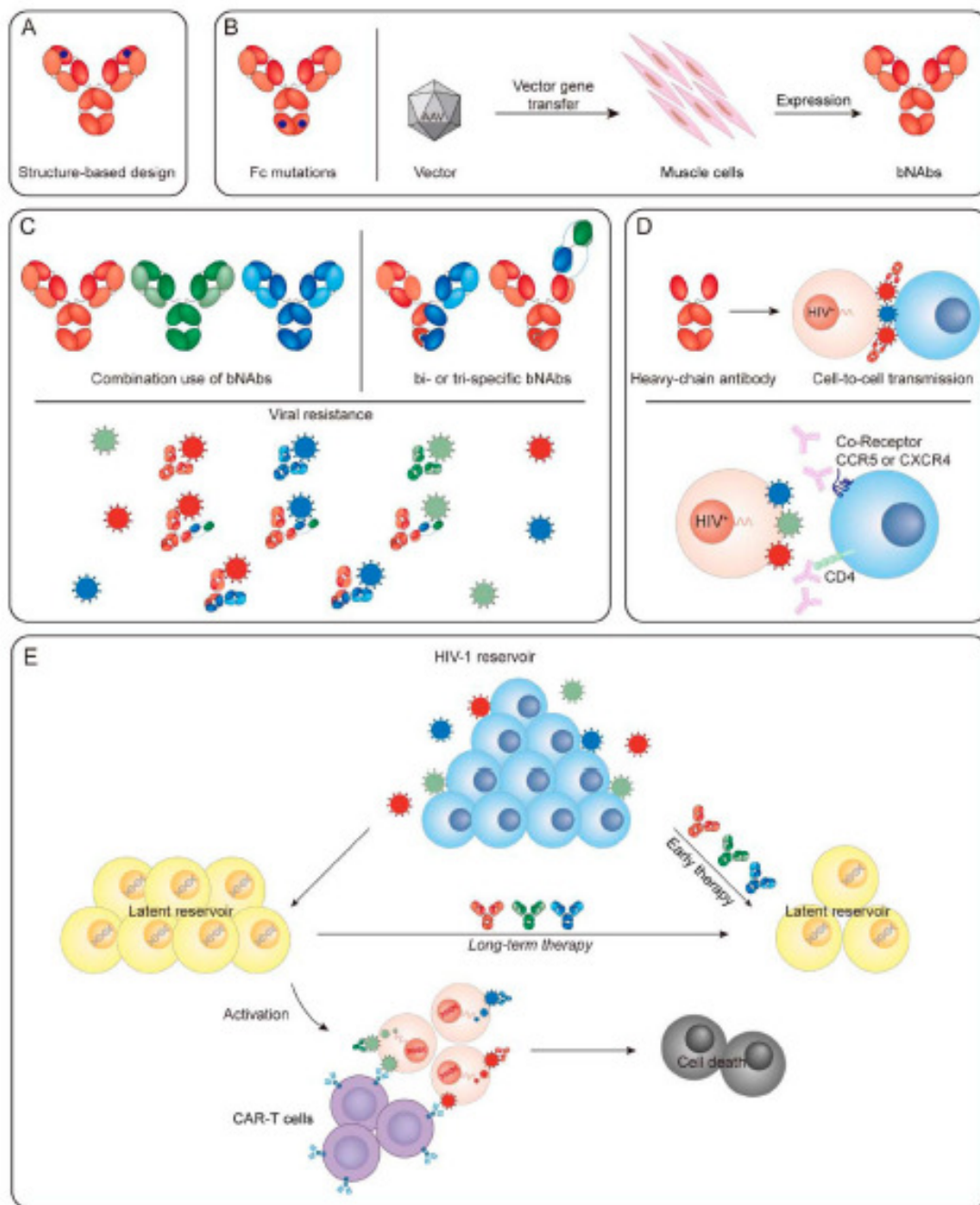
Figure 1.9 *Approaches to enhance bNAbs efficacy. (A) Structure-based design strategies (B) Mutations on Fc region to increase biological half-life (C) Combination of multi-specific bNAbs to overcome viral resistance. (D) Heavy chain antibody mediated prevention of viral cellular transmission and CD4+ coreceptors targeting for the inhibition of viral spread. (E) Administration of combination of bNAbs, CAR-T and latency reversal agents to affect HIV-1 reservoir [170].*

1.6.5. **Transdermal Systems**

With similar advantages to subdermal implants, transdermal delivery route for development LA therapeutics are being explored to enhance patient compliance and improve adherence outcomes. Transdermal delivery approaches are meant to improve patient compliance since these could be self-administered once and be self-disabled by patient at the end of the treatment thereby by-passing the need for daily cART regimen and incase of injectables, the need of health care workers. Microarray patch (MAP) technology form the principal strategy for transdermal delivery of therapeutics [175]. MAPs are essentially micron scale system used for both drugs and vaccine delivery through intra-dermal route [176, 177]. Ideal properties of drugs delivered through MAP include their molecular weights of 500 dalton, melting points of <250 ^{0}C, and log P value of 3 [178]. MAPs offer additional benefits of avoiding injuries related to needle stick and the risk of transmission of blood borne diseases related to accidental exposure to needle specially in the developing world [179]. Keeping in mind the advantages offered by MAPs, novel dissolving microarray patch of rilpivirine LA was developed for its intradermal delivery [180]. The authors anticipated that RPV LA when delivered through MAP would form a depot in the skin and dissolved in the interstitial fluid and released and absorbed in the systemic circulation [181]. Given the hydrophobicity of RPV, the released drug from MAP would target secondary lymph nodes which sites of latent HIV infection [182]. In developing MAPs of RPV LA formulation, low molecular weight PVA (9-10kDa) was employed. Several batches of RPV LA MAPs were made by varying the composition of PVA and RPV LA. Base plate used in MAPs was an aqueous solution having a composition of 20 % w/w PVA (3600kDa) and 1.5 % (w/w) glycerol. The sequential process of preparation of RPV LA MAPs is summarized in **Figure 1.10.** RPV LA MAPs when evaluated in invitro drug release model demonstrated penetration of RPV through the skin and maintained its physico-chemical integrity. Additionally, in-vivo evaluation of

RPV MAPs in rats reached plasma levels of 431 ng/mL at day 7th which was 10 times higher compared to trough concentration obtained after single administration in previous clinical trials [180].

Similarly, transdermal delivery of TAF was explored to achieve sustained release of TAF in comparison to orally delivered 25 mg/ day TAF. One of issues with orally delivered TAF is its poor bioavailability which is 25%. Hence, authors targeted 8 mg/day TAF release in the blood as target dose bioequivalent to orally delivered TAF [120]. Two types of transdermal TAF delivery systems were developed i.e. transdermal TAF patches composed of acrylate adhesive (DURO-TAK 87-2516) and suspension patches composed of silicone (BIO-PSA 7-4301) and polyisobutylene (DURO-TAK 87-6908) adhesives. In-vitro permeation studies in human epidermis were carried out using vertical Franz diffusion cell for period of one week. Acrylate patches composed of 2% TAF and permeation enhancers showed flux of 0.60 ± 0.09 µg/cm^2/h. In contrast, silicone-based patches composed of 15 % TAF demonstrated flux of 7.24 ± 0.47 µg/cm^2/h. However, the optimized TAF loaded transdermal silicone patch – SP7 was further characterized for drug loading, in-vitro release, coat weight and thickness. The optimum SP7 patch was reported to have percent in-vitro drug release of 97.43 ± 19.03, drug content of 6.26 ± 0.32 mg/cm^2, coating thickness of 186 ± 4 and coat weight of 29.39 ± 4.67 mg/cm^2 at room temperature for the duration of 3 months.
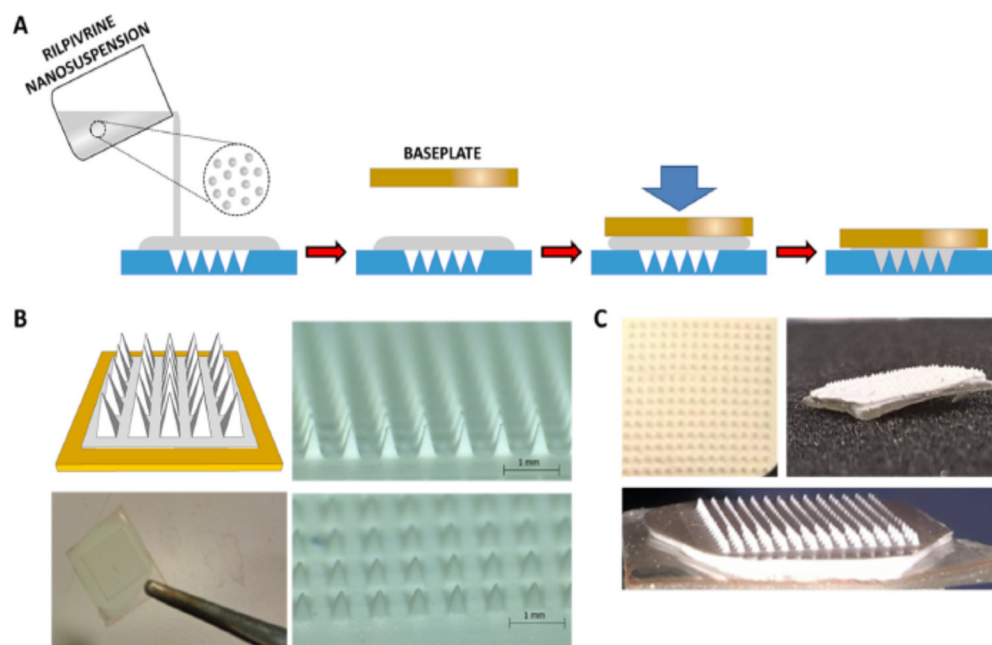
Figure 1.10. *Schematic representation of RPV LA MAP manufacturing process **(A)** RPV LA MAPs micrographs **(B)** and **(C)** digital images of RPV LA MAPs* [180].

1.6.6. Vaginal Rings

On July 24th 2020, the European Medicines Agency (EMA) announced that LA Dapivirine ring received a positive benefit risk opinion from human medicines committee for HIV prevention [183]. Dapivirine LA vaginal ring is made of silicone and meant to sustain the release Dapivirine over duration of 28 days in healthy women which are at the higher risk of HIV infection. After 28 days, LA ring is needed to be replaced with a new ring. Dapivirine LA vaginal ring is a complementary approach to high-risk women when access to the oral PrEP is not feasible [184]. In A Study to Prevent Infection with a Ring for Extended Use (INSPIRE, MTN-020) showed that monthly LA Dapivirine ring containing 25 mg of Dapivirine when used regularly could reduce the risk of acquiring HIV infection in women up to 56 % [185, 186]. Dapivirine is an NNRTI that has activity against a broad range of HIV-1 subtypes and was developed for topical administration. It

has been studied in 2 phase 3 studies and showed HIV risk reduction of 27 and 31%. Follow-on extensions showed even better results and improved adherence.

1.6.7. LA Oral Therapy

Though oral route of administration is feasible and non-invasive high pill burden and fatigue related to ART forms one of the major hurdles in achieving medication adherence [101], [187]. In order to overcome the need of taking multiple pills, simplified dosage forms with a single pill regimen such as Truvada, Atripla, Complera, and Stribild have been approved by the FDA for prevention and treatment of HIV infection [188]. However, these tablets need to be taken daily and any occasion of missed dose could lead to emergence of resistant viral strains leading to treatment failure [103, 189]. Thus, there is a need to develop drug delivery technology that could be given orally releasing drug for a sustained period thereby reducing dosing frequency and improve patient adherence and treatment success. In order to achieve extended release kinetics per oral delivery, a gastro-retentive drug delivery system with abilities to sustain drug delivery form a principal choice in the formulation development [190]. With these goals in mind, the authors attempted to develop a star shaped polymeric gastric resident dosage form with the ability of load and release multiple drugs to achieve sustain release dosage form for HIV maintenance therapy [191]. In this research the authors developed modular polymeric drug delivery system having star shaped external morphology loading DTG, CAB and RPV which folds and recoils in stomach and releases these drugs over a period of week in a swine model. The authors believe if this technology becomes successful in clinical trials it could bring about a substantial paradigm shift in HIV-1 treatment. In addition to tablets, liquid capsules, soft gels, suspensions and emulsions are other forms of drug, a polymer stabilized nanoemulsion of poorly water-soluble drugs efavirenz and lopinavir was developed and optimized to achieve on-demand concentrations at the patient's end. The apparent permeability of drug loaded nanoemulsion demonstrated

improved in-vitro transcellular permeation with no negative effects on anti-retroviral effects [192]. More interestingly, in order to achieve a customized release profile of drugs, a novel 3D- printing technology was been explored for oral delivery of combination of drugs in a single pill regimen [193]. Taking advantage of the controlled release kinetics offered by 3-D printed pills, guaifenesin loaded polymeric 3D-printed tablets were developed and their release kinetics were compared with the commercially available guaifenesin bi-layer tablets. A comparable release profile and similar physico-chemical and mechanical properties were noted for 3D-printed tablets compared to commercial formulation [194]. With these advantages, 3D- printed tablets loading multiple ARVs with desired release kinetics could be developed and explored as sustained release oral delivery technology.

Chapter 2

Project Hypotheses and Research Goals

2.1. Hypotheses and Aims

Project 1: Development of LA Nanoformulated NRTI ProTides against HIV-1 infection - **(Chapters 3, 4, 5)**

Project 2: Development of LA Nanoformulated Prodrugs against HBV infection - **(Chapter 6)**

Project 1 Hypothesis

We hypothesize that developing a library of LA slow effective release emtricitabine (FTC) ProTide nanoformulations will provide potent antiretroviral activities by increasing the developed FTC ProTide's apparent half-life, improving plasma stability and thereby targeting HIV reservoir sites to reduce dosing frequency for continual viral suppression. By employing LA ProTide nanocrystal strategy to create a LA FTC, we hoped to bypass the first step of phosphorylation in FTC's intracellular activation pathway thereby enhancing FTC's potency. Additionally, docosyl phenylalanyl/alanyl ester in FTC ProTide would enhance nanoparticle stability and prolong FTC monophosphate's intracellular delivery. Docosanol component in FTC ProTide would enhance therapeutic synergism in the infected cells [195, 196]. The objective of this project is to develop a LA nanoformulated FTC ProTide for pre-exposure prophylactic treatment in combination with a LA TFV prodrug nanoformulation developed in our laboratory.

Project 2 Hypothesis:

We hypothesize that the development of LA lipophilic and hydrophobic tizoxanide (TIZ) prodrug nanoformulation (NM1NIT) would sustain the biological activity of TIZ leading to generation of potent LASER nanoformulation of TIZ for effective

treatment individually and in combination with tenofovir prodrug nanoformulation against HBV infections.

Project 1: Specific Aims

Aim 1: Synthesis and physicochemical characterizations of M2FTC, M3FTC and M4FTC ProTides.

Aim 2: Nanoformulation of M2FTC, M3FTC and M4FTC ProTides and their cell-based characterizations.

Aim 3: Evaluation of PK and BD of NM2FTC in sprague dawley rats at 45mg/kg FTC equivalents and NM4FTC in NSG and Balb/c mice in combination with NM2TFV at 75 mg/kg FTC/TFV equivalents following I.M. administration.

Developmental Aim: Preliminary evaluation of optimum viral dose for pre-exposure prophylactic study of combination of NM4FTC and NM2TFV treatments at 75 mg/kg of FTC/TFV equivalents in humanized mouse model of HIV-1 infection.

Project 2: Specific Aims:

Aim 1: Synthesis of LA NIT prodrug (M1NIT) and its physicochemical characterization.

Aim 2: Nanoformulation of NIT (NM1NIT) and its physicochemical characterization

Aim 3: Evaluation of anti-HBV efficacy of combination of NM1NIT and NM1TFV treatments at 75 mg/kg of FTC/TFV equivalents administered I.M. in humanized HBV infected TK-NOG mice.

Chapter 3

Synthesis of a LA Nanoformulated

Emtricitabine ProTide

3.1 Abstract

While antiretroviral therapy (ART) has revolutionized treatment and prevention of human immunodeficiency virus type one (HIV-1) infection, regimen adherence, viral mutations, drug toxicities, access stigma and pill fatigue are treatment limitations. These have led to new opportunities for the development of LA ART including implantable devices and chemical drug modifications. Herein, medicinal and formulation chemistry were used to develop LA prodrug nanoformulations of FTC). A potent lipophilic FTC phosphoramidate prodrug (M2FTC) was synthesized then encapsulated into a poloxamer surfactant (NM2FTC). These modifications extended the biology, apparent drug half-life and antiretroviral activities of the formulations. NM2FTC demonstrated a > 30-fold increase in macrophage and CD4+ T cell drug uptake with efficient conversion to triphosphates (FTC-TP). Intracellular FTC-TP protected macrophages against an HIV-1 challenge for 30 days. A single intramuscular injection of NM2FTC, at 45 mg/kg native drug equivalents, into Sprague Dawley rats resulted in sustained prodrug levels in blood, liver, spleen, lymph nodes and FTC-TP in lymph node and spleen cells at one month. In contrast, native FTC-TP was present for one day. These results are an advance in the transformation of FTC into a LA agent.

3.2 Introduction

There is an emerging need for LA nanoformulations for both treatment and prevention of HIV-1 infection [160, 197]. Parenteral cabotegravir and rilpivirine (CAB and RPV) LA antiretroviral drug (ARV) formulations [197, 198] and a dapivirine vaginal ring [184] have generated significant enthusiasm and will soon occupy a position in the HIV therapeutic armamentarium [199]. However, there are limitations of each [200]. They include, but are not limited to, required large injection volumes, site reactions [201],

limited viral reservoir drug penetrance [202], cost, access [203] and drug delivery [204]. While broad numbers of drug-loaded implants and LA nanomedicines are being developed few provide immediate remedies [205]. To these ends our laboratory has developed prodrug nanoformulations stabilized by poloxamer surfactants and lipids as LA agents [206, 207]. The rationales are based demonstrating that prodrugs present effective and inexpensive opportunities for improved drug delivery. These include their readily upscale potential and their prior and extensive use as a delivery systems for infectious [208], neuropsychiatric [209] and metabolic disorders [210]. Added to these advantages is the use of the prodrug approach for more than four decades in clinical practice [211-213]. Thus, we contend that parenteral ARV prodrug formulations may be developed as suitable LA injectables. Our works and those of others have offered this track as a creative solution for the current challenges seen in developing LA ARVs as a mainstream HIV treatment strategy.

There are number of prodrug advantages in the development of LA ARVs. *First*, after physicochemical drug modifications, improvements in drug potency and apparent plasma half-life of the native drug can be realized [212],[214]. *Second*, prodrugs are pharmacologically inactive requiring chemical transformation to produce the parent drug [215] that ensures their retention for extended time periods. This occurs either at the site of injection or in tissue and as such can significantly extend the pool of active drug in plasma and tissue after a single injection. *Third*, prodrugs can positively affect absorption, biodistribution and excretion based on lipophilic and hydrophobic properties. Such modifications of therapeutic compounds facilitates their passive transport across cell and tissue membranes [216]. This also effects depot formation in endosome vesicles [150, 217, 218]. *Fourth*, potent ARVs remain underutilized due to their biologic PK and PD or physiochemical properties that would benefit from prodrug transformations [219]. Indeed, ARVs that currently have short half-lives with hydrophilic properties provide opportunities

for chemical conversions. Conversions from native hydrophilic agents to hydrophobic and lipophilic prodrugs are possible. To these ends, we developed research platforms to transform existing ARVs into LA agents [220] [206, 207, 221, 222].

ARV potency and bioavailability improvements by production of fatty acid ester prodrugs of nucleoside reverse transcriptase inhibitor (NRTI) compounds were accomplished [221]. Notably and in pursuit of potent LA NRTI inhibitor analogs, design of carbon chain modifications and ProTide strategies were completed. These led to development of a first lipophilic abacavir (ABC) ProTide through screening a range of amino acid and ester promoieties [223]. However, intracellular delivery of LA active drug metabolites remains elusive. Thus, in the present study, we applied a unique LA ProTide nanocrystal strategy to create a LA FTC. We assumed that by bypassing the first phosphorylation step in FTC's intracellular activation pathway could further enhance drug potency. We also reasoned that inclusion of a docosyl phenylalanyl ester in FTC ProTide would confer prodrug nanoparticle stability and would enhance intracellular delivery of the nucleoside monophosphates [224]. Once cleaved, docosanol would promote drug-drug synergy [225, 226].

3.3 Materials and Methods

3.3.1 Materials

All chemical synthesis reactions were performed under a dry argon atmosphere unless otherwise noted. Reagents were obtained from commercial sources and used directly; exceptions are noted. FTC was purchased from HBCChem (Fremont, CA). Phenyl dichlorophosphate, N-(carbobenzyloxy)-*L*-phenylaline, docosanol, dichloromethane (DCM, CH_2Cl_2), chloroform ($CHCl_3$), N,N dimethylformamide (DMF), triethylamine (Et_3N), diethyl ether, tetrahydrofuran (THF), *tert*-Butylmagnesium chloride

solution (*t*BuMgCl, 1.0 M in THF), triethylsilane (Et₃SiH) and methanol were purchased from Sigma-Aldrich (St. Louis, MO).1-[Bis(dimethylamino)methylene]-1H-1,2,3-triazolo[4,5-b]pyridinium3- oxidhexafluorophosphate (HATU) was obtained from Chem Impex Intl. Inc. (Wood Dale, IL) and palladium, 10% on activated carbon was purchased from STREM Inc. (Newburyport, MA). Flash chromatography was performed using flash silica gel (32-63 µ) from SiliCycle Inc. (Quebec, Canada). Chemical reactions were analyzed by thin layer chromatography (TLC) on precoated silica plates (200 µm, F-254) from Sorbtech technologies Inc. (Norcross, GA). The compounds were visualized by UV fluorescence or by staining with ninhydrin or $KMnO_4$ reagents. Pyridine, poloxamer 407 (P407), ciprofloxacin, 3-(4,5-dimethylthiazol-2yl)-2,5-diphenyltetrazolium bromide (MTT), dimethyl sulfoxide (DMSO), paraformaldehyde (PFA), and 3,3'-diaminobenzidine (DAB) were purchased from Sigma-Aldrich (St. Louis, MO). Cell culture grade water (endotoxin free), gentamicin, acetonitrile (ACN), bovine serum albumin (BSA), and LC-MS-grade water were purchased from Fisher Scientific (Hampton, NH). Heat-inactivated pooled human serum was purchased from Innovative research (Novi, MI). Phosphatase, acid from sweet potato (P1435-500UN) was purchased from Sigma Aldrich. Dulbecco's Modification of Eagle's Medium (DMEM) was purchased from Corning Life Sciences (Tewksbury, MA) and RPMI 1640-*L*-glutamine (SKU# 11875-093) was purchased from Gibco, ThermoFisher Scientific. LiveDead Fixable Blue Dead Cell Stain kit was purchased from Invitrogen, ThermoFisher. CEM-ss CD4+ T-cells were obtained from the National Institutes of Health cell repository.

3.3.2 Synthesis of A Phosphorylated FTC Prodrug

FTC (1.5 g, 6.02 mmoles, 1 equivalent) was dried from anhydrous pyridine (15 mL), resuspended in anhydrous THF (30 mL) and then cooled at -78 °C under an argon

atmosphere. *t*BuMgCl (12.04 mmoles, 2 equivalents) was then added and allowed to stir for 15 minutes under protection from light. A solution of phenylalanine docosyl phosphochloridate [223] (3.89 g, 6.02 mmoles, 1 equivalent) in THF (20 mL) was then added dropwise to the anion at -78 °C. The reaction mixture was gradually warmed to room temperature for 1 day and heated at 45 °C for 24 h. The mixture was then cooled at -78 °C and quenched using methanol and concentrated to remove solvents. The residue was purified by silica column flash chromatography eluting with 95% then 90% DCM in methanol to give M2FTC as a colorless powder after lyophilization (61 % yield). The chemical structure of M2FTC was confirmed by proton, carbon and phosphorus nuclear magnetic resonance (^{1}H, ^{13}C and ^{31}P NMR) spectra recorded on a Varian Unity/Inova-500 NB (500 MHz; Varian Medical Systems Inc., Palo Alto, CA, USA) (**Figure 6 (A, B, C)**). FT-IR analysis was performed on a Spectrum Two FT-IR spectrometer (PerkinElmer, Waltham, MA, USA). Comparative crystallographic analyses of FTC and M2FTC by powder X-ray diffraction (XRD) were carried out in the 2ø range of 2-500 using PANalytical Empyrean diffractometer (PANalytical Inc., Westborough, MA, USA) with Cu-Ka radiation (1.5418 Å) at 40 kV, 45 mA setting. FTC and M2FTC quantitation were performed on a Waters ACQUITY ultra performance liquid chromatography (UPLC) H-Class System with TUV detector and Empower 3 software (Milford, MA, USA) using a Phenomenex Kinetex 5 μ C18 100 Å column (150, 4.5 mm) (Torrence, CA) for separation. Molecular mass was determined by direct infusion into a Waters TQD mass spectrometer. The UPLC-TUV and mass spectrometric methods for FTC and M2FTC quantitation are included in the supplementary information.

3.3.3 M2FTC Characterization

3.3.3.1 Solubility

To determine solubility of FTC and M2FTC in water and 1 – octanol, excess amount of drug was added to each media to form saturated solutions. The homogeneous saturated solutions were mixed at room temperature for 24 h and centrifuged at 14,000 x g for 10 minutes to separate insoluble drug. The amount of drug in the supernatants was quantified by UPLC TUV method.

3.3.3.2 Prodrug Chemical Stability

Chemical stability at acid, alkaline and neutral pH was determined as described by Gupta et al. [227]. M2FTC stock solution at a concentration of 2 mg/mL was prepared in optima-grade methanol in a glass amber vial. For acidic, alkaline and neutral hydrolysis, 100 μL of M2FTC stock solution was added to 1900 μL each of 0.1 M HCl, 0.1 M NaOH or optima-grade water, respectively. The samples were then incubated at room temperature under shaking conditions (innova® 42 shaker incubator, 150 rpm). Samples were withdrawn at predetermined time points (0, 4, 8 h and 1, 3 and 7 days) and stored at -80 °C until analysis by UPLC-TUV.

3.3.3.3 Plasma Stability

To evaluate prodrug stability, 100 μL plasma from different species (rat, mouse, rabbit, dog, monkey and human) were incubated with 1 μM of M2FTC at 37 °C. At different time points (0, 2, 6, and 24 h), 1 mL methanol was added to each sample and vortexed for 3 min to stop the reaction. For 0-min time-point, a 100 μL ice cold plasma was spiked with 100-x prodrug spiking solution in 20%DMSO/80% methanol and immediately 1 ml of ice-cold methanol was added. Heat-inactivated plasma was incubated at the same conditions and used as a negative control to differentiate chemical vs. biological instability. Following the addition of methanol, samples were centrifuged at 15,000 g for 10 min, 10 μL supernatant was mixed with 90 μL 80 % methanol containing IS, and then 10 μL was used for UPLC-MS/MS analysis.

3.3.4 Nanoformulation of M2FTC and Physicochemical Characterization

P407 stabilized M2FTC nanosuspensions (NM2FTC) were prepared by high-pressure homogenization on an Avestin EmulsiFlex-C3 (Ottawa, ON, Canada) homogenizer. Specifically, P407 (0.5% w/v) was dissolved in PBS followed by addition of M2FTC (1% w/v) to the surfactant solution at a drug to polymer ratio of 2:1 and mixed to form a pre-suspension. The suspension was then homogenized (~20,000 psi) until the desired particle size was achieved. Particle size (D_{eff}), polydispersity index (PDI), and zeta potential were determined by dynamic light scattering (DLS) on a Malvern Nano-ZS (Worcestershire, UK). The stability of NM2FTC nanoparticles was monitored at 25 and 37°C over 2 months. Encapsulation efficiency was calculated using the following equation: Encapsulation efficiency (%) = (weight of drug in formulation/initial weight of drug added) x 100. In-vitro nanoparticle release kinetics were determined by dialysis (membrane MWCT 2000, Spectrum laboratories, Inc.) against PBS containing 1% v/v Tween 80 at 37 °C with constant shaking (New Brunswick™ Innova® 42, 150 rpm). One milliliter aliquot was withdrawn at predetermined time points and replaced with equal amounts of dispersion medium. Samples were then centrifuged at 10,000×g for 10 min and then lyophilized followed by reconstitution in 100 μL of methanol and quantification for total M2FTC concentration using LC-MS/MS method using Waters Xevo TQD UPLC MS system, chromatographic separation was performed on a CSH analytical column (2.1×100 mm, 1.7µm; Waters) equipped with a guard column (Waters, Milford, MA). Mobile phase A was ammonium formate (10 mM, pH 3.2), while mobile phase B was 100% methanol (mobile phase A: B was 2:98 v/v). The LC method was 7 minutes, run isocratically at 0.35 mL/minute. The following transitions were monitored for M2FTC: m/z 859.19→229.98 and m/z 859.19→276.07.

Nanoparticle morphology was analyzed by transmission electron microscopy (TEM). Samples for TEM imaging were fixed by immersion in a solution of 2% glutaraldehyde, 2% paraformaldehyde in a 0.1M Sorenson's phosphate buffer (pH 7.2) at 4℃ for 24 h and processed as previously described [223].

3.3.5 Macrophage Drug Uptake, Retention and Triphosphate Production.

Characterization of NM2FTC in MDM was performed as previously described [13, 14, 30, 31, 37] [38]. Human monocytes were obtained by leukapheresis from HIV-1/2 and hepatitis B seronegative donors, and then purified by counter-current centrifugal elutriation [228]. Human monocytes were plated in 12-well plates at a density of 1.0×10^6 cells per well using DMEM supplemented with 10% heat-inactivated pooled human serum, 1% glutamine, 10 μg/mL ciprofloxacin, and 50 μg/mL gentamicin. Cells were incubated at 37 ℃ in a 5% CO_2 incubator. After 7 days of differentiation in the presence of 1000 U/mL recombinant human macrophage colony stimulating factor (MCSF), MDM were treated with 100 μM FTC or NM2FTC. Uptake of drug was assessed by measuring intracellular drug concentrations at 2-8 h after treatment [207]. For drug retention studies, MDM were treated with drug formulations for 8 h then washed 2 times with PBS and maintained with half-media changes every other day until collection from days 1 to 30. For both studies, adherent MDM were washed with PBS, then scraped into PBS, and counted at predetermined time points using an Invitrogen Countess Automated Cell Counter (Carlsbad, CA). Cells were pelleted by centrifugation at 3,000 rpm for 8 min at 4℃. The cell pellets were then sonicated in 200 μL methanol using a probe sonicator to extract drug and centrifuged at 20, 000 g for 10 min at 4℃ to separate cell debris. FTC and M2FTC drug contents were determined by UPLC-UV/Vis. For measurements of FTP formed during uptake and retention studies, MDM were treated with FTC and M2FTC with 100 μM concentration using protocol described previously. Cell pellets were suspended in 70% aqueous methanol (v/v) and FTC-TP extraction was performed as

described previously with some modifications [32]. Briefly, Sep-Pak QMA cartridges were used to separate FTC-TP from its mono- and di-phosphate forms. The triphosphate fractions were eluted and dephosphorylated using type XA sweet potato acid phosphatase. The $^{15}N_2$$^{13}C$-3TC internal standard was added following the incubation (final concentration of 0.5 ng/mL). Dephosphorylated samples were then subjected to 2nd SPE extraction step using Waters OASIS HLB cartridges. The FTC were then eluted with 1.4 ml of methanol and evaporated under vacuum. Once dry, the residues were reconstituted with 100 μL 25% methanol before performing LC–MS/MS analyses. To assess cell viability, MTT assay was performed [229]. Briefly, MDM were seeded on 96-well plates at a density of 80.0 x 10^5 cells per well and treated with various concentrations (10 - 400 μM) of FTC or NM2FTC for 6-24 h. After drug treatment, cells were washed twice with PBS and incubated with 100 μL/well of MTT solution (5 mg/mL) for 45 min at 37 °C. After incubation MTT was removed, and 200 μL/well of DMSO was added and mixed thoroughly. Absorbance was measured at 490 nm on a Molecular Devices SpectraMax M3 plate reader with SoftMax Pro 6.2 software (Sunnyvale, CA).

3.3.6. CEM-ss CD4+ T cell Drug Uptake and Triphosphate production.

These expeiments were performed in twelve-well plates were coated with poly-L-lysine solution (100 μg/mL in distilled water) for 1 h. Wells were then washed once with sterile water then seeded with CEM-ss cells at a density of 1 x 10^6 cells/well followed by further incubation at 37 °C for at least 30 minutes. Cells were then treated with 100 μM of FTC or NM2FTC to evaluate drug uptake and retention as previously described [206, 207]. At each time point, cells were washed twice and scraped into PBS, centrifuged at 650 x g for 5 minutes and intracellular drug quantitation was performed using TQD MS method as previously described. To determine intracellular FTC triphosphate (FTC-TP) levels, CEM-ss CD4+ T-cells were treated with 100 μM FTC or NM2FTC and processed for uptake [43].

3.3.7. Half maximum Effective Concentration (EC_{50}) Measurements

MDM were seeded in round bottom 96 well plates at a density of 80,000 cells/well. Various concentrations of NM2FTC or FTC in the range of 0.01 nM-10 μM were added for 60 min prior to infection with HIV-1$_{ADA}$ media at a MOI of 0.1 infectious particles per cell for 4 h. After 4 h, infection media was removed, and the cells were incubated an additional 10 days in the presence of the same concentration of drug. Half media changes were done every other day. After 10 days, culture media was collected to measure HIV-1 reverse transcriptase (RT) activity as previously described [148, 230, 231]. Parallel studies were performed in transformed CD4+ T cells. Briefly, CEM-CD4+ T cells were cultured in suspension in 96 well plates, centrifuged at 650 x g and re-dispersed in 100 μL drug-containing media. After 60 minutes, cells were challenged with HIV-1$_{NL4-3-eGFP}$ (MOI 0.1) by spin-inoculation (1125 g for 2 hours, 25ºC) followed by incubation in drug-containing media for 16 h. The cells were then washed 3x with PBS to remove extracellular virus and incubated in drug-containing media. Media exchanges occurred every 2 days with drug-containing media. Ten days post HIV-challenge, cell pellets were fixed in 2% PFA and fluorescence was analyzed by flow cytometry. The EC_{50} was calculated using sigmoidal 4-point logarithmic regression using GraphPad Prism v7. RT activity was measured in culture media.

3.3.8. Measurements of Antiretroviral Activities

To assess long-term antiretroviral efficacy, MDM were treated with 100 μM NM2FTC or FTC as described above for 8 h. After treatment, cells were washed with PBS and cultured with fresh media without drug followed by half-media exchanges every other day. At days 1-30 after treatment, cells were challenged with HIV-1$_{ADA}$ at a MOI of 0.1 for 16 h. After viral infection, the cells were cultured an additional 7 days with half-media exchanges every other day followed by full media change on the 8th day post

challenge. Culture fluids were collected on the 10th day for measurement of RT activity, while adherent MDM were fixed with 4% PFA and HIV-1p24 protein expression assayed by immunohistochemistry [35, 36].

3.3.9. PK and BD Assessments

All animal studies were approved by the University of Nebraska Medical Center Institutional Animal Care and Use Committee in accordance with the standards incorporated in the Guide for the Care and Use of Laboratory Animals (National Research Council of the National Academies, 2011). Male Sprague Dawley rats (250g; Jackson Labs, Bar Harbor, ME) were maintained on normal diet and water. Animal weights were monitored at the start and weekly throughout the study duration of study. The rats were administered a single 45 mg/kg FTC-equivalent dose of FTC or NM2FTC intramuscularly (IM) into the caudal thigh muscle to determine PK over 4 weeks. Blood was collected 2 h and 1, 7, 14, 21, and 28 days. Tissues were collected at days 1, 7, 14 and 28 days. Lymph node cells and splenocytes were isolated on days 1, 7, 14 and 28 days for determination of FTC-TP levels**.** Prodrug and FTC were quantitated in whole blood and tissue samples by UPLC-MS/MS method (Waters Xevo TQS micro., Milford, MA). For FTC quantification in cell samples and injection solutions, U.V. detection at 278 nm and mobile phase composition of acetonitrile and ammonium acetate buffer (20 mM, pH 3.9) in the ratio 10:90 v/v and flow rate of 1.0 mL/min was used. For M2FTC quantification, HPLC grade methanol and ammonium formate (10 mM, pH 3.1) in the ratio of 98:2 v/v, flow rate of 1 mL/min and detection at 250 nm was carried out. Retention times for FTC and M2FTC attained were 4.5 and 5.5 minutes respectively. LC-MS single quadrupole compound infusion was recorded on a Waters TQD (Boston, MA) to confirm [M+1] m/z of 860. Isotopic distribution was (m/z): 858.45 (100%), 859.46 (48.7%), 860.46 (11.6%). For M2FTC quantification using Waters Xevo TQ-XS UPLC-MS/MS method, ACQUITY UPLC® BEH Shield RP18 Column-4 (2.1×30 mm, 1.7μm; Waters, Part No.: 186003909,

Serial No.: 01633604918114) was used with LC conditions of ammonium formate pH 3.0 (7.5 mM) and methanol used as gradient mobile phases and MRM of 8 min with wash: purge: 80% methanol, strong wash: 50% methanol + 30% H_2O + 20% Acetone. Sample was maintained at 4°C advanced with needle placement from bottom 1.2 mm, pressure limits: Low: 0 psi, High: 15000 psi and seal wash 3.0 min. The initial mobile phase composition was 88% B for the first 5 min at which time it was increased to 95% B over 0.25 mins and held constant for 1.55 min and then reduced to 88 % B after 0.2 mins and held constant for further 10 min.

Parent FTC was generated from FTC-TP during sample preparation and then subjected to UPLC-MS/MS analyses. The UPLC-MS/MS system comprised of a Waters ACQUITY ultra-performance liquid chromatography (UPLC) system (Waters, Milford, MA) coupled to a triple quadrupole mass spectrometer with electrospray ionization (ESI) source (Waters Xevo TQ-XS). An ACQUITY UPLC using a CSH C18 analytical column (2.1×100 mm, 1.7µm; Waters) equipped with a guard column (Waters, Milford, MA) were used for analyte separation. The transition of 248.08 < 129.95 m/z and 232.96 < 115.00 m/z were used for FTC and IS quantification. Mobile phase A consisted of 7.5mM ammonium bicarbonate in water (MS grade, Fisher), pH was adjusted to 7.0 with glacial acetic acid (ACS grade, Sigma). Mobile phase B was 100% methanol (MS grade, Fisher). The flow rate was 0.25 mL/min.

Drug concentration in whole blood and tissues was determined by UPLC-MS/MS using a Waters Acquity UPLC- Xevo TQ-S micro mass spectrometry system (Milford, MA). For blood analysis, 10 µL of internal standard (IS) solution was added to each sample. 3TC-d3 and myristoylated dolutegravir (MDTG) were used as IS for FTC and M2FTC analysis, respectively. Chromatographic separation of 10 µL sample injections of M2FTC was achieved with an ACQUITY UPLC-BEH Shield RP18 column (1.7 µm, 2.1 mm × 33 mm) using a 6.75 min gradient of mobile phase A (7.5 mM

ammonium formate in Optima-grade water adjusted to pH 3 using formic acid) and mobile phase B (100% Optima-grade methanol) at a flow rate of 0.35 mL/ min. The initial mobile phase composition was 88% B for the first 5 min at which time it was increased to 95% B over 0.25 mins and held constant for 1.50 min. For FTC quantitation, chromatographic separation was carried out on UPLC CSH C18 (1.7 µm, 2.1 mm × 100 mm) column. Mobile phase A consisted of ammonium bicarbonate (90%) and mobile phase B consisted of 100 % Optima grade methanol at a flow rate of 0.25 mL/min and run time of 7 mins. Multiple reaction monitoring (MRM) transitions used for M2FTC, MDTG, FTC, 3TC – d3, were 859.394 > 276.014, 630.2 > 126.94, 247.98 > 129.80, 233.39 > 114.97 m/z, respectively. Spectra were analyzed and quantified by MassLynx software version 4.1. Quantitation was based upon drug peak area to internal standard peak area ratios.

3.4. Statistics

For all studies, data were presented as mean ± standard error of mean (SEM), and experiments were preformed using a minimum of three biological replicates. For in-vivo studies, each group contained 5 rats (pharmacokinetic studies). For comparison of two groups, Student's t-test (two-tailed, paired and unpaired) were used. One way ANOVA was performed for comparison between 3 groups. $P < 0.05$ was considered to be significant (*$P < 0.05$, ****$P < 0.0001$). All the data were analyzed using GraphPad Prism 7.0 software (La Jolla, CA).

3.5. Study Approval

All animal studies were approved by the University of Nebraska Medical Center Institutional Animal Care and Use Committee in accordance with the standards incorporated in the Guide for the Care and Use of Laboratory Animals (National Research

Council of the National Academies, 2011). Human monocytes were isolated by leukapheresis from HIV-1/2 and hepatitis seronegative donors according to an approved UNMC IRB exempt protocol.

3.6. Results

3.6.1. Synthesis and Characterization of M2FTC

Phenylalanine docosyl ester was reacted with preformed phenyl phosphorodichloridate in the presence of triethylamine (**Figure 3.1A).** This generated a phenylalanyl docosyl ester phosphorochloridate masking group [223]. The amino ester was then coupled with FTC (**Figure 3.1B)** and purified by silica gel column chromatography producing 61% of M2FTC [232].

Nuclear magnetic resonance, Fourier transform infrared spectroscopy and mass spectrometry (NMR, FTIR and MS) confirmed the formation of the prodrug. The M2FTC physicochemical properties consisted of broad singlets at 0.84 ppm and 1.4 ppm and multiplet at 1.1-1.3 ppm in the ^{1}H NMR spectrum corresponding to the terminal methyl and symmetrical methylene protons of the fatty alcohol. Additionally, the multiplet at 7.09-7.32 ppm corresponds to the aromatic protons from the aryl and phenylalanine promoieties (**Figure 3.1C**). ^{13}C NMR spectrum of NM2FTC showed additional peaks corresponding to the carbonyl ester (172.2 ppm) and aromatic carbon atoms (124.7, 124.3, 119.9, 119.8 ppm) **(Figure 3.1D)**. ^{31}P NMR spectrum of M2FTC demonstrated a dominant single peak (**Figure 3.1E)**. M2FTC spectra data ^{1}H NMR (500 MHz, $(CD_3)_2S=O$): 7.89 (app. d, J = 6.8 Hz 1H), 7.64 (b, 1H), 7.09-7.32 (m, 8 H), 7.03 (app. d, J = 8.0 Hz 2H), 6.22 (t, J = 11.5 Hz 1H), 6.16 (br, 1H), 5.19-5.25 (m, 1H), 3.85-4.05 (m, 4H), 3.30-3.40 (m, 4H), 3.05 (dd, J = 11.5, 6.1 Hz 1H), 2.82 (dt, J = 15.5, 7.6 Hz 1H), 2.76-2.85 (m, 1H), 1.40 (br, 2H), 1.10-1.30 (m, 38H), 0.84 (br, 3H). ^{13}C NMR (125 MHz,

(CD$_3$)$_2$S=O): δ 172.2, 157.5, 124.7, 124.3, 119.9, 119.8, 86.9, 81.4, 66.4, 64.4, 56.0, 35.3, 35.1, 31.2, 28.9, 28.8, 28.7, 28.6, 27.9, 27.8, 25.1, 22.0, 13.7; ^{31}P NMR (202 MHz, (CD$_3$)$_2$S=O); 5.68. Infusion of M2FTC into Waters TQD mass spectrometer confirmed a M2FTC molecular ion peak of 859.19 **(Figure 3.1F)**.
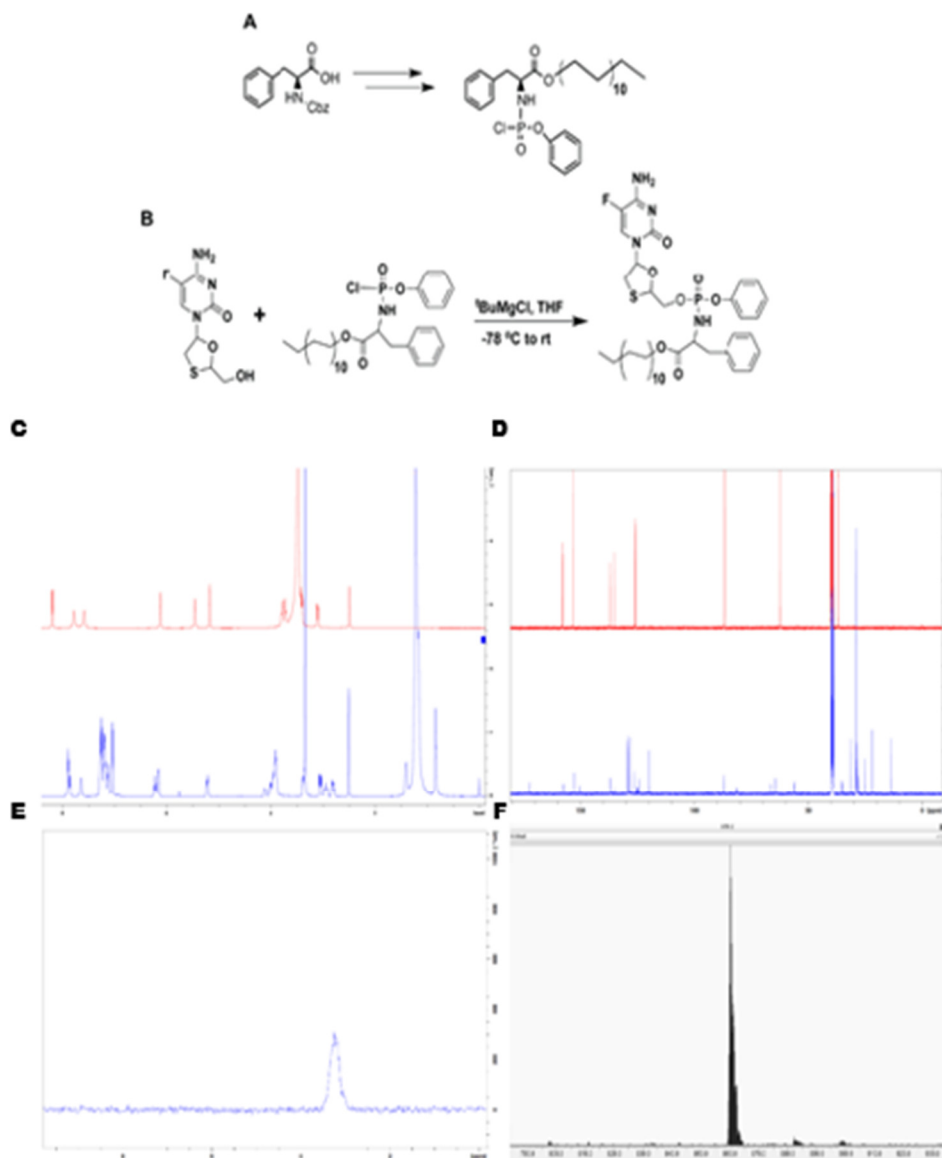
Figure 3.1. Synthesis of M2FTC and NMR spectroscopic and Mass spectrometric characterization.

(A) Synthesis of aryl amino phosphochloridate. N-Cbz-L-Phenylalanine was dissolved in DMF and CFM. Cooled on ice. HATU, docosanol, imidazole and Et$_3$N were added and reaction was stirred at RT for 48 h. Product was dissolved in CFM and MeOH. Palladium on carbon was added and cooled to 4 ºC, Et$_3$SiH was

*added and stirred for 16 h. Product was dissolved in DCM at -78 ºC, Phenyl dichlorophosphate was then added, followed by Et₃N/CFM addition, stirred at 48 h RT. **(B)** FTC was dissolved in THF at -78 ºC, ᵗBuMgCl was added and stirred at 48-90 h at RT. FTC was then reacted with product formed in previous step with a 61% yield. **(C)** ¹H NMR spectra of FTC (red), M2FTC (blue). **(D)** ¹³C NMR spectra of FTC (red), and M2FTC (blue). (E) ³¹P NMR spectrum of M2FTC (F) Mass spectrometric infusion of M2FTC.*

A 4000-fold decrease in aqueous solubility (0.0366 ± 0.0093 mg/mL) for M2FTC compared to FTC (142.97 ± 11.24 mg/mL) was observed. This corresponded to a 90-fold improvement in M2FTC octanol solubility (87.56 ± 0.236 mg/mL) compared to 0.97 ± 0.027 mg/mL for FTC. These data confirmed the prodrug lipophilicity enhancements ($p < 0.0001$) (**Figure 3.2A**). Additional absorption bands at $2921 - 2846$ cm^{-1} and $1800 - 1700$ cm^{-1} in the FTIR spectrum of M2FTC were seen representing the C-H and C=0 stretches in docosanol and phenylalanine esters, respectively (**Figure 3.2B**). XRD spectra demonstrated difference in the crystallographic spectrum of M2FTC compared to FTC (**Figure 3.2C**). Changes in the crystallinity of M2FTC compared to FTC was due to conjugation of lipophilic promoieties to the FTC structure during M2FTC synthesis followed by lyophilization, thus affecting its polymorphic form [233, 234].

Figure 3.2 Physicochemical characterization of M2FTC (A) *Solubility of FTC and M2FTC in 1-octanol and water was measured at 37℃. Data are expressed as mean ± SEM for n = 3 samples were evaluated. Statistical significance was measured using one-way ANOVA at ****P < 0.0001.* ***(B)*** *Fourier transformed infra-red spectroscopic (FT-IR) analysis showed the presence of carbonyl and aromatic stretching vibrations in the region of 2900 - 3100 cm^{-1} for FTC and M2FTC and phosphoramide (P-N-H) bending vibrations between 1600 – 1700 cm^{-1} in M2FTC, confirming the presence of these functionalities.* ***(C)*** *XRD analysis of FTC and M2FTC supporting unique atomic arrangement in the compounds crystal lattice.* ***D)*** *Hydrolysis study in different species' plasma demonstrated chemical stability of M2FTC over 90% in both normal and heat inactivated human plasma up to 24 h at 37 ℃ and gradual hydrolysis observed of up to 40% in mice and rats, dog, rabbit and in monkey plasma over 24 h.*

3.6.2. M2FTC Chemical Stability

Chemical stability for M2FTC was determined at room temperature in buffers of different pH solutions. At neutral pH, M2FTC was stable over 7 days (**Figure 3.3A)**. However, after 24 h of incubation under acidic and alkaline pH, 10% of the prodrug degraded presumably through ester bond cleavage.

3.6.3. Plasma Metabolic Stability

The stability of M2FTC was further investigated using plasma from different species. After 24 h of incubation at 37℃, degradation of M2FTC was high in rodent, dog, rabbit and monkey plasma. However, M2FTC remained stable in both normal and heat inactivated human plasma over 24h (**Figure 3.2D**). The observed differences in plasma stability of M2FTC in different species were due to differences in the esterase expression in these tested species [235]. These data sets support the stability of M2FTC in blood for both intracellular and tissue prodrug uptake and FTC triphosphate conversions.

3.6.4. Physico-chemical Characterization of M2FTC Nanoformulations

We next developed stable nanoformulations of the prodrug by a single step scalable nanoparticle manufacturing scheme [236]. P407 stabilized nanosuspensions of M2FTC (NM2FTC) were prepared by high-pressure homogenization with a drug encapsulation efficiency of ≥70%. Particle size, polydispersity index (PDI), and zeta potential were determined by DLS and were 359.4 ± 13 nm, 0.37 ± 0.02, and -44.8 ± 0.2 mV, respectively. NM2FTC remained stable at 25 and 37 °C (**Figure 3.3A** and **Figure 3.4C**) for up to 60 days. The high negative charge provides electrostatic repulsion between the particles to minimize aggregation. Nanoparticle morphologies by TEM showed fairly uniform and spherical particles with diameters less than 400 nm (**Figure 3.3D**) and validated the particle size. The high drug loading, smaller particle size and minimal excipient usage in NM2FTC nanosuspensions could potentially reduce injection site reactions. HIV-1 RT activity measurements demonstrated that the EC_{50} of FTC (0.5 nM), M2FTC (0.11 nM), and NM2FTC (0.04 nM) against HIV-1$_{ADA}$ in MDM were comparable (one-way ANOVA, p=0.74) indicating that conversion of FTC to M2FTC and NM2FTC did not compromise drug potency (**Figure 3.3B**). Similarly, the EC_{50} of NM2FTC in CEM CD4+ T-cells was not different from FTC (15.55 nM and 25.71 nM, respectively; P = 0.5873, two tailed t test with Welch correction). These data further confirmed that the antiretroviral activity of the prodrug formulation was not altered by its chemical modification (**Figure 3.3E**). The reduction in the EC_{50} for M2FTC was likely due to poor solubility of the hydrophobic prodrug in aqueous culture media. Administration of the prodrug nanoparticles (NM2FTC) with improved dissolution properties confirmed the expected improvement in drug potency. Since mitochondrial dysfunction is a major adverse effect of NRTIs [237], we performed mitochondrial dehydrogenase activity assessment of FTC, M2FTC and NM2FTC in MDM at 10-400 μM using 3-(4,5-dimethylthiazol-2-yl)-2,5-diphenyltetrazolium bromide (MTT). No effects on mitochondrial reductase activity was observed at all tested drug concentrations. However, M2FTC and

NM2FTC exhibited a slight reduction in cell viability above 100 μM, presumably caused by enhanced cellular drug uptake (**Figure 3.3C**). In CEM CD4+ T-cells, neither FTC, M2FTC nor NM2FTC affected cell viability at $\leq$ 200 μM by LiveDead staining (**Figure 3.3F**). Hence, 100 μM drug concentrations were used in subsequent CEM-ss CD4+ T-cell studies. TEM imaging performed in MDM and CEM CD4+ T cells showed NM2FTC within cytoplasmic vesicles. After 8 h of drug treatment, NM2FTC nanoparticles accumulated in cytoplasmic vesicles in both cell lines (**Figure 3.3G**).
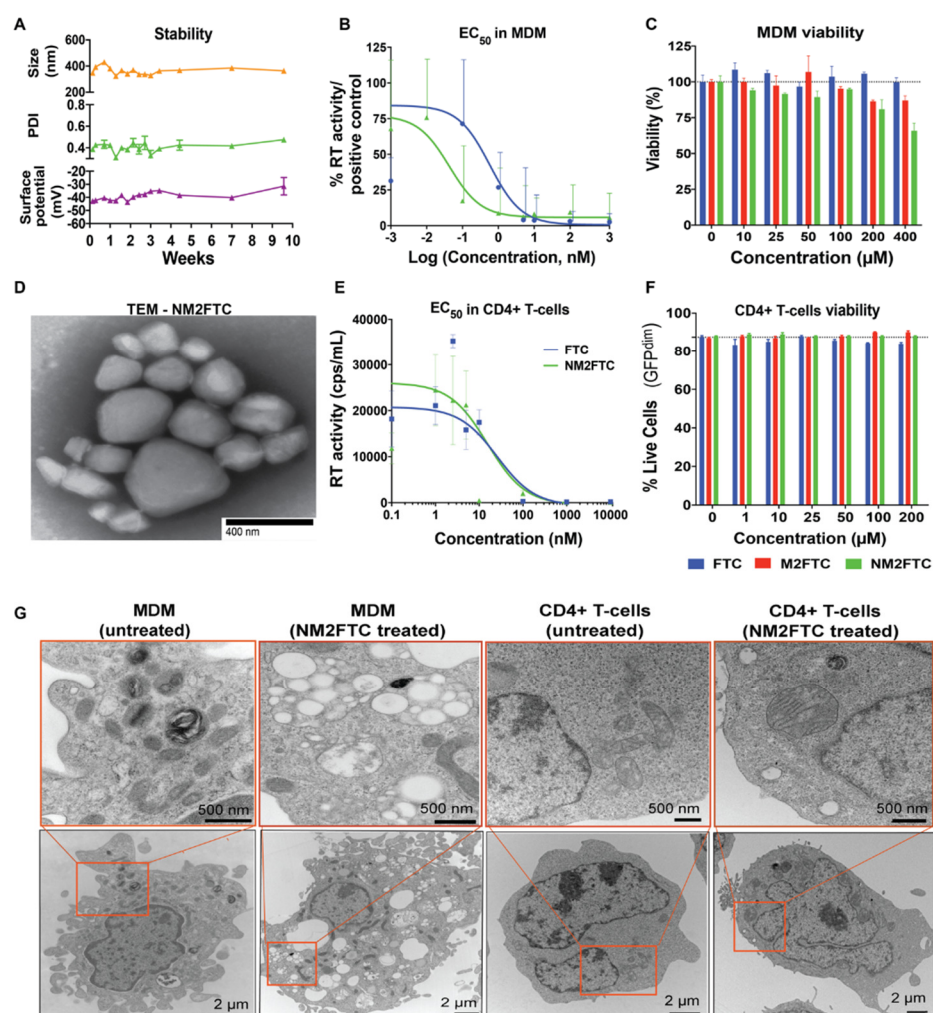
Figure 3.3 NM2FTC characterizations. A) *Physico-chemical stability evaluation of NM2FTC at 25 °C in terms of particle size, zeta potential and polydispersity index over 1 month. **(B)** EC_{50} was determined in MDM over a range of concentrations (0.001–1000 nM) by determining HIV-1 RT activity after FTC or NM2FTC treatments in cells infected with HIV-1$_{ADA}$. Results were analyzed by nonlinear regression least squares fit.*

*Results are shown as the mean ± SEM of three replicates. **C)** Cell vitality was assessed in MDM by MTT assay 24 h after FTC, M2FTC or NM2FTC treatments over a range of concentrations (10 – 400 µM). Results were normalized to untreated control cells. Both M2FTC and NM2FTC were found to be non-cytotoxic at 100 µM or less. Data are represented as mean ± SEM for n = 3 samples per group. **D)** Transmission electron microscopy (TEM) of NM2FTC showed presence of nanoparticles predominantly in the size range of 100-250 nm. **E)** EC_{50} was determined in CEM CD4+ T-cells by RT activity measurement in the supernatant after FTC or NM2FTC treatments over a range of concentrations (0.1–10,000 nM). Results were analyzed by nonlinear regression least squares fit. **F)** CEM-ss CD4+ T-cell vitality using LiveDead staining. All the treatments were non-toxic at 200 µM of drug or less. **G)** TEM morphological evaluation in MDM and CEM-ss CD4+ T-cells after NM2FTC (100 µM) treatment for 8 h, washing with PBS (2x) and re-suspension in TEM fixation buffer.*

Particle dissolution and release of M2FTC from NM2FTC across a dialysis membrane (MWCT 2000) were characterized by an initial burst prodrug release of 40% within 90 minutes. This was followed by sustained release for over 72 h (**Figure 3.4B**). Analysis of particle size distribution by size statistical histogram plot employing ImageJ software on TEM images showed 71, 18 and 9 % of the nanoparticle population in the range of 100-250 nm, 250-400 nm and 400-550 nm respectively (**Figure 3.4D**). These observations were further confirmed by quantitation of HIV-1$_{NL4-3\ GFP}$ expression on fixed cell samples by flow cytometry (**Figure 3.4E**).
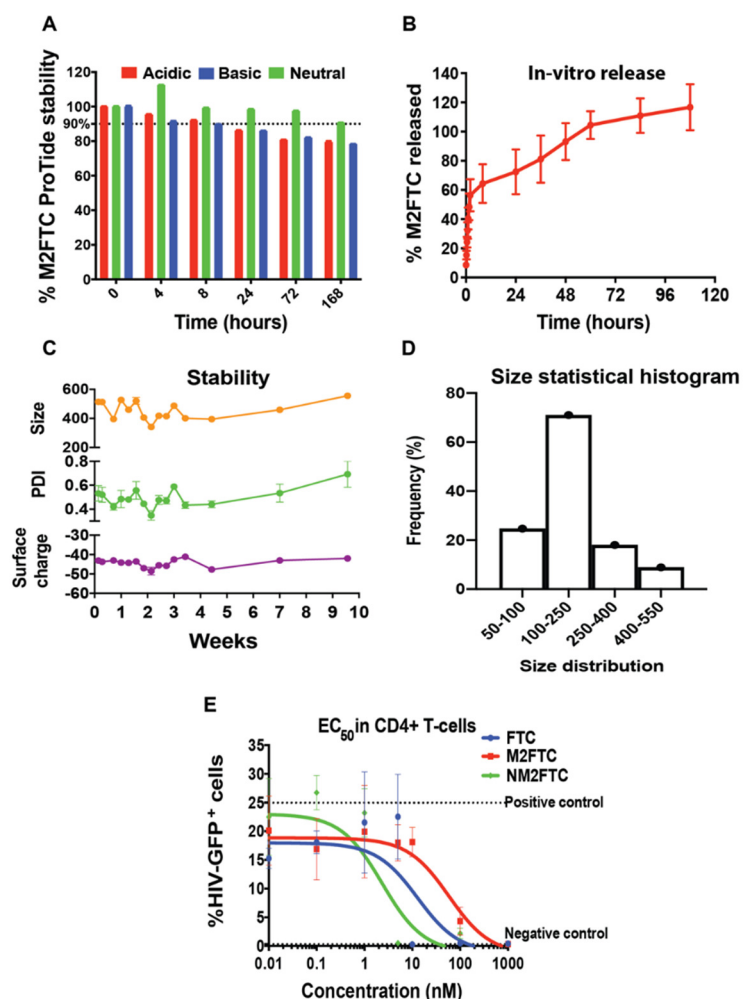
Figure 3.4 Physicochemical and efficacy evaluations of M2FTC and NM2FTC A). *Chemical stability of M2FTC in different pH conditions at room temperature. M2FTC was found to maintain its chemical stability up to 24 hours at room temperature with highest stability observed in neutral pH conditions up to 7 days. However, there was gradual hydrolysis in acidic and alkaline pH conditions beyond 24 hours at room temperature. Samples were analyzed using UPLC method. Data are expressed as mean ± SEM for n = 2 samples per group.* ***B)*** *In vitro release of M2FTC from NM2FTC using dialysis membrane (MWCT 2000) in 1 % Tween 80 PBS as dispersion medium at 37 °C and shaking at 150 rpm.* ***C)*** *Physico-chemical stability evaluation of NM2FTC at 37 °C in terms of particle size, zeta and polydispersity index distributions over a month period* ***D)*** *Size statistical histogram demonstrating particle size distribution of NM2FTC predominantly in 100-250 nm range using ImageJ processing of TEM images.* ***E)*** *EC_{50} was determined in CEM-ss CD4+ T-cells by flow cytometry. % HIV-1$_{NL4-3eGFP}$ was determined after FTC, M2FTC and NM2FTC treatments over a range of concentrations (0.01–1000 nM). Chemical modification of FTC followed its nanoformulation (NM2FTC) did not affect antiretroviral drug activity (12.91 nM, 58.45 nM and 2.34 nM for FTC, M2FTC and NM2FTC respectively). Results were analyzed by nonlinear regression least squares fit.*

3.6.5. Cell Based Evaluations of NM2FTC Particles

3.6.5.1. NM2FTC Uptake, Retention and FTC TP Formation

NM2FTC was rapidly taken up by MDM and intracellular concentrations increased over 8 h (**Figure 3.5A**). Intracellular drug concentrations were 34.6 *nmoles*/10^6 cells for NM2FTC and >100-fold higher than FTC (< 0.1 *nmoles*/10^6 cells) after equimolar drug concentration exposures. NM2FTC was also retained within MDM for up to 30 days (15.9 *nmoles*/10^6 cells) while native FTC was undetectable at 8 h (**Figure 3.5B**). In order to probe activation of M2FTC inside cells, we quantified intracellular FTC triphosphate (FTC-TP) levels in MDM treated with equivalent concentrations of FTC or M2FTC. For MDM uptake studies, NM2FTC and FTC treatments produced 28,2541 fmoles/10^6 cells and 21,7276 fmoles/10^6 cells of FTP respectively which were comparable over the 8 h test period (**Figure 3.5C**). NM2FTC also provided high sustained FTC-TP levels up to day 30 where TP concentration was 312 fmoles/10^6 cells compared to 19.1 fmoles/10^6 cells for FTC (**Figure 3.5D**). Sustained retention of the active TP metabolite from NM2FTC demonstrates slow prodrug release from the nanoparticle then intracellular activation/phosphorylation. Similarly, NM2FTC exhibited enhanced uptake in CEM CD4+ T cells with peak drug concentration of 10,300 *pmoles*/10^6 cells at 8 h (**Figure 3.5E**). Parallel quantitation of FTC-TP in CEM CD4+ T-cells after single exposure to NM2FTC demonstrated active metabolite levels of 508.6 ± 56.14 fmoles/10^6 cells at 8 h (**Figure 3.5F**). Overall, these data suggest that NM2FTC could be transformed into a long-acting slow-release formulation. Maintaining therapeutic drug levels at cellular sites of infection could potentially disrupt viral replication cycle and prevent further dissemination [238]. Studies performed in human MDM suggest that despite the ability of native ART formulations to achieve high drug concentrations in plasma, viral replication continues to occur due, in part, to restricted drug cell entry across lipid membranes [206, 207]. The inherent lipophilicity of NM2FTC and enhanced intracellular uptake of the prodrug could potentially overcome limitations of native FTC cell delivery.
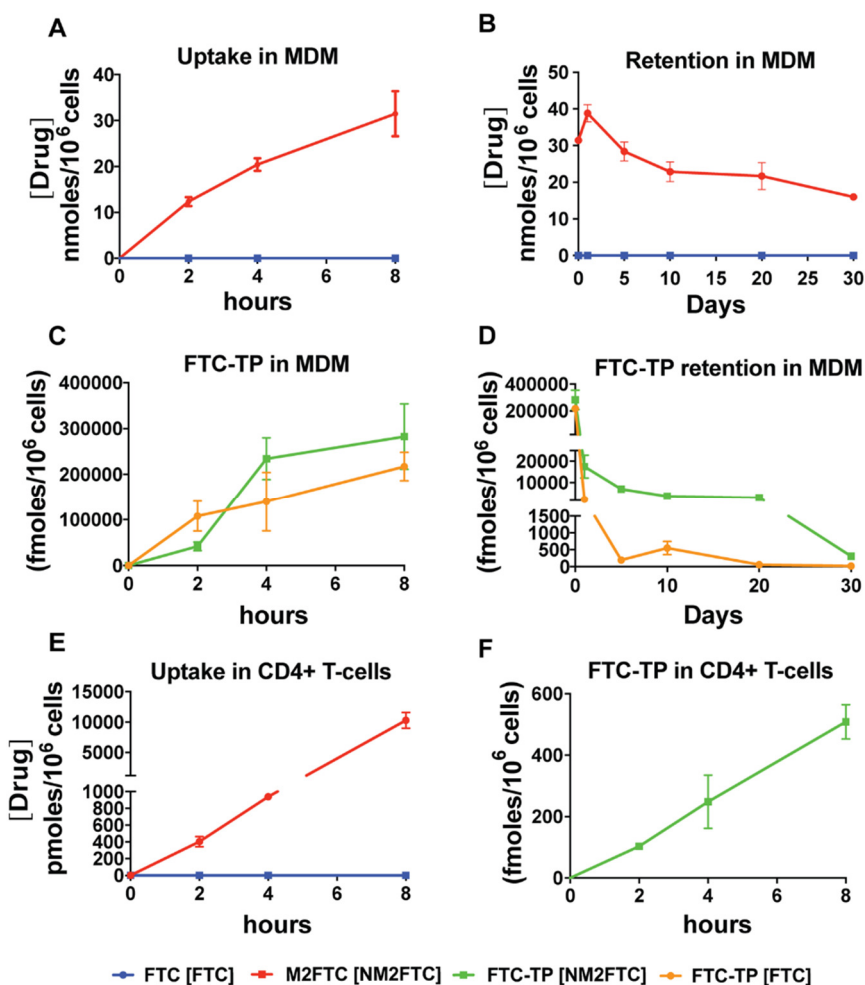
Figure 3.5. NM2FTC uptake, retention and triphosphate (TP) conversion. *A) For uptake, MDM were treated with equal drug concentrations (100 µM) and uptake was determined over 8 h. **B)** For retention study, MDM were loaded with FTC or NM2FTC for 8 h followed by PBS washing and maintaining half media changes every other day for 30 days. (**C**) Intracellular FTC TP levels during uptake studies was quantified at various time points over the 8h experiment time course. (**D**) Intracellular FTC TP levels were measured at different time points over 30-days. **E)** M2FTC, and **F)** FTC TP levels in parallel uptake studies in CEM-ss CD4+ T-cells were carried out as for MDMs.*

3.6.5.2. Anti-retroviral Efficacy

To assess antiretroviral activity of NM2FTC, MDM were challenged with HIV-1_{ADA} for up to 30 days after a single 8 h treatment with 100 μM of the prodrug formulation or native drug. As a result of enhanced MDM drug uptake and sustained retention,

NM2FTC exhibited superior antiretroviral activity compared to FTC as measured by HIV RT activity **(Fig. 3.6A)** and HIV-1 p24 antigen staining **(Fig. 3.6B)**. Notably, complete viral inhibition was maintained for up to 30 days with NM2FTC compared to minimal protection at day one (40%) and no viral inhibition at later time points for FTC treatment **(Fig. 3.6C)**. The ability of NM2FTC to protect MDM from HIV-1 infection for extended periods of time is a significant step towards transforming FTC into a potent long-acting cell and tissue targeted formulation that could be used in pre-exposure prophylaxis or in combination with other LA ART for HIV-1 treatment.
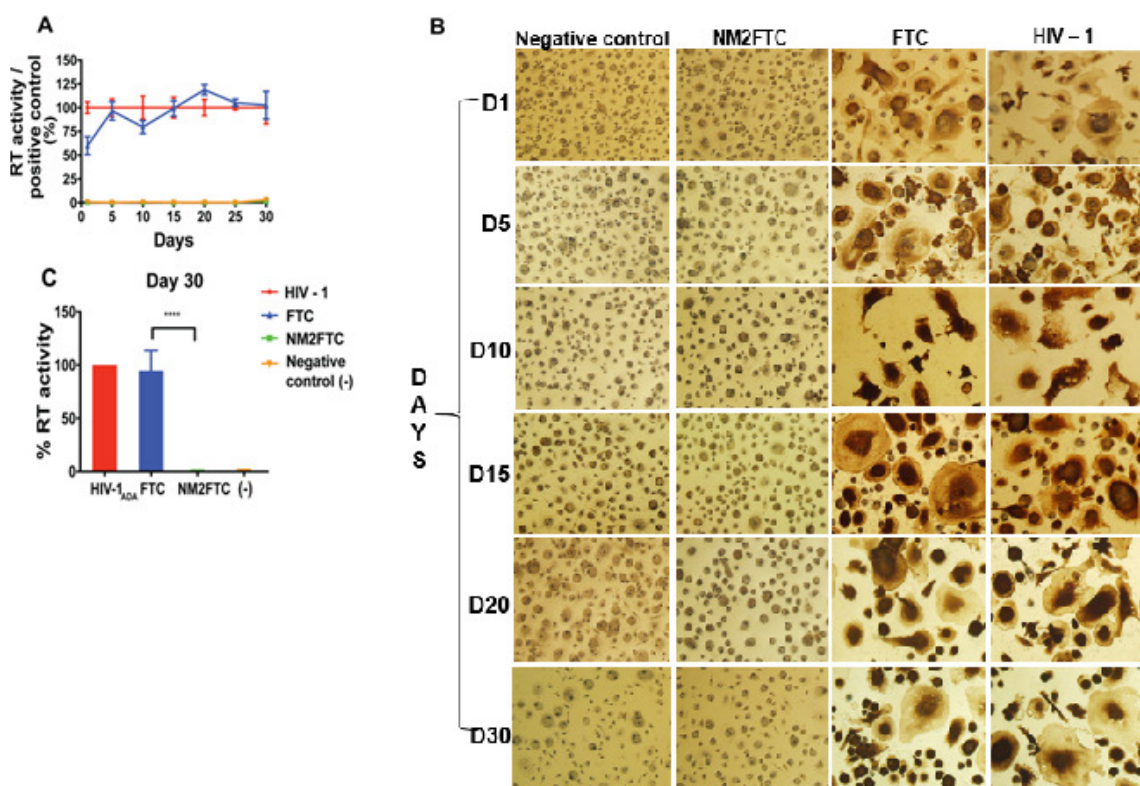
Figure 3.6 Cell-based antiretroviral activities. *Antiretroviral activity was determined in MDM treated for 8 h with 100 µM FTC or NM2FTC and then infected with HIV-1$_{ADA}$ at 1 to 30 days following drug loading. HIV-1 replication was determined 10 days after infection by **A)** Time course HIV-1 RT activity in culture supernatants. RT activity results were confirmed by **B)** HIV-1p24 antigen expression (brown stain) of adherent MDM. NM2FTC protected MDM from HIV-1 infection at all time points. Results were normalized to*

positive control cells. All results are shown as the mean ± SEM with n = 3 **C)** *Comparative HIV-1 RT activity at day 30 showing statistical significance in the % RT activity between FTC and NM2FTC treatments using unpaired two tailed t-test at ****P < 0.0001.*

3.6.6. PK and BD Studies

Male Sprague Dawley (SD) rats were administered a single 45 mg/kg FTC or FTC-equivalent (equimolar FTC) dose of NM2FTC IM into the caudal thigh muscle to determine PK and tissue drug distribution over 4 weeks. Administration of NM2FTC provided sustained drug levels in blood over four weeks (**Figure 3.7A**). The measured prodrug blood concentrations were 472.7 ± 35.4 ng/mL and 50 ± 6.4 ng/mL at days 1 and 28, respectively. In contrast, native FTC showed rapid drug decay with levels below 2 ng/mL by day 7. Notably, spleen (152 ng/g), liver (79 ng/g) and lymph nodes (152 ng/g) showed high M2FTC concentrations at day 28 (**Figures 3.7 B-D)** with detectable FTC-TP levels **(Figures 3.7 E, F)** all following a single NM2FTC injection**.** In contrast and like blood**,** native FTC treatment elicited low drug levels in tissues that rapidly fell below the limit of quantitation **(Figures 3.7 B-D).** The high drug levels in tissues after NM2FTC treatment suggest controlled prodrug release from the nanoparticle with enhanced accumulation of FTC-TP in tissue [156].
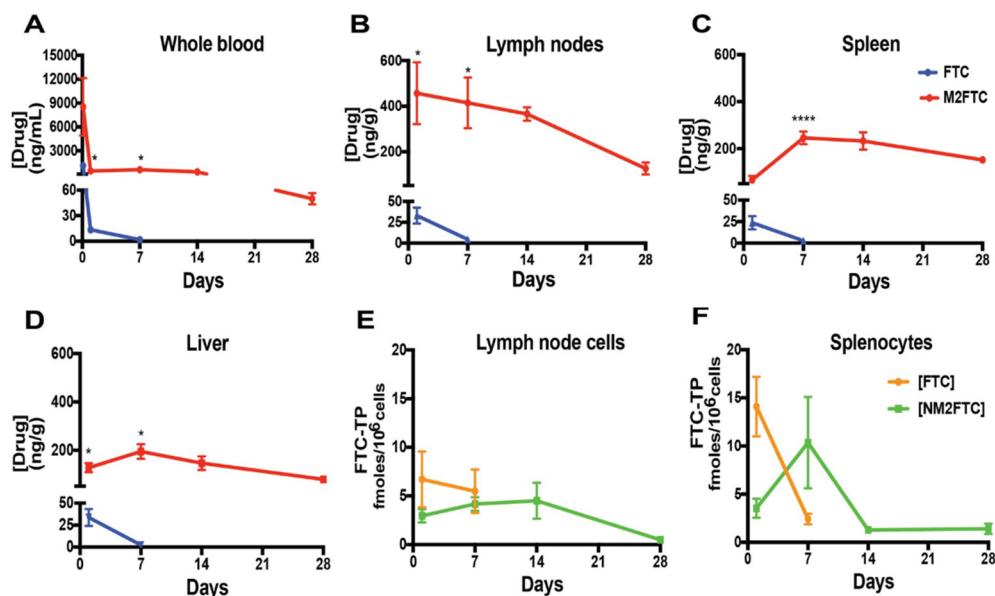
Figure 3.7 PK and biodistribution of FTC and NM2FTC in rats. *Blood and tissue M2FTC and FTC concentrations were determined over 28 days.* ***A)*** *FTC and M2FTC levels in whole blood after a single IM injection of FTC or NM2FTC in Sprague Dawley rats (45 mg/kg FTC equivalents). M2FTC and FTC concentrations were determined in* ***(B)*** *lymph nodes,* ***(C)*** *spleen, and* ***(D)*** *liver. Data are expressed as mean ± SEM for n = 5 rats per group. Formation of FTC-TP in* ***(E)*** *lymph node and* ***(F)*** *spleen cells were determined. Drug concentrations were quantified by UPLC-MS/MS.*

3.7. Discussion

FTC is an NRTI with potent activity against HIV-1 and HBV infections [239, 240]. Daily pre-exposure prophylaxis with a combination of FTC and tenofovir is effective at preventing HIV-1 transmission. Combinations of BIC, FTC and TAF are a mainline therapy for HIV-1 treatment [241]. Despite its effectiveness, limitations of FTC include regime adherence and restricted viral reservoir penetrance. These offer the needs for improved formulation strategies. Thus, LA ARV formulations were developed to extend dosing intervals, reduce systemic toxicity, and improve PK profiles [206, 207, 222, 223, 242, 243]. The formulations made were maximized for drug loading and excipient usage. Drug formulation scalability and stability after long-term storage were achieved.

As FTC is highly water-soluble, drug transformation into sustained release solid drug nanocrystals is required. Thus, we designed and applied an optimized ProTide strategy to generate hydrophobic and lipophilic ProTides drug nanocrystals. These extended the drug's apparent half-life through slow nanoparticle dissolution [244] and controlled ProTide hydrolysis and activation [223, 245]. The created FTC prodrug bypassed the initial rate-limiting phosphate kinase activation step and improved its potency. Development of LA nanoformulations with slower hydrolysis rates can sustain therapeutic drug concentrations in plasma and tissue [144] while improving cell penetrance and drug tissue biodistribution [246]. Despite such benefits, only two LA ARVs, RPV and CAB LA, have progressed to phase III clinical trials [198, 247-250]. It is noteworthy that inherent hydrophobicity is critical in creating nanoparticles. However, most ARVs cannot be easily converted into stable aqueous nanosuspensions [251]. These challenges could be overcome by encapsulation of lipophilic ARV prodrugs into poloxamer coated nanocrystals enabling slow release and hydrolysis rates [206, 207, 221-223].

We reasoned that optimal formulation design should maximize delivery of ART to macrophages and CD4+ T cells, the principal targets of HIV-1 infection, in spleen, gut and lymphoid organ reservoirs. This would improve delivery over native ART nanosuspensions [252] and improve the abilities of highly mobile macrophages with large storage capacities to transfer drug to CD4+ T cells and ultimately to virus tissue compartments [207]. Drugs stored in macrophages as nanocrystals can also protect drugs from systemic metabolism, prolonging drug half-lives to enhance efficacy. Such events would lead to improved PK and drug biodistributions [206, 207]. We have also shown that once inside macrophages, drug particles are stored in late- and recycling-endosomes, as well as autophagosomes [253, 254]. Thus, cell drug delivery serves multiple purposes especially in conjunction with prodrug activation. Activation of ProTides

involves protease and peptidase mediated processes to release nucleoside monophosphates, which undergo further phosphorylation into active triphosphate forms [255, 256]. Following intracellular uptake, M2FTC nanocrystal undergo slower dissolution mediated by esterase induced hydrolysis [257-260]. Intracellular M2FTC activation would include cleaving off docosanol from docosyl phenylalanine ester carried out by cathepsin A or carboxyesterases induced ester hydrolysis. This is then followed by intracellular cyclization to form a cyclic intermediate which would then undergo further hydrolysis by phosphoramidase leading to release of FTC monophosphates [241, 261-264]. In All, the creation of NM2FTC significantly improved ProTide stability, enhanced intracellular and sustained delivery of the active triphosphate metabolite compared to native FTC. Consequently, the antiviral activity of the drug was extended from hours to weeks for NM2FTC after single drug treatment of MDM. These results demonstrate that NM2FTC could potentially provide maximal intracellular viral restriction.

Development of optimal therapeutic regimen for effective treatment and prevention of HIV-1 requires sustained delivery of therapeutic drug concentrations in plasma and target tissues [265, 266]. We therefore investigated the abilities of NM2FTC to improve drug PK and biodistribution. A single intramuscular injection of NM2FTC in rats provided sustained and high prodrug concentrations in blood and tissues for one month. In contrast, drug concentrations from FTC treatment declined to undetectable levels within a day. Thus, high intracellular and tissue drug levels for NM2FTC could potentially translate to improved drug efficacy and reduced dosage. Additionally, NM2FTC treated animals showed sustained but low levels of FTC-TP in lymph nodes and spleen at one month compared to undetectable levels for FTC treatment. The observed low FTC triphosphate levels were not surprising since ProTides have been shown to undergo rapid degradation [267] and that cleavage of the phosphoramide bond could be limited in rodents [268]. Therefore, future PK evaluations should be conducted

in non-rodent species. Our data sets are particularly encouraging since evaluation of the prodrug in human macrophages and CD4+ T cells strongly suggest that M2FTC is efficiently metabolized into the active triphosphate form. The developed M2FTC formulation could potentially enhance uptake and sustain therapeutic concentration of FTC TP at restricted reservoirs of infection.

Chapter 4

Development of Second Generation

LASER FTC ProTides

4.1 Abstract

ART has revolutionized treatment and prevention of HIV-1 infection. We have also demonstrated that application of a modified PROdrug and nucleoTide technology (ProTide) could potentially transform FTC into LA formulations. First generation FTC ProTide, M2FTC demonstrated detectable levels of FTP in rat's lymph node and spleen cells over 28 days post injection. However, we observed lower levels of FTP in cells of lymphatic tissue likely due to slower hydrolysis of M2FTC's P-N bond caused by HINT1 phosphoramidase in rodents [268] or the steric hindrance from the bulky phenyl alanine benzyl group. To further enhance intracellular and tissue FTP levels, second- generation lipophilic FTC ProTides (M3FTC, M4FTC) were developed and then stabilized into poloxamer 407 coated LASER ART aqueous nanosuspensions (NM3FTC and NM4FTC). Both M3FTC and M4FTC were characterized by mass spectrometry, nuclear magnetic resonance and Fourier transform infrared spectroscopy. NM3FTC and NM4FTC were prepared by high-pressure homogenization and characterized for drug loading, particle size, cell viability, drug uptake, and EC_{50} studies in MDM and CD4+ T cells. Both NM3FTC and NM4FTC demonstrated particle sizes of 150-300 nm, polydispersity indices of 0.2-0.3, negative zeta potentials and drug encapsulation efficiency of 80-93%. Additionally, NM3FTC and NM4FTC nanoformulations showed enhanced stability at 25°C for at least 2 months, were found to be non-cytotoxic in MDM at 100 µM concentration, and exhibited intracellular prodrug levels of 15-20 µg/10^6 cells compared to undetectable levels for FTC treatment over an 8 hour time course in MDM. Enhanced potency (EC_{50}) of NM3FTC (2.63 nM) and NM4FC (1.33 nM) in MDM compared to FTC (19.56 nM) was observed. Thus, NM4FTC LASER ART with improved antiretroviral efficacy could be a promising candidate for further pre-clinical development.

4.2 Introduction

Creation of a LA potent and highly lipophilic/hydrophobic nucleoside reverse transcriptase inhibitor (NRTI) for the treatment and prevention of HIV-1 infection is a need of present day therapeutic [269, 270]. Lipophilic compounds are reported to demonstrate enhanced biodistribution and targeting to the lymphatic system [271]. Additionally, sustained delivery of active drugs from LA formulations at virus target sites could further prevent ongoing viral replication at reservoir sites, thereby limiting transmission of infection to healthy individuals [272]. Extended release of potent nucleoside analogs and their active metabolites at cellular sites of infection could also improve patient tolerability towards treatment regimen through dose reduction [273, 274]. Reduction of effective dose due to enhanced potency and pharmacokinetics could result in lower toxicity profiles thereby improving the risk to benefit ratio (therapeutic index) of these treatments [275].

In this phase, we employed phosphoramidate chemistry with alanine modification aimed at developing LA second generation emtricitabine ProTides with improved hydrolysis profiles. We derived inspiration from US FDA approved ProTides that utilize L – alanine as the amino acid. Such marketed products include tenofovir alafenamide fumarate (Descovy) and sofosbuvir (Sovaldi) for HIV and HCV infections, respectively [276].

Thus, in our present work of developing newer generation of FTC ProTides, we theorized that the combination of ProTide stability in plasma and less bulky L – alanyl amino acid masking group would enhance activation of FTC ProTides to produce high concentrations of FTP in various cell and tissue compartments.

With these goals, we designed second generation lipophilic LA FTC ProTides with the aim of enhancing bioactivation (eventual FTP formation) in target cells (MDM and CD4+ T-cells). The developed FTC ProTides were nanoformulated into surfactant stabilized aqueous nanosuspensions. Both M3FTC and M4FTC have docosyl alanyl

phosphoramidate modification that is expected to provide improved plasma stability, prodrug activation, tissue targeting and enhanced anti-HIV-1 efficacy profiles.

4.3 Materials and Methods

All chemical synthesis reactions were performed under a dry argon atmosphere unless otherwise noted. All the reagents used for synthesis and characterization of M3FTC and M4FTC were similar to those used for M2FTC synthesis and characterization and request to refer to Chapter 3 for materials with exception of Z-*L*-alanine which was purchased from Millipore sigma (St. Louis, MO, USA).

4.3.1 Synthesis of Second - Generation LASER FTC ProTides

Similar to the synthesis process employed in chapter 3 for phenylalanine docosyl phosphochloridate [223], an alanyl octadecanoyl (C_{18}) and alanyl docosyl phosphochloridates (C_{22}) were synthesized and then conjugated to FTC using reaction schemes described previously (**Figure 3.1**) with minor modifications. The concentration of reactants and reagents used in the synthesis of M3FTC and M4FTC ProTides are represented in **Table 4.1**. Post reaction completion, mother liquor was purified using silica column flash chromatography eluting with 95% then 90% DCM in methanol to give M3FTC (C_{18}) and M4FTC (C_{22}) alanine ProTides as colorless powder (60-65 % yield) post lyophilization process as described previously in chapter 3.

Reagents	M3FTC (alanyl C_{18} ProTide	M4FTC (alanyl C_{22} ProTide
Alanylphosphochloridate	1.36 g, 1 eq.	2.55 g, 1 eq.
Tert-Butylmagnesium chloride (1 M in THF)	5.34 mL, 2 eq.	8.65 mL, 2 eq.

FTC (dried from 10 mL pyridine)	1.08 g, 1 eq.	1.07g, 1 eq.

Table 4.1. Reagents used for the synthesis of M3FTC and M4FTC

4.3.2 M4FTC Characterization

4.3.2.1 NMR and Mass Spectrometric Evaluations

The chemical structures of M3FTC and M4FTC were confirmed by proton, carbon and phosphorus nuclear magnetic resonance (^{1}H, ^{13}C and ^{31}P NMR) spectra recorded on a Varian Unity/Inova-500 NB (500 MHz; Varian Medical Systems Inc., Palo Alto, CA, USA). Additionally, the newly synthesized ProTides were subjected to mass spectrometric infusion into Waters TQD mass spectrometer for the determination of molecular ion peak at mass to charge ratio (m/z) of their respective molecular weights.

4.3.2.2 Aqueous Solubility

Solubility of M3FTC and M4FTC in HPLC grade water was determined by adding excess amount of each ProTide to aqueous media leading to the formation of saturated solution followed by mixing at 37^{0}C for 24 h under shaker incubator (innova® 42 shaker incubator). After 24 hours, the samples were centrifuged at 14,000 x g for 10 minutes to separate insoluble drug. Supernatant was then carefully removed and lyophilized. Each sample was then re-dispersed in methanol before quantitation by validated UPLC TUV method for M3FTC and M4FTC analyses.

4.3.2.3 FTIR and UPLC Method Development

The synthesized M3FTC and M4FTC ProTides were further characterized for the presence of desired functional moieties using FT-IR spectroscopy employing Spectrum Two FT-IR spectrometer (PerkinElmer, Waltham, MA, USA).

Analytical method developments for M3FTC and M4FTC quantifications were performed on Waters ACQUITY ultra performance liquid chromatography (UPLC) H-Class System with TUV detector and Empower 3 software (Milford, MA, USA) and Kinetex 5 μ C18 100 °A Phenomenex column (150, 4.5 mm) (Torrence, CA) used for separation. Mobile phase composition consisted of methanol (organic phase) and ammonium formate (10 mM, pH 3.2) (served as aqueous phase) in the ratio 95:5 for M3FTC and 98:2 for M4FTC quantitation. FTC was quantified using method as described previously in Chapter 3.

4.3.2.4 Chemical Stability Evaluation

Evaluations of chemical stability of M4FTC was carried out at different pH conditions. Briefly, M4FTC stock solution (2 mg/mL) was prepared in optima-grade methanol in a glass amber vial. For acidic and neutral hydrolysis, 100 μL of M4FTC stock solution was added to 1900 μL each of 0.1 M HCl or optima-grade water. The samples were then incubated at room temperature under shaking conditions (innova® 42 shaker incubator, 150 rpm). Samples were aliquoted at predetermined time points (0, 4, 8, 24 and 72 hours) and stored at -80 °C until analysis. At the time of analysis, samples were lyophilized, and then redispersed in methanol, centrifuged at 14, 000 g for 10 mins and supernatant was collected and analyzed by validated UPLC method for quantitation.

4.3.2.5 Nanoformulation Physicochemical Characterization

The nanoformulations of M3FTC and M4FTC i.e. NM3FTC and NM4FTC were prepared by high-pressure homogenization on an Avestin EmulsiFlex-C3 (Ottawa, ON, Canada) homogenizer using poloxamer P407 surfactants as described in Chapter 3. However, drug to poloxamer ratio for NM3FTC batch was maintained at 2:1 w/w. For NM4FTC batch, drug to poloxamer ratio was maintained at 1:1 w/w. Particle size (D_{eff}), polydispersity index (PDI), and zeta potential were determined by dynamic light scattering

(DLS) on a Malvern Nano-ZS (Worcestershire, UK). The physico-chemical stability of NM3FTC and NM4FTC nanoparticles was monitored at 25 ^{0}C over 2 months duration. Encapsulation efficiency was calculated as described in Chapter 3. For in-vivo studies, NM4FTC formulation was centrifuged at 4˚C for 10 minutes at 200 x g, supernatant was removed and further centrifuged at 15000 x g for 20 minutes at 4˚C. Pellet thus obtained was dispersed in minimum volume of poloxamer to achieve the required dose of 75 mg/kg. DLS parameters i.e. size, PDI, zeta potential and concentration of the formulation were then measured.

4.3.2.6 MDM Uptake, Retention, and Triphosphate Measurement

The developed second generations of FTC ProTides i.e. NM3FTC and NM4FTC were characterized for in-vitro evaluations in MDM comparing NM2FTC as previously described [277, 278]. MDM uptake studies were performed over 2- 8 hours after treatment as described in Chapter 3. Briefly, MDM were treated with 100 µM each of NM2FTC, NM3FTC and NM4FTC and MDM uptake studies were performed 2-8 hours after treatment [207]. Moving forward, NM4FTC retention studies were carried out in MDM for the duration of one month. MDM were treated with NM4FTC at a concentration of 100 µM for 8 hours followed by washing with PBS to remove treatments and replacing with fresh media B and maintaining half-media changes every other day until collection days 1, 5, 10, 20 and 30. Both on each of the time points during uptake studies and retention collection, cells were washed twice with PBS and then scrapped in PBS, counted, and centrifuged at 3,000 rpm for 8 min under 4℃. During intracellular drug quantitation, cell pellets were sonicated in 200 µL methanol to extract drug and centrifuged at 14,000 rpm for 10 min at 4℃ to pellet cell debris. Resultant supernatant was then quantitated for M2FTC, M3FTC and M4FTC levels using validated UPLC-UV/Vis methods.

4.3.2.7 Potency (EC$_{50}$) Studies

Initially, MDM were plated at a density of 80,000 cells/well in 96 welled plates. MDM were then treated with various concentrations of M2FTC, M3FTC and M4FTC and their nanoformulations i.e. NM2FTC, NM3FTC and NM4FTC respectively in the range of concentrations 0.001 – 10, 000 nM for 60 min prior to infection with HIV-1$_{ADA}$ media at a MoI of 0.1 for 4 hours. Infectious media was then removed, and cells were incubated an additional 10 days with intermittent half media changes with the same amount of drug performed every other day. After 10 days, culture media was collected to measure HIV-1 reverse transcriptase activity as previously described [148, 230, 231]. The EC$_{50}$ was calculated using sigmoidal 4-point logarithmic regression using GraphPad Prism v7.

4.3.2.8 Cytotoxicity Evaluations in CEM-ss CD4+ T-cells

For cytotoxicity evaluations of FTC, NM3FTC and NM4FTC treatments in MDM at various concentrations (1 – 800 µM), MTT assay was performed. Briefly, MDM were cultured in 96 welled plates at a density of 80,000 cells/ well. MDM were then treated with the above treatments for 24 hours. Cells were then washed with PBS to remove treatments post 24 hours followed by addition of 200 µL of MTT solution to each well. Cells were incubated at 37 ^{0}C for 45 minutes. Plates were removed from incubator and MTT solution was then carefully removed from each of the well. Now, 200 µL of DMSO was added into each well, mixed to dissolve formed formazan crystals and then subjected to measuring absorbance at 490 nm on a U.V. vis plate reader. Percent viability of cells after various treatments was then calculated and normalized with absorbance received from untreated cells.

4.3.2.9 Potency (EC$_{50}$) Studies in Primary CD4+ T-cells

Initially, primary CD4+ T cell blasts were expanded from human PBMCs (huPBMC) via interleukin-2 (IL-2) + phytohemagglutinin (PHA) mediated immune stimulation. Briefly, stimulation culture medium was composed of 90% RPMI with L-glutamine + 9% FBS + 1% PenStrep + 4 µg/mL (PHA) + 20 U/mL interleukin-2 (IL-2). PBMC were seeded in a T150 culture flask at 1 x 10^6 cells /mL and cultured for 48 hours followed by examination for blast-formation. Stimulated PBMC were exposed to various concentrations of the drug (e.g. 10000, 1000, 100, 10, 1, 0.5, 0.25, 0.1, 0.01 nM) for 60 min. After 1 hour of treatment incubation, these cells were then challenged with HIV-1$_{NL4-3}$ at a MoI of 0.05 in 50 µL drug-containing stimulation- growth media (containing IL-2, PHA) via spin-inoculation (1035 RCF, 2 hours, 25^{0}C). Cells were then incubated for additional 6 hours at 37 ^{0}C. Stimulation-growth media (100 µL) was then added and cultures were further incubated for 16 hours 37 ^{0}C. Cells were then washed 3X with PBS and then incubated with the same concentrations of drug in simulation growth media used before infection. Full media change was done every other day with equivalent replacement of drug containing media. 7 days after infection, cell supernatant was collected for RT-assay. Cell fractions were collected for GFP readout by flow cytometry.

4.3.2.10 Efficacy Studies in CEM-ss CD4+ T-cells

Long term efficacy studies were carried out in CEM-ss CD4+ T-cells after FTC, NM2FTC, NM3FTC and NM4FTC treatments at 50 µM concentration. Post 24 hours of treatment incubation, CEM-ss CD4+ T-cells were infected with HIV-1$_{NL4-3}$ at a MOI of 0.05 using spin inoculation procedure described in **section 4.3.8**. After 24 hours post HIV-1$_{NL4-3}$ challenge, infected cell cultures were washed with PBS thrice and then replaced with drug containing media for additional 5 days (7 days post treatment) with full media changes with drug containing serum free RPMI media. On 7th day post treatment, cell

culture supernatant was collected and then assay for RT activity using RT assay protocol described in Chapter 3.

4.3.2.11 In-vivo FTP Measurement in Balb/c and NSG Mice

For in-vivo measurement of FTP formed after NM4FTC treatment when given in combination with NM2TFV, Balb/c (n=6) and NSG (n=6) mice were treated with NM4FTC and NM2TFV each at 75 mg/kg FTC/TFV equivalents via I.M. injection on right and left caudal thigh muscle respectively at day 0. Subsequently on day 10th post treatment, blood and plasma were isolated and mice were then sacrificed to collect organs and tissues. PBMCs and splenocyte cells were isolated and FTP levels in these cells were analyzed using FTP extraction protocol and MS-MS quantitation as described previously [279].

4.4 Study Approval

All animal studies were approved by the University of Nebraska Medical Center Institutional Animal Care and Use Committee in accordance with the standards incorporated in the Guide for the Care and Use of Laboratory Animals (National Research Council of the National Academies, 2011). Human monocytes were isolated by leukapheresis from HIV-1/2 and hepatitis seronegative donors according to an approved UNMC IRB exempt protocol.

4.5 Code of Ethics for Animals

Mice were maintained in a pathogen-free facility and treated humanely. All mouse studies were conducted in strict accordance with the Guide for the Care and Use of Laboratory Animals from University of Nebraska Medical Center (UNMC). All experimental protocols were approved by the Animal Care and Use Committee of UNMC.

4.6. Results

4.6.1 Synthesis and Characterization of Second - Generation FTC ProTides

Synthesis of second generation M3FTC and M4FTC ProTides was performed by analogy to M2FTC synthesis [223, 277]. Briefly, alanine octadecanoyl (C_{18}) and alanyl docosyl (C_{22}) ester promoieties were prepared and then reacted with phenyl phosphorodichloridate in the presence of triethylamine (**Figure 4.1)**. The formed alanyl octadecanoyl / alanyl docosyl ester phosphorochloridates were then coupled [232] with FTC to form M3FTC and M4FTC ProTides. The compounds were then purified by silica gel column chromatographic to yield M3FTC and M4FTC ProTides (**Figure 4.1)**. The synthesized M3FTC and M4FTC ProTides were then characterized by nuclear magnetic resonance (^{1}H, ^{13}C, ^{31}P), Fourier transform infrared spectroscopy and mass spectrometric infusion to determine compound purity. ^{1}H NMR spectrum of both M3FTC and M4FTC showed a triplet at 0.8 – 1.2 ppm, and a broad singlet between 1.4 – 1.6 ppm and a multiplet at 1.8 ppm representing terminal methyl, and symmetrical methylene protons of the fatty acid conjugations. Additionally, the multiplet signals at 7.09-7.7 ppm correspond to the aromatic protons representing aryl promoieties in both M3FTC (**Figure 4.2.A**) and M4FTC (**Figure 4.2.B**). ^{13}C NMR spectrum of NM4FTC showed peaks between 172.9 and 172.7 ppm corresponding to the carbonyl moieties, peaks between 157.2 – 119.6 ppm represent aromatic carbon atoms with C=C functionality, and peaks between 86.7 – 81.1 ppm represent carbons from fatty ester close to oxygen, peaks

between 66 – 64 ppm represent carbons close to nitrogen group, peaks in the range of 21.7 – 35.17 correspond to aliphatic carbons of fatty acid conjugation in the synthesized M4FTC (**Fig. 4.2.C**). ^{31}P NMR spectra of M4FTC (dissolved in DMSO) showed splitting peaks in the region of 3.34 and 3.72 ppm due to presence of enantiomeric forms of M4FTC resulting from chiral phosphorus center in the compound (**Fig. 4.2.D**). Additionally, mass spectrometric infusion of M3FTC and M4FTC ProTides in Waters Acquity TQD system showed molecular ion sodium adduct peaks at m/z of 757 (**Fig. 4.3.A)** and 805 (**Fig. 4.3.B)** respectively. The expected molecular weights of M3FTC and M4FTC were 734 and 782 Daltons respectively. We compared the functional groups present in M3FTC and M4FTC against parent FTC using FTIR spectroscopy. Prominent peaks corresponding to C-H and C=0 stretching vibrations in the regions of 2900 – 2800 cm^{-1} and 1800 - 1700 cm^{-1} respectively in M3FTC and M4FTC spectra confirmed the presence of aliphatic fatty alcohol group and ester moieties in the synthesized ProTides (**Fig. 4.3.D**). Aqueous solubility evaluations of M3FTC, M4FTC, M2FTC and parent FTC was carried out at 37 ^{0}C and shaking conditions. The aqueous solubilities of M3FTC and M4FTC were 31.87 ± 0.154 µg/mL and 3.13 ± 0.607 µg/mL respectively compared to M2FTC (30.185 ± 0.315 µg/mL) and FTC as reported previously (**Fig. 4.3.D**). Thus, reduction in aqueous solubility of the synthesized ProTides, especially M4FTC is indicative of inherent hydrophobic and lipophilic nature of the compound. Lipophilic and hydrophobic compounds have enhanced lymphatic targeting and biodistribution profiles [280-282] thus an ideal characteristic for enhancing pharmacokinetics and tissue targeting of these compounds to the sites of HIV-1 latency [283, 284]. We further carried out chemical stability evaluations of M4FTC under different pH conditions at 25 ^{0}C for up to 72 hours. M4FTC was found to be chemically stable for up to 24 hours at 25 ^{0}C when incubated in both acidic and neutral pH conditions. Under neutral pH conditions, M4FTC

stable for up to 72 hours. However, there was gradual hydrolysis in acidic conditions beyond 24 hours likely to due to acid mediated ester hydrolysis in M4FTC (**4.3.E**).
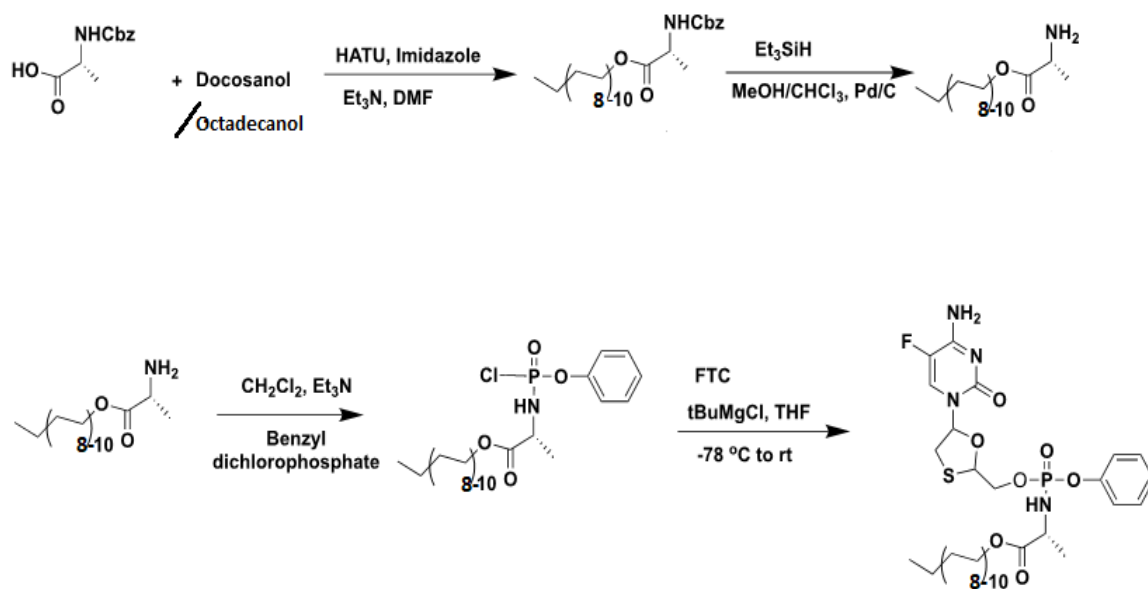
Figure 4.1. *Scheme of synthesis of fatty acid conjugated alanyl FTC ProTides - M3FTC and M4FTC.*
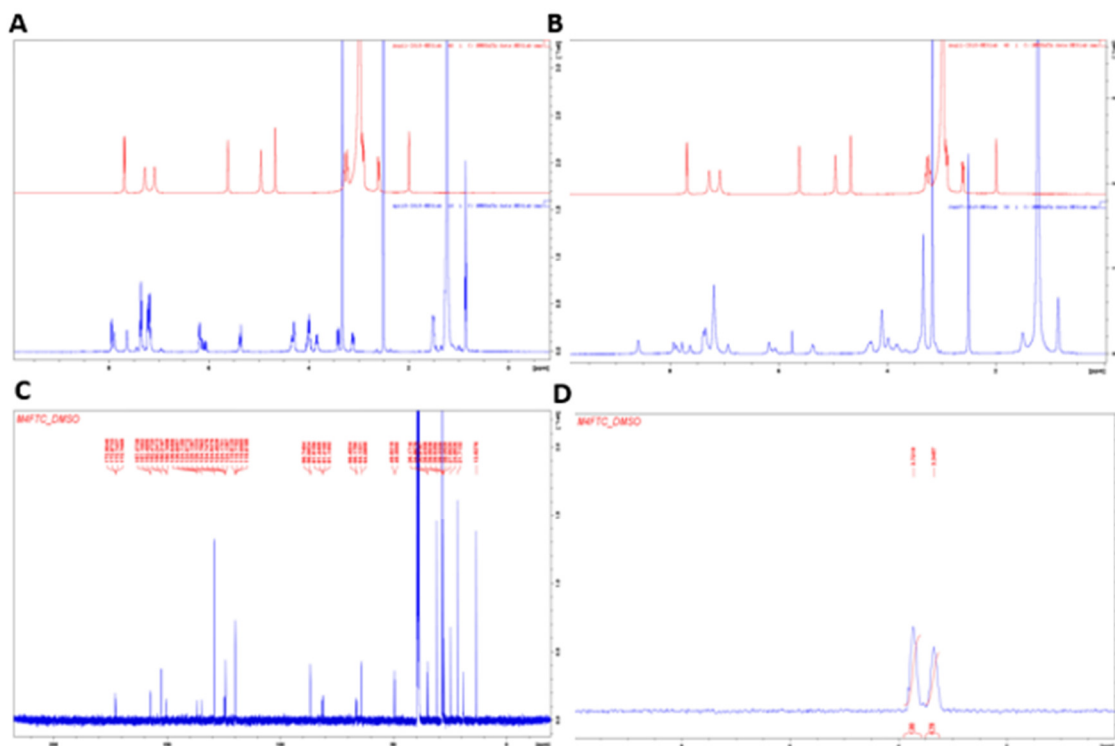
Fig. 4.2. NMR Characterizations of M4FTC *¹H NMR spectra of (A) M3FTC (blue) (B) M4FTC (blue) compared against parent FTC (red) confirming successful modifications in the synthesized M3FTC and M4FTC ProTides. (C) ¹³C NMR spectra of demonstrating the presence of functional carbons in the modified M4FTC ProTide. (D) ³¹P NMR spectra of M4FTC illustrating splitting patterns at chiral phosphorus atom confirming the presence of two isomers.*
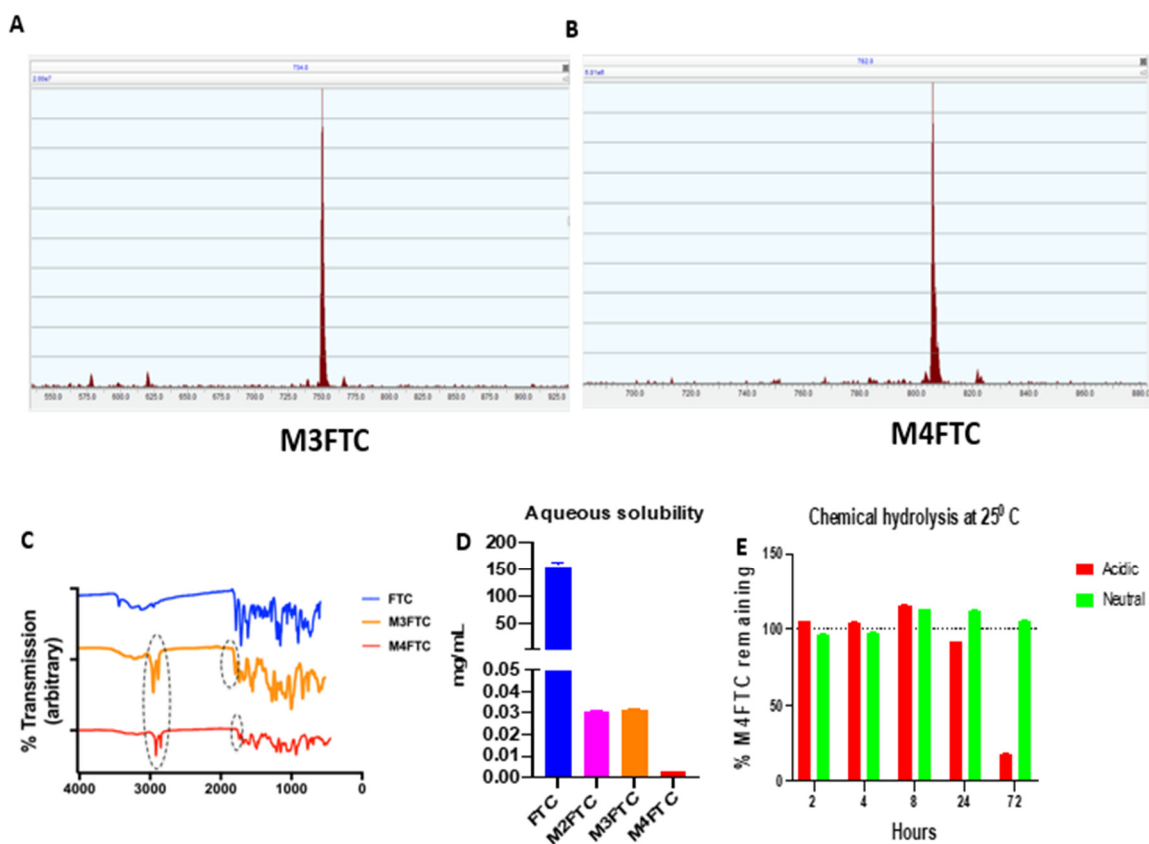
Figure. 4.3. Physicochemical characterizations of second generation of FTC ProTides. *MS infusion in Waters Acquity TQD showed (A) M3FTC molecular ion sodium adduct peak at m/z of 745 (B) M4FTC molecular ion sodium adduct peak at m/z of 805 (C) FT-IR spectra showed the presence of carbonyl (C=0), aliphatic and aromatic C-H stretching vibrations in synthesized M3FTC and M4FTC ProTides. (D) Aqueous solubilities of FTC, M2FTC, M3FTC and M4FTC comparing FTC at 37℃. (E) Chemical stability evaluations of M4FTC in acidic and neutral pH conditions at 25⁰C. Data are expressed as mean ± SEM for n = 2 samples evaluated.*

4.6.2 Physicochemical Characterization of Nanoformulations

High pressure homogenization technique [236] was employed for the preparations of NM3FTC and NM4FTC nanoformulations (**Figure 4.4.A**). Poloxamer P407 was used as surfactant in drug to poloxamer ratio of 2:1 and 1:1 w/w for NM3FTC and NM4FTC nanosuspensions, respectively. Both nanoformulations were analyzed for percent encapsulation efficiencies using validated UPLC U.V. methods. Physicochemical characterizations of NM3FTC and NM4FTC formulations i.e. particle size, polydispersity index (PDI), and zeta potential were determined by DLS and are summarized in **Table 4.2**.

Formulation	NM3FTC	NM4FTC
Stabilizer	Poloxamer P407	Poloxamer P407
Prodrug : P407	2:1	1:1
Dispersion medium	PBS	PBS
Size (nm)	117.1 ± 1.3 nm	150 ± 4.5 nm
Zeta potential (mV)	- 21.4 ± 0.15	- 14.7 ± 0.41
Percent encasement	80-93	85

Table 4.2. Preparation of NM3FTC and NM4FTC using high pressure homogenization. These formulations were then subjected to physicochemical characterization i.e. percent encapsulation, size, PDI and zeta potential measurements.

Additionally, we evaluated physicochemical stability of NM3FTC and NM4FTC for over 2 months at 25 ^{0}C. Both NM3FTC and NM4FTC maintained their physicochemical stability at 25 ^{0}C as evidenced by absence of major changes in their DLS measurements over the duration of 2 months. NM3FTC and NM4FTC had sizes in the range of 120 – 300 nm, PDI in 0.2 – 0.4 range, and zeta potentials between -20 to -30 mV as measured by Malvern zeta sizer. Particle sizes less than 300 nm, a narrow PDI

and negative zeta potential constitute suitable formulation's physicochemical parameters for parenteral delivery [285] (**Figure 4.4. B and Figure 4.4.C**).
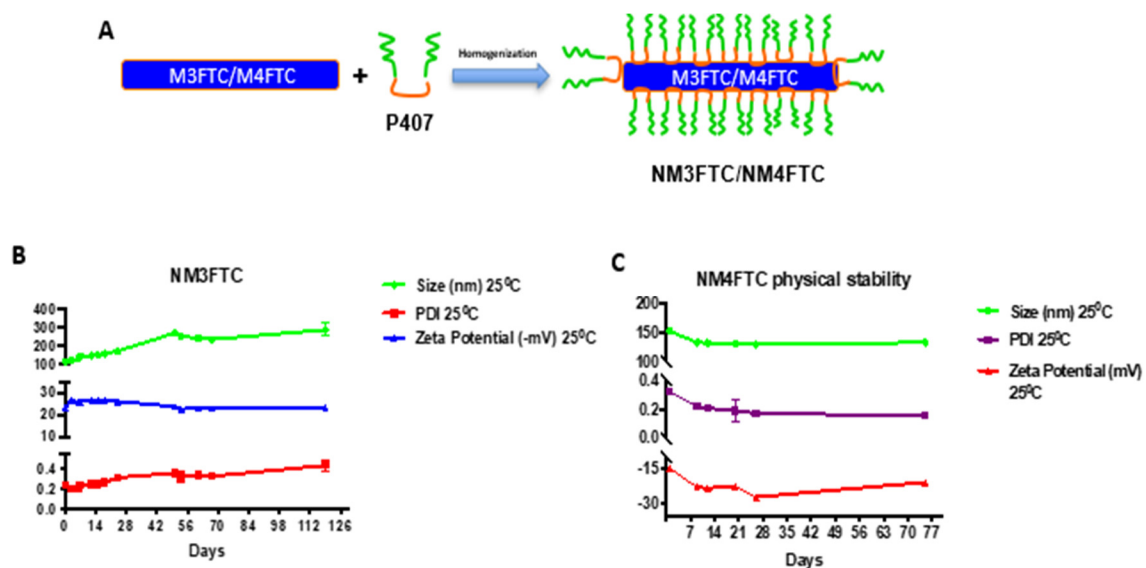
Figure 4.4 Formulation and physico-chemical stability evaluations (A) *Formulation of M3FTC and M4FTC nanosuspension stabilized by poloxamer P407 and high-pressure homogenization technique. Nanoformulations' physico-chemical stability evaluations at 25 ^0C for* *(B)* *NM3FTC and* *(C)* *NM4FTC over 2 months duration.*

We further characterized NM3FTC and NM4FTC formulations in-vitro for their uptake, retention, FTP formation and EC_{50} in MDM. During uptake studies, all the formulations demonstrated robust uptake in MDM over an 8-hour study period. NM3FTC and NM4FTC showed prodrug uptake of 18 – 20 µg/10^6 MDM over 8 hours (**Figure 4.5.A**). Additionally, we observed sustained retention of M4FTC ProTide after a single exposure of NM4FTC treatment at 100 µM dose in MDM for a period of up to a month. On day 30, 10 µg/10^6 MDM of M4FTC was recorded, demonstrating macrophage storage and sustained intracellular hydrolysis of M4FTC over extended periods (**Figure 4.5. B**). Parallel FTP measurement in MDM after FTC or NM4FTC treatments at 100 µM concentration showed 93917.93 fmoles/10^6 FTP formed after NM4FTC treatment

compared to 62683.36 fmoles/10^6 FTP formed after FTC treatment over 8 hours period (**Figure 4.5.C**). Thus, we observed the ability of M4FTC ProTide to form FTP in comparable levels to those formed after FTC treatments in MDM over 8 hours experimental period. Additionally, we carried out EC_{50} studies in MDM. EC_{50} values are represented in **Table 4.2.** EC_{50} studies in MDM demonstrated enhanced potency of 2nd generation FTC ProTides (M3FTC, M4FTC) and their nanoformulations i.e. NM3FTC and NM4FTC against HIV-1_{ADA} infection in MDM (**Figure 4.5. D**).

Sr. No.	Sample	EC_{50} value (nM) in MDM against HIV-1_{ADA}
1	FTC	19.56
2	M2FTC	24.63
3	M3FTC	4.389
4	M4FTC	16.43
5	NM2FTC	4.097
6	NM3FTC	2.626
7	NM4FTC	1.33

Table 4.3 EC_{50} values of various treatments in MDM against HIV-1_{ADA} infection
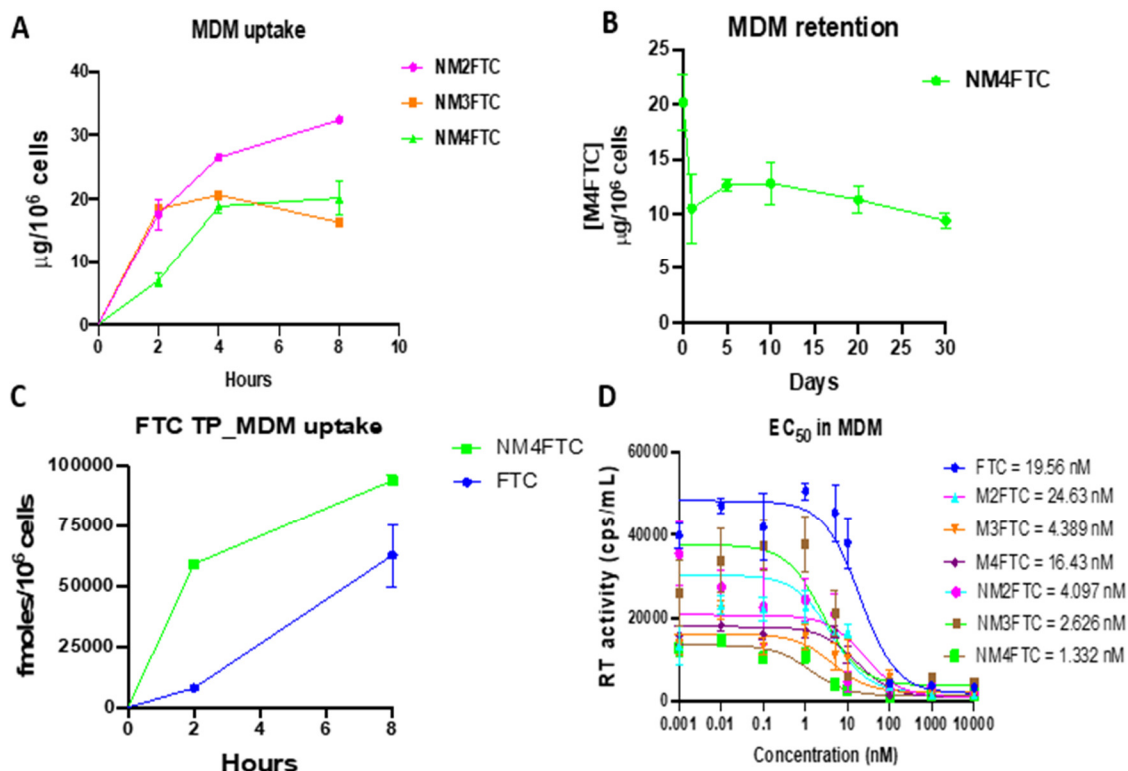
Figure 4.5 *Characterization of nanoformulations in MDM*. (*A*) *Uptake studies in MDM over 2-8 hours duration after NM2FTC, NM3FTC and NM4FTC treatments at 100 µM concentration.* **(B)** *Retention studies in MDM after single NM4FTC treatment at 100 µM dose carried out over 30 day experimental period.* **(C)** *FTP measurement during uptake studies in MDM over 8 hours period after FTC and NM4FTC treatments at 100 µM dose.* **(D)** *EC_{50} potency studies in MDM after FTC, M2FTC, M3FTC, M4FTC and their nanoformulations treatments at various concentrations (10000 – 0.001 nM) over 10 days experimental period.*

We then performed MTT vitality assay in CEM-ss CD4+ T-cells after FTC, NM3FTC, NM4FTC treatments at concentrations of 1 – 800 *µM.* After 24 hours of treatment incubation, drug treatments were removed and then incubated with MTT dye for 45 mins at 37 ^{0}C. All the treatments were found to be non – cytotoxic at 100 µM concentration when normalized with un – treated cell control (**Figure 4.6.A***).* Additionally, we performed long term efficacy studies in CEM-ss CD4+ T-cells after FTC, NM2FTC, NM3FTC and NM4FTC treatments with cells infected with HIV-1$_{NL4-3}$ acting as positive

control at MoI of 0.05 and negative control constituted of cells devoid of infection and treatment. On day 5 post treatment, we evaluated RT activity in the supernatants of both treated and un – treated positive infected cells.   We observed infection in positive control group and in FTC treated cells evidence by their increased RT activity. FTC ProTide nanoformulation treatments (i.e. NM2FTC, NM3FTC and NM4FTC) at 50 µM concentration showed minimal RT activity that was similar to negative control samples demonstrating sustained long-term inhibition of HIV-1_{NL4-3} infection (**Figure 4.6.B***)*. Selection of 50 µM for in vitro studies was based on MTT data sets. We then performed potency assay in terms of EC_{50} studies in PBMCs stimulated with IL-2 and PHA for 48 hours. After FTC and NM4FTC treatments in the range of concentrations (0.01 – 10000 nM) in stimulated PBMCs, we noted EC_{50} values of FTC and NM4FTC treatments as 6.45 and 35.82 nM respectively using RT assay as end read out in the supernatant of these cultures (**Figure 4.6.C***)*. However, we did not observe statistically significant differences between FTC and NM4FTC treatments across the potency curve using non-parametric analysis (Mann Whitney t-test). We further performed flow cytometric evaluations in these cultures and quantitated % of GFP positive CD4+ T-cells (as % of CD3+) after HIV-$1_{NL4-3\ GFP}$ infection plotted against log concentration of treatments given to these cells. We noted EC_{50} values for FTC and NM4FTC as 1.146 and 19.25 nM respectively using GFP intensity as end read out in flow cytometric analysis (***Figure 4.6.D)***. Thus, relatively higher EC_{50} values for NM4FTC compared to FTC could be attributed to slower hydrolysis and processing of M4FTC in stimulated PBMCs likely leading to sustained but delayed formation of FTC monophosphate. Stimulation of PBMCs with IL-2 and PHA could result in differences in their functional metabolism[286][287] and could delay the activation FTC monophosphate to FTC triphosphate (carried out by intracellular phosphokinases). Additionally, since PBMCs constitute (70 – 90 %) of lymphocytes[288], the enzymatic

repertoire required for M4FTC processing and activation may not be sufficient for immediate action[289][290].
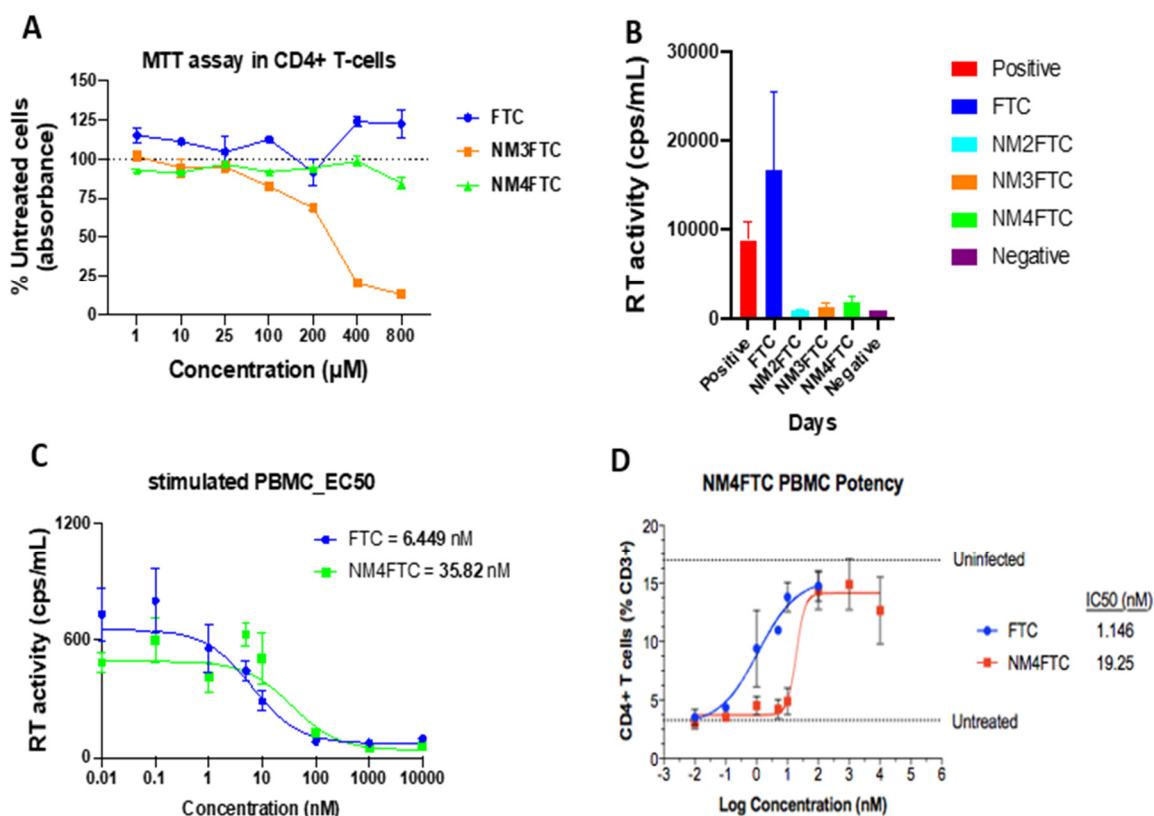
Figure 4.6. Characterizations in CEM-ss CD4+ T-cells and stimulated PBMCs. (A) *Cell vitality was assessed in CEM-ss CD4+ T-cells using MTT assay after FTC, NM3FTC and NM4FTC treatments (1 – 800 µM) for 24 hours* **(B)** *RT activity in the supernatants of CEM-ss CD4+ T-cells 5 days post treatment with FTC, NM2FTC, NM3FTC and NM4FTC at 50 µM dose during long term efficacy study. EC_{50} potency study in PBMCs stimulated by IL-2 and PHA after FTC and NM4FTC treatments in the range of concentrations (0.01-10000 nM). EC_{50} potency assay with* **(C)** *RT activity in the supernatants of the cell cultures used as the end read out.* **(D)** *using flow cytometric analysis carried out as CD4+ T-cells (% CD3+) vs log of concentration of NM4FTC treatment. Data are represented as mean ± SEM for n = 4 samples per group.*

4.6.3 FTP Measurement in Balb/c and NSG Mice

To measure FTP levels, Balb/c (n=6) and NSG (n=6) mice were administered NM4FTC and NM2TFV formulations via I.M. injection at 75 mg/kg FTC/TFV equivalents.

Since FTC and TFV combination are recommended for PrEP therapy, we sought to quantify FTP formed after administration of NM4FTC and NM2TFV (prodrug of tenofovir developed by our laboratory) via single I.M injections to NSG and Balb/c mice. On Day 10th post administration, PBMCs were isolated and mice were sacrificed. Mice's spleens were collected and splenocytes were isolated using cell isolation protocol described in chapter 3. FTP levels were then quantitated in these samples using validated MS method [277]. Quantitation of FTP levels in PBMCs and splenocytes isolated from Balb/c mice demonstrated levels of 1059.56 ± 296.3 and 109.45 ± 87.14 fmoles/10^6 cells respectively on day 10 after treatment. Similarly, FTP levels in NSG mice showed 33669.287 ± 29873 and 169.27 ± 103.08 fmoles/10^6 cells respectively on day 10 post administration. Thus, we recorded high levels of FTP in PBMCs and splenocytes isolated from NSG and Balb/c mice on day 10 after NM4FTC and NM2TFV administration. Detectable FTP levels (**Figure 4.7**) after NM4FTC and NM2TFV treatments at 75 mg/kg FTC/TFV equivalents in these mice demonstrated the likelihood of protection against HIV-1 infection when used as pre-exposure prophylactic preventive therapy.
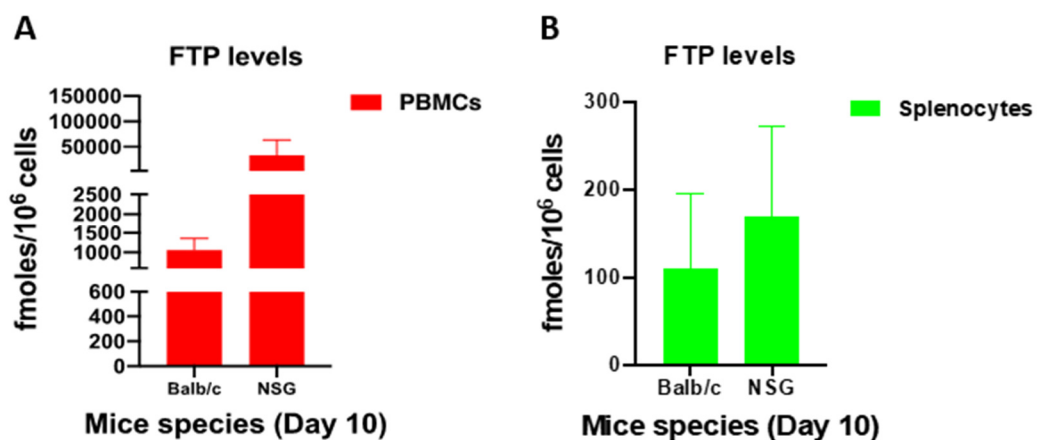
Figure 4.7 Evaluation of FTP levels in Balb/c and NSG mice after NM4FTC and NM1TFV treatments at 75 mg/kg FTC/TFV equivalents on day 10. **(A)** FTP levels in PBMCs isolated from balb/c and NSG mice **(B)** FTP levels in splenocytes isolated from balb/c and NSG mice.

4.7 Discussion

With the goal of developing next generation PrEP therapeutic [291], we continued our efforts in exploring highly potent LA FTC ProTides effective in various subsets of cells infected with HIV-1. Thus, we aimed to develop 2nd generation LA FTC ProTides (i.e. M3FTC and M4FTC) that would overcome challenges related to patient adherence, improve patient compliance, and eventually enhance the efficacy of PrEP treatment in all groups of susceptible individuals. Alanine modification in M3FTC and M4FTC ProTides is expected to enhance potency in different subsets of infected cells [261].

To achieve this goal, we employed phosphoramidate conjugation chemistry in the synthesis process. ProTides with phosphoramide (P-N) bonds have been shown to improve plasma hydrolytic stability to facilitate tissue targeting and biodistribution profiles of compounds [292, 293]. We further incorporated alanyl octadecanol (C_{18}) and docosanol (C_{22}) fatty alcohols in the structure of M3FTC and M4FTC ProTides respectively to enhance their lipophilicity/ hydrophobicity profiles which play vital role in lymphatic tissue targeting of compounds [233, 262] to affect efficacy at restricted sites of infection [294]. Alanine was incorporated in these modifications because it less hindered and also been shown to efficiently undergo intracellular processing of ProTides by carboxypeptidases (CES) and amidases (HINT1) [295, 296] in different cell types, specifically monocyte derived macrophages and CD4+ T-cells which constitute first line of defense against the virus and thus the primary site of infection [94, 297]. The synthesis of M3FTC and M4FTC ProTides were characterized by ^{1}H, ^{13}C, ^{31}P NMR and FTIR spectra. Mass spectrometric infusion of M3FTC and M4FTC in Waters Acuity TQD system showed the presence of the desired molecular ion peak thereby confirming the

successful synthesis of the target compounds. Solubility evaluations of M3FTC and M4FTC showed reduced aqueous solubilities due to their hydrophobic/lipophilic properties. Additionally, M4FTC was found to be chemically stable at 25 ^{0}C for upto 24 hours. In order to enhance dissolution properties of the synthesized hydrophobic/lipophilic ProTides and make them amenable to delivery, we nanoformulated M3FTC and M4FTC ProTides using Poloxamer (P407) stabilized aqueous solution by high pressure homogenization. The nanosuspensions had particle sizes < 300 nm, negative zeta potential and narrow PDI over 2 months duration which make them suitable candidates for LA parenteral delivery [298, 299]. Additionally, the uniformly dispersed lipophilic ProTide nanoformulations (NM2FTC, NM3FTC and NM4FTC) were readily internalized by monocyte derived macrophages with subsequent formation of FTP after drug treatment. LA NM4FTC particles were also found to be retained in MDM over a month. We observed improvement in potency for these ProTides and their nanoformulations in MDM when compared against FTC. Notably, NM4FTC demonstrated lowest EC_{50} value correlating to its enhanced potency in infected MDM. Thus, this second generation FTC ProTide nanoformulation could potentially lead to reduced dosage and efficacy.

The ProTide nanoformulations were also evaluated in stimulated PBMCs and CEM-ss CD4+ T-cells. Since, T-cells are important virus targets [300], we sought to evaluate efficacy of these nanoformulations in inhibiting HIV-1 infection in T-cells. Initial cytotoxicity evaluations using MTT assay in CEM-ss CD4+ T-cells after FTC, NM3FTC and NM4FTC treatments assay demonstrated no negative effects in cell viability at doses of up to 100 µM of drug. We then carried out long term efficacy studies in CEM-ss CD4+ T-cells after FTC, NM2FTC, NM3FTC or NM4FTC treatments at 50 µM concentration. After 24 hours of treatment and infection with HIV-1$_{NL4-3\ eGFP}$ as described in chapter 3, we evaluated RT activity in culture supernatants at 5 days post challenge. We observed

sustained inhibition of viral replication after single administration of either NM2FTC, NM3FTC or NM4FTC compared to FTC and positive control cells that were infected with no drug. Additionally, we carried out EC_{50} studies for FTC and NM4FTC in stimulated PBMCs and found no statistically significant differences between treatments demonstrating chemical modification of FTC into a ProTide followed by its nanoformulation does not alter anti-viral potency in stimulated PBMCs. We noted higher EC_{50} values for NM4FTC treatment compared to FTC in stimulated PBMC which may be due the effect of PBMC stimulation [301-303] and presence of divergent population of cell types such as PBLs, macrophages, dendritic cells (DC) in stimulated PBMCs [303].

We then evaluated the levels of FTP formed in PBMCs and spleen cells of balb/c and NSG mice 10 days after NM4FTC or NM2TFV treatment at 75 mg/kg FTC/TFV equivalents. We extracted FTP from PBMC and splenocytes samples using solid phase extraction as described in the previous chapter and quantitated using validated Waters Acquity TQS MS-MS system. We observed PBMC FTP levels of 1059.56 ± 296.3 to 33669.287 ± 29873 fmoles/10^6 cells and splenocytes FTP levels of 109.45 ± 87.14 to 169.27 ± 103.08 fmoles/10^6 in balb/c and NSG mice respectively. Human pharmacokinetic study of TFV and FTC combination treatment in healthy volunteers after daily dosing (HPTN 066) for establishing adherence bench-marks, FTP median (IQR) of 1500 - 2600 fmoles/10^6 PBMCs was observed in daily dosing cohort at 49 week post treatment [304]. Similar observation was noted in one such study in which study participants were taking four or more Truvada™ doses per week, FTC-TP >600 fmol/10^6 PBMC was reported while 11 out of 12 participants had FTC-TP concentrations (>2200 fmol/10^6 PBMC) which are consistent with daily dosing with Truvada [302]. Thus, we observed similar levels of FTP in PBMCs isolated from balb/c and NSG mice after single intramuscular injection of NM4FTC and NM2TFV administered separately in combination at 75 mg/kg dose on day 10 post administration. In conclusion, NM4FTC is a promising

nanoformulation candidate to be explored further for once a month or longer treatment

modality as PrEP preventive strategy in humanized mice model of HIV-1 infection.

Chapter 5

Preliminary Evaluation of

Optimum Viral Dose for Pre-Exposure

Prophylactic Study of Combination of

NM4FTC and NM2TFV Treatments in

Humanized Mouse Model of HIV-1

Infection.

5.1. Abstract

There is a need of developing newer PrEP therapies with the focus in enhancing patient adherence and compliance. With these goals, we aimed to evaluate our second-generation FTC ProTide, M4FTC nanoformulation (NM4FTC) in combination with NM2TFV at 75 mg/kg FTC/TFV equivalents in humanized mice model of HIV-1 infection. In our preliminary study of evaluating the optimum HIV-1 $TCID_{50}$ dose (10^2, 10^3, 10^4), we injected NM4FTC and NM2TFV I.M. in each of the caudal thigh muscle of humanized mice a week after these mice's immune subcellular distributions were evaluated by flow cytometry. After 2 weeks, these mice were randomly distributed into separate groups and challenged at various $TCID_{50}$ doses of 10^2, 10^3, 10^4 viral copies/mL. We then evaluated plasma viral loads in mice after 4 and 8 weeks post challenged with HIV-1 viral inoculum. After 4 and 8 weeks, we observed protection from HIV-1 infection as evidenced by 75 and 80 % of mice in 10^4 $TCID_{50}$ inoculum dose group showed viral levels below the level of detection, respectively.

5.2. Introduction

In this phase, we sought to identify an optimal viral dose required to prevent HIV-1 infection in humanized mouse during PrEP evaluation of combination treatments of NM4FTC and NM2TFV formulations administered I.M. at 75 mg/kg of FTC and TFV equivalents. The rationale for the drug panel was based on approved PrEP recommendations [305, 306].

Thus, in our current study we evaluated pre-exposure prophylactic efficacy of combination of NM4FTC and NM2TFV in preventing HIV-1 infection in humanized mouse model. NM2TFV was chosen because in rat PK studies, the alanine modification in M2TFV provided enhanced tenofovir diphosphate levels in lymphocytes and PBMCs. M4FTC ProTide nanoformulation was selected because in-vitro studies demonstrated

alanine modifications in M4FTC provided higher potency and long-term efficacy in CD4+ T-cells compared to other FTC ProTides developed.

5.3 Methods

5.3.1 Preparation of Formulations

NM4FTC was prepared by high-pressure homogenization (14% (w/v) of M4FTC and 14% (w/v) P407) in PBS. Final drug concentration in the nanoformulations was determined by validated UPLC-UV/Vis method. NM2TFV was prepared (3.33% (w/v) M2TFV and 1.67% (w/v) P407) by high-pressure Avestin C3 homogenizer in 10 mM HEPES pH 7. Final drug concentration was determined using UPLC-UV/Vis. The nanosuspensions were then characterized for size, charge, and PDI following production as well as just before and after injection. A volume of ≤ 50 µL per 25 g mouse for each nanoformulation was administered by I.M. injection in each of thigh muscle separately. After homogenization, the formulation was concentrated by differential centrifugation and used without further processing. The final drug content was determined using UPLC-UV/Vis analytical method. Pre- and post-dose injection samples were collected for size, charge, and PDI as determined by DLS. Pre- and post-dose injection samples were collected for drug concentration analysis by UPLC-UV/Vis.

5.3.2 Animal Grouping

For the present study, NOD.Cg-Prkdc^{scid} Il2rgt^{m1Wjl}/SzJ (NSG) mice reconstituted with human hematopoietic stem cells (HSC) which are reported to generate human T cells susceptible to HIV-1 infection were used [206, 307, 308]. Since we are aiming at evaluating long term efficacy of our developed nanoformulations in combination, NOD.Cg-Prkdcscid Il2rgtm1Wjl/SzJ (NSG) mouse model was expected to assist in developing long term infection both in blood and tissue compartments [294].

Group	Treatment	# of mice

1	Infected control at 10^2 TCID$_{50}$	5
2	Infected control at 10^3 TCID$_{50}$	5
3	Infected control at 10^4 TCID$_{50}$	5
4	NM4FTC+ NM2TFV (10^2 TCID$_{50}$ infection)	5
5	NM4FTC+ NM2TFV (10^3 TCID$_{50}$ infection)	5
6	NM4FTC+ NM2TFV (10^4 TCID$_{50}$ infection)	5

Table 5.1 *Groups of positive and treatment control humanized mice infected with different HIV-1 TCID$_{50}$ inoculum (10^2, 10^3, 10^4) doses.*

5.3.3 Dose Treatments and Viral Challenge

Mice were injected NM4FTC intramuscularly in one thigh, and NM2TFV in the other at a dosage of 75 mg FTC/TFV-eq./kg at Day 0. One week before and every two weeks after drug treatment, human CD45+, CD3+, CD4+, CD8+, and CD14+ populations were assessed by flow cytometry. 14 days after drug treatment, mice were challenged with HIV-1$_{ADA}$ (100-200 µL, each of the doses of 10^2, 10^3 and 10^4 tissue culture infection dose 50 (TCID$_{50}$)/mL by IP injection. Mice were bled every after 2 weeks for flow cytometric evaluations and plasma samples were collected 4 weeks and 8 weeks post viral challenge for viral load and drug level quantitation and flow cytometric evaluations and further monitored for viral loads in both untreated (HIV-1 positive) and treatment infected mice groups. Humanized mice (both positive infected and treated) in 10^4 TCID$_{50}$ group were then sacrificed on week 9th post challenge. Humanized mice in 10^2 and 10^3 TCID$_{50}$ group (both positive infected and treated mice) were monitored every alternate week for viral load quantitation and were sacrificed on week 14th post challenge. Whole blood was collected for cell phenotyping analysis by flow cytometry and drug level quantitation. On sacrifice day, whole blood, spleen, lung, liver, kidney, lymph nodes, brain, and gut were collected for drug level analysis (without perfusion). Spleen, lung,

liver, kidney, brain, gut, and bone marrow were collected for viral RNA/DNA detection by qRT-PCR. Spleen, lung, liver, kidney, brain, and gut were collected for RNAscope analysis.

5.3.4 Experimental Study Design
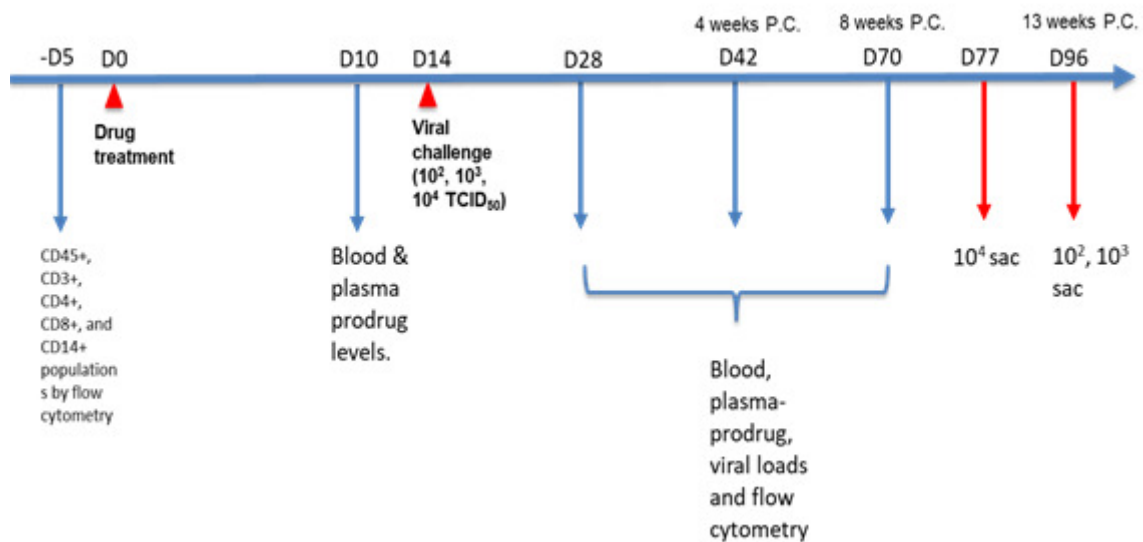
Fig 5.1 *Scheme and timeline of PrEP study in humanized mice.* *Initially, a week before the treatment, humanized mice were evaluated for blood sub-cellular populations by flow cytometry. These mice were then treated with NM4FTC and NM2TFV on each of the different thigh muscles at 75 mg/kg FTC/TFV equivalents I.M. on day 0. 2 weeks after treatment, humanized mice both infected and treated (n=5) per group were infected with HIV-1$_{ADA}$ at 10^2, 10^3 and 10^4 TCID$_{50}$ inoculum and mice were monitored for 14 weeks after infection. On weeks 4th and 8th, both infected and treated mice were evaluated for plasma viral loads, flow cytometric analysis and blood drug quantitation. On week 9th after viral challenge, mice infected with 10^4 TCID$_{50}$ dose were sacrificed and blood, and tissues were collected. However, mice in 10^2 and 10^3 TCID$_{50}$ group were further monitored for plasma viral load and blood drug quantitation. On week 13th post HIV-1 challenge, both infected and treated mice in 10^2 and 10^3 TCID$_{50}$ group were sacrificed and plasma, blood and tissues were collected for viral load and drug quantitation, respectively.*

5.3.5 Flow Cytometry Analysis

Blood was collected at mentioned time points post-treatment by facial vein bleeding. Final blood collection was done by heart puncture into EDTA tubes (BD Biosciences). For cell phenotyping analysis, human CD45+, CD3+, CD4+, CD8+, CD14+, CD19+ populations were examined using antibody used for each of the cell types and detecting fluorescence intensity by flow cytometry.

5.3.6 Viral DNA/RNA Measurements

Quantitative real-time PCR was performed to detect viral DNA and RNA in tissue samples. Spleen, lung, liver, kidney, brain, gut, and bone marrow were collected at the time of euthanasia and stored at -80˚C until processing. Then, DNA and RNA were isolated to perform viral quantitation by real-time PCR. Human CD45 and GAPDH primers were used for normalization.

5.3.7 Drug Quantitation

Whole blood (25 µL) was immediately added to 1 mL of methanol with 0.1% FA and 2.5 mM ammonium formate on ice. EDTA tubes were then centrifuged to separate plasma from blood cells at 1800 g for 10 minutes. Plasma was be removed and transferred to a clean 0.6 mL Eppendorf tube and stored at -80˚C. Whole blood samples in methanol were used for drug level determination. The remaining plasma was stored (-80˚C) for viral load analysis and other tests. Spleen, lung, liver, kidney, brain, and gut was collected at time of sacrifice. One-third of each of these tissues was frozen at -80˚C for drug analysis, 1/3 was frozen for viral DNA/RNA quantitation, and the other 1/3 was frozen for RNAscope analysis. Each organ piece for drug level analysis was weighed and the weight was recorded.

5.4 Results

NM4FTC formulation was characterized for physico-chemical parameters post centrifugation. NM4FTC showed particle size of ˗ 340 nm, PDI between 0.3 – 0.4 and had a negative surface zeta potential. Additionally, both of NM4FTC and NM2TFV nanoformulations were characterized for percent drug loading and encapsulation efficiencies using validated UPLC/U.V.-Vis method and the injection volumes used for administration are presented in **Table 5.2.**

Formulation	Target drug dose (mg/kg)	Concentration quantitated (mg/mL) post Centrifugation	% Encapsulation	Injection volume	Injection volume in μL/g mice
NM4FTC	237	146.46	87.91	40	1.60
NM2TFV	193.5	129.65	64.83	37.41	1.49

Table 5.2 Quantitation of drug content and injection volumes used for I.M. administration in humanized mice PrEP study.

One week prior to challenge with HIV-1$_{ADA,}$ humanized mice were subjected to evaluation of sub-cellular population of human CD45+, CD3+, CD4+, CD8+, CD14+, CD19+ cells by flow cytometric analysis. These mice were then treated with each of the infections of NM4FTC and NM2TFV at 75 mg/kg of FTC/TFV equivalents by I.M. injection. Mice were then kept for 2 weeks (pre-exposure) before challenging them with HIV-1$_{ADA}$ at three different TCID$_{50}$ (10^2, 10^3 and 10^4) doses. On week 4th post challenge, we quantitated plasma viral loads in both untreated positive and treated infected mice and represented in **Figure 5.2**. More importantly, humanized mice in positive HIV-1$_{ADA}$ infected with 10^4 TCID$_{50}$/mL group showed viral outbreak in 3 out of 4 mice (75%). However, in treated HIV-1$_{ADA}$ infected mice, 3 out of 4 mice (75%) showed viral loads

below the level of detection (500 viral copies/mL). Humanized mice in positive HIV-1$_{ADA}$ infected with 10^3 TCID$_{50}$/mL group showed viral outbreak in 2 out of 4 mice (50%). However, in treated HIV-1$_{ADA}$ infected mice, 2 out of 2 mice (100%) showed viral loads below the level of detection. Additionally, in positive HIV-1$_{ADA}$ infected 10^2 TCID$_{50}$/mL group of mice, 5 out of 5 mice (100%) did not show viral outbreak 4 weeks post challenge. Similar observations were noted in treated HIV-1$_{ADA}$ infected 10^2 TCID$_{50}$/mL group of mice wherein 4 out of 5 mice did not show viral outbreak and one mouse had viral load at the level of detection 4 weeks post HIV-1$_{ADA}$ challenge.
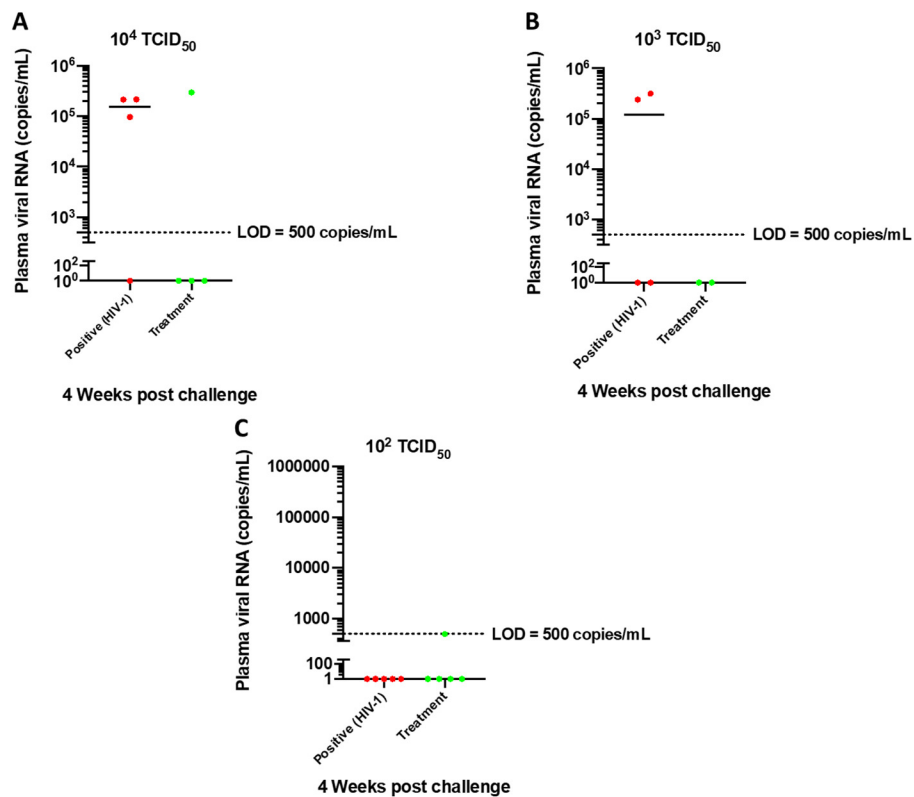
Figure 5.2 Plasma viral load quantitation in treated and positive (HIV-1) infected humanized mice (10^2, 10^3, 10^4 TCID$_{50}$ inoculum group). *After 4 weeks of viral challenge, humanized mice in both treated and positive control group were bled and plasma viral loads were quantitated using viral load RT-PCR detection kit with the limit of detection (LoD) of 500 copies/mL.*
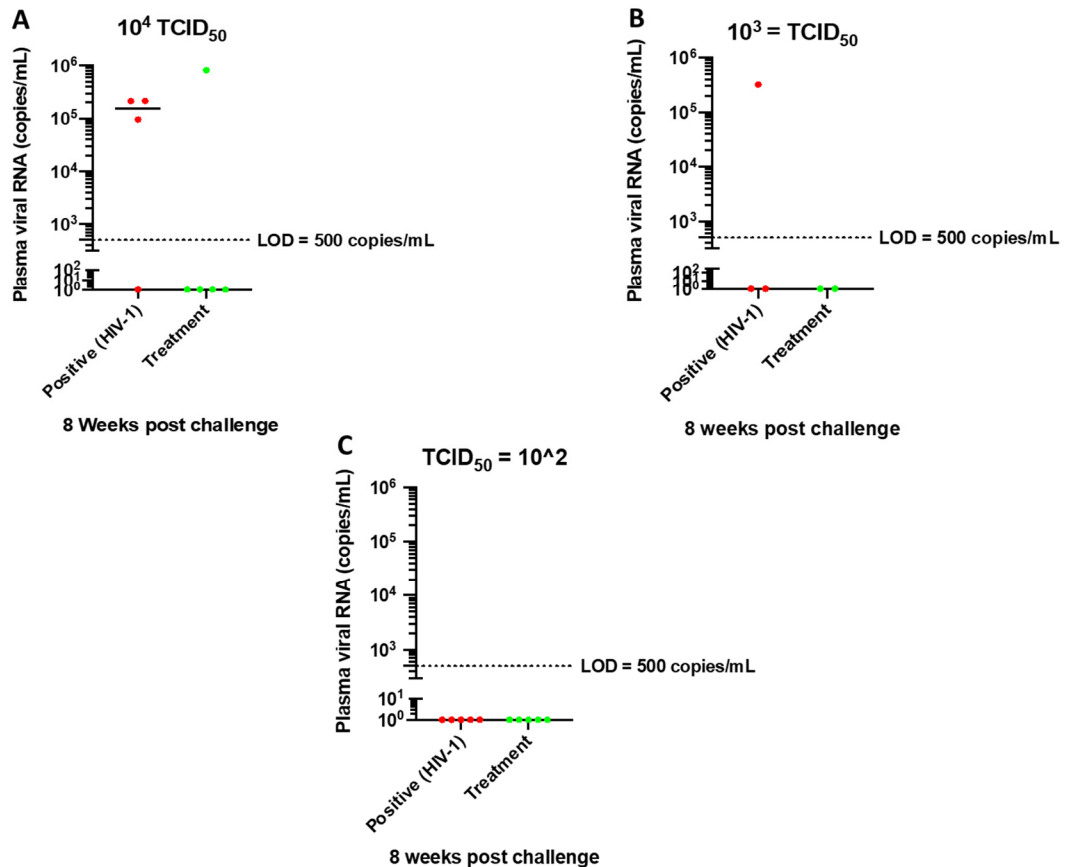
Figure 5.3 Plasma viral load quantitation in infected positive (HIV-1_ADA) and infected treated humanized mice (10^2, 10^3, 10^4 TCID_50 inoculum group). *After 8 weeks of viral challenge, humanized mice in both untreated infected positive control and treated infected group were bled and plasma viral loads were quantitated using viral load RT-PCR detection kit having limit of detection (LoD) = 500 copies/mL.*

Moving forward, we measured plasma viral loads in both positive and treated infected mice on week 8th post HIV-1_ADA challenge (**Figure 5.3**). Humanized mice in positive HIV-1_ADA infected with 10^4 TCID_50/mL group showed viral outbreak in 3 out of 4 mice (75%). Excitingly, in treated HIV-1_ADA infected mice, 4 out of 5 mice (80%) showed viral loads below the level of detection (500 viral copies/mL). Humanized mice in positive HIV-1_ADA infected with 10^3 TCID_50/mL group showed viral outbreak in 2 out of 3 mice (~67%). However, in treated HIV-1_ADA infected mice, 2 out of 2 mice (100%) showed viral loads below the level of detection. Additionally, in both positive HIV-1_ADA infected 10^2

$TCID_{50}$/mL group of mice, 5 out of 5 mice (100%) did not show viral outbreak 8 weeks post challenge. Similar observation was noted in treated HIV-1$_{ADA}$ infected 10^2 $TCID_{50}$/mL group of mice wherein 5 out of 5 mice did not show viral outbreak.

Thus, in conclusion the combination of single I.M. administration of NM4FTC and NM2TFV nanoformulations at 75 mg/kg FTC/TFV equivalent dose demonstrated plasma viral loads below the level of detection in 75 and 80 % of treated mice infected with HIV-1$_{ADA}$ inoculum dose of 10^4 $TCID_{50}$/mL at 4 and 8 weeks post challenge respectively. Additionally, further investigation of variation in terms of a later challenge time point (i.e. 4 weeks after treatment instead of current 2 weeks post treatment) and multiple viral challenge to demonstrate continued protection against HIV-1 infection are needed to be included in future evaluations of these nanoformulation efficacy as pre-exposure prophylactic treatment modality against HIV-1 infection.

5.5 Discussion

The efficacy and success of combination therapy of TDF/FTC is proportional to the level of patient adherence and compliance achieved. By developing LASER ProTide nanoformulations of FTC (M4FTC) and TFV (M2TFV) that would maintain therapeutic levels of active metabolites i.e. FTP and TFV-DP in the target tissues after single I.M. administration would constitute a major step forward in achieving improved patient adherence (single I.M. injection leading to reducing dosing frequency). Additionally, these LA formulations would enhance patient compliance by lowering the frequency of dose administration. Together, these would result in increased protection from prospective infections in susceptible healthy individuals and cause reduction in rate of transmission thereby enhancing the success of PrEP in HIV-1 treatment.

Chapter 6

Long-Acting Nitazoxanide and Tenofovir Prodrug Nanoformulations Suppress HBV Replication in Humanized Mice

6.1 Abstract

We tested the potency of nitazoxanide (NTZ), a broad-spectrum antiviral and immune stimulating agent and TFV, a nucleoside reverse transcriptase inhibitor in HBV mouse model. This drug combination was transformed into hydrophobic prodrug nanocrystals, and then stabilized into aqueous nanosuspensions. NTZ (M1NIT) and TFV (M1TFV) prodrugs were synthesized and nanoformulated creating NM1NIT and NM1TFV. NM1NIT had average particle sizes of 250-350 nm, polydispersity index of <0.2 and drug loading capacity of 45 - 70%. Suppression of HBV DNA release from cccDNA pools were recorded.

6.2 Introduction

Chronic HBV infection represents a major global public health threat with approximately 257 million people in 2015 having chronic HBV infection and 887,000 reported to have died of infection [309, 310] HBV causes acute and chronic infections and is responsible for considerable liver-related morbidity and mortality [311]. HBV is primarily transmitted through either percutaneous, mucosal exposures to infected biological fluids or through perinatal or parenteral routes of transmission (areas of drug misuse)[21]. Standard of care treatments are effective in many cases in HBV and HCV infections. However, therapeutic outcome is suboptimal and do not cause clinical cures in treated individuals [312].

Chemically, nitazoxanide (NTZ) is a thiazolide based anti-infective compound with broad activity against anaerobic bacterial, protozoan, and viral infections [313-315]. NTZ is marketed under the trade name Alinia® by Romark Laboratories, Tampa, Florida USA for the treatment of diarrhea and enteritis. Later on it was discovered that NTZ was also effective against many viruses [68]. NTZ and its active circulating metabolite tizoxanide (TIZ) were reported to inhibit HBV DNA transcription as well as the hepatitis B core

antigen, hepatitis B e antigen (HBeAg), and HBsAg in-vitro [316]. TIZ, a desacetyl NTZ is a metabolite of 3TC [316]. Additionally, NTZ also inhibits expression of HBV cccDNA and HBV RNA transcription by targeting the hepatitis B X protein (HBx)–damage-specific DNA-binding protein 1(DDB1) interaction [64]. A pilot clinical trials of NTZ against chronic HBV infection was recently conducted [68]. NTZ given at a dose of 500 mg (Romark, Tampa, FL) orally twice daily with food for up to 48 weeks showed undetectable HBV DNA levels (<38 IU/mL) in the serum of 8 of the 9 subjects (89%) after 4 to 20 weeks of treatment. Interestingly, 2 subjects became HBeAg negative which were initially reported to be HBeAg positive after 4 and 16 weeks of treatment, respectively. Additionally, NTZ was reported to be tolerated and showed transient mild to moderate side effects in patients primarily related to diarrhea and epigastric pain [317]. Thus, given the broad spectrum anti-viral efficacy and safety profile of NTZ, we aimed to develop LA NTZ prodrug nanoformulation with improved biological half-life and evaluate its efficacy against HBV infection in combination with LA tenofovir prodrug nanoformulation in humanized liver TK NOG mice having chimeric humanized liver infected with HBV [317-319].

6.3 Materials and Methods

All chemical synthesis reactions were performed under a dry argon atmosphere unless otherwise noted. Reagents were obtained from commercial sources and used directly; exceptions are noted. Nitazoxanide and tizoxanide were purchased from BOC Sciences, NY 11967, USA. Stearoyl chloride, sodium chloride (NaCl), sodium bicarbonate (NaHCO$_3$), Sodium sulphate (Na$_2$SO$_4$), N,N-diisopropylethylamine (DIEA), dichloromethane (DCM, CH$_2$Cl$_2$), chloroform (CHCl$_3$), N,N dimethylformamide (DMF), triethylamine (Et$_3$N), diethyl ether, tetrahydrofuran (THF), and methanol were purchased from   Sigma-Aldrich   (St. Louis, MO). Flash silica gel (32-63 μ) was purchased from

SiliCycle Inc. (Quebec, Canada). Precoated silica plates (200 µm, F-254) were purchased from Sorbtech technologies Inc. (Norcross, GA). The compounds were visualized by UV fluorescence or by staining with ninhydrin or $KMnO_4$ reagents. Poloxamer 407 (P407), ciprofloxacin, 3-(4,5-dimethylthiazol-2yl)-2,5-diphenyltetrazolium bromide (MTT), dimethyl sulfoxide (DMSO) were purchased from Sigma-Aldrich (St. Louis, MO). Cell culture grade water (endotoxin free), gentamicin, acetonitrile (ACN), bovine serum albumin (BSA), and LC-MS-grade water were purchased from Fisher Scientific (Hampton, NH). Heat-inactivated pooled human serum was purchased from Innovative research (Novi, MI). Dulbecco's Modification of Eagle's Medium (DMEM) was purchased from Corning Life Sciences (Tewksbury, MA).

6.3.1 Screening of Compounds for Anti-HBV Efficacy

For evaluating anti-HBV activity of drugs, HepG2.2.15 cells were used. Hep G2.2.15 cells are derived from human hepatoblastoma cell line Hep G2 and been characterized for having stable HBV expression [320]. Initially, HepG2.2.15 cells were plated in 6 welled plates. After 24 hours, these cells were treated with tizoxanide (10, 25 µM), and nitazoxanide (10, 25, 50 and 100 µM) (stock solutions were made in DMSO) for 8 hours. After 8 hours, cells were washed twice slowly with media (DMEM) and then fresh media was added. After 72 hours, cells were then washed with PBS and scrapped into PBS. Samples were then centrifuged at 2000 rpm for 5 minutes; supernatant PBS was removed and pellet thus obtained was frozen for future DNA isolation. DNA was isolated using Qiagen DNA kit. DNA samples, extracted from HepG2.215 cells were used as a template input for digital droplet polymerase chain reaction PCR (ddPCR) amplification. The copy number of HBVccc DNA were represented out of total input DNA. Briefly, to detect the HBV cccDNA by the ddPCR, 20 µL ddPCR mixture was reconstituted with 10 µL 2x ddPCR Supermix (Bio-Rad); 900 nM HBV cccDNA primers; 250 nM

corresponding probe; and 1 µL digested DNA template and droplets were produced by a droplet generator of the QX100 Droplet Digital PCR system (Bio-Rad). The droplets, which contain the PCR reaction mixture and droplet generation oil, were then transferred to a 96-well PCR plate for amplification using the C1000 Thermal Cycler and subsequently to a droplet reader to calculate the number of both positive and negative droplet events from each PCR reaction mixture. The software determines the number of positive droplets per µL by calculating the ratio of the positive droplets over the total droplets combined with Poisson distribution. Thus, the value of the template equals the number calculated by the software multiplied by the dilution factor of the template in the reaction system.

6.3.2 Synthesis of LA Prodrug of Tizoxanide (M1NIT)

Tizoxanide was chemically modified with C_{18} fatty acid to form LA tizoxanide prodrug M1NIT. Briefly, TIZ (2 g, 7.54 mmol, 1 eq.) was dissolved in DMF (20 mL) under an argon atmosphere and cooled on a regular ice bath. We then added DIEA (2.63 mL, 15.08 mmol, 2 eq.) and   stearoyl chloride (3.89 g, 11.31 mmol, 1.7 eq.) followed by warming up of the reaction mixture to room temperature for at least 16h. The reaction progress was monitored by thin layer chromatography (TLC). Following reaction completion, DMF was evaporated followed by partitioning the solids in a mixture of DCM and 0.1 M HCl. The aqueous HCl layer was back extracted twice with DCM (80 mL). DCM layers were combined and further washed with 100 mL saturated $NaHCO_3$ and brine. The organic phase was then dried over Na_2SO_4 and concentrated. The resultant solid was then purified by column chromatography eluting with 2:1 hexane: ethyl acetate solvent mixture. The desired compound (M1NIT) was further precipitated from hexanes and dried to obtain an off white powder.

6.3.3 M1NIT Physicochemical Characterization

6.3.3.1 Solubility

Solubility of M1NIT in water (aqueous) and 1 – octanol (lipid) was determined by adding excess amount of drug to each of these media leading to the formation of saturated solutions. The homogeneous saturated solutions were mixed at 37^0C for 24 h under shaker incubator (innova® 42 shaker incubator) and centrifuged at 14,000 x g for 10 minutes to separate insoluble drug. The amount of drug in the supernatant was quantified by validated UPLC TUV method for M1NIT analysis.

6.3.3.2 NMR and Mass spectrometric evaluations

The chemical structure of M1NIT was confirmed by proton, and carbon nuclear magnetic resonance (^{1}H, and ^{13}C NMR) spectra recorded on a Varian Unity/Inova-500 NB (500 MHz; Varian Medical Systems Inc., Palo Alto, CA, USA) and molecular ion peak was determined by mass spectrometric infusion into a Waters TQD mass spectrometer.

6.3.3.3 FTIR and DSC Evaluations

Characterization of NIT and M1NIT prodrug by FT-IR was performed on a Spectrum Two FT-IR spectrometer (PerkinElmer, Waltham, MA, USA).

TIZ, NIT and M1NIT were subjected to DSC analysis to determine their thermal behavior by observing the dependence of changing sample heat capacity (mW/mg) on temperature variations (in ^{0}C). DSC evaluations of the samples were performed on differential scanning calorimeter (204 F1 Phoenix) on DSC 204F1 t-sensor/E with Pan Al and pierced lid crucible. Heating rate was 10 ^{0}C)/min ranging from 30 – 600 ^{0}C in nitrogen atmosphere with corr/m. range of 000/5000 µV.

6.3.3.4 Analytical Method Developments

M1NIT quantifications were performed on a Waters ACQUITY ultra performance liquid chromatography (UPLC) H-Class System with TUV detector and Empower 3

software (Milford, MA, USA) and Kinetex 5 µ C18 100 °A Phenomenex column (150, 4.5 mm) (Torrence, CA) used for separation. Mobile phase used was mixture of acetonitrile as organic phase and HPLC grade water as aqueous phase in the ratio 90:10 and flow rate of 1 mL/min and wavelength of 244 nm.

6.3.3.5 Nanoformulation of M1NIT and Physicochemical Characterization

The nanoformulation of M1NIT i.e. NM1NIT was prepared by high-pressure homogenization on an Avestin EmulsiFlex-C3 (Ottawa, ON, Canada) homogenizer using poloxamer P407 surfactant as stabilizer. Briefly, P407 (0.5% w/v) was weighed and dissolved in PBS. The prodrug (1% w/v) was then added to the surfactant solution at a drug to surfactant ratio of 2:1 and then continued stirring leading to formation of microparticle pre-suspension. The microparticles were then homogenized (~20,000 psi) on Avestin homogenizer until the desired nanoparticle size was achieved. Particle size (D_{eff}), polydispersity index (PDI), and zeta potential were determined by DLS on a Malvern Nano-ZS (Worcestershire, UK). The physico-chemical stability of NM1NIT nanoparticles was monitored at 25 ^{0}C over 70 days. Encapsulation efficiency was calculated using the following equation: Encapsulation efficiency of M1NIT (%) = (weight of M1NIT in formulation/initial weight of M1NIT added) x 100. For in-vivo dosing, the prototype formulation was concentrated by differential centrifugation at 4˚C for 10 minutes at 200 x g. The supernatant was carefully transferred to another centrifuge tube and then centrifuged at 15000 x g for 20 minutes at 4˚C. NM1NIT was re-dispersed in minimum volume of poloxamer to achieve the desired dose of 75 mg/kg for in-vivo anti-HBV efficacy studies. Resulting size, PDI, zeta potential and concentration of the formulation were measured.

6.3.3.6 Chemical stability and TEM morphological evaluations of NM1NIT

The percent encapsulation was calculated on Day 0 and Day 30 which is indicative of chemical stability of M1NIT in the nanoformulation.

The NM1NIT morphological evaluation was performed using transmission electron microscopy (TEM). The processing for TEM sample was done as follows: Initially, a 10 µL NM1NIT nanosuspension was placed on a formvar/silicon monoxide 200 mesh copper grid, allowed to settle for 2 min, and the excess solution was wicked off and grid was further allowed to dry. A drop of NanoVan vanadium negative stain was placed on the grid for 1 min, then stain was wicked away and further allowed to dry (2-5 mins). Grids were examined on a FEI Tecnai G2 Spirit TWIN transmission electron microscope (Hillsboro, OR) operated at 80 kV, and images were acquired digitally with an AMT digital imaging system (Woburn, MA).

6.3.3.7 MDM Cytotoxicity Evaluations of NM1NIT

For cytotoxicity evaluations of TIZ, NIT, M1NIT and NM1NIT treatments in MDM at various concentrations (1 – 400 µM), MTT assay was performed. Briefly, MDM were cultured in 96 welled plates at a density of 80,000 cells/ well. MDM were then treated with different concentrations of TIZ, NIT, M1NIT and NM1NIT for 24 hours. DMSO (0.1 % v/v) in media B was used as media control. Treatments were then washed with PBS and then 100 µL of MTT solution was added to each well. Cells were then incubated at 37^0 C for 45 minutes. Plates were removed from incubator and MTT solution was then aspirated from each of the well. Immediately, 200 µL of sterile DMSO was added into each well. Plates were shaken and then subjected to measuring absorbance at 490 nm on a microtiter plate reader.

6.4 Study Approval

All animal studies were approved by the University of Nebraska Medical Center Institutional Animal Care and Use Committee in accordance with the standards incorporated in the Guide for the Care and Use of Laboratory Animals (National Research Council of the National Academies, 2011). Human monocytes were isolated by leukapheresis from HIV-1/2 and hepatitis seronegative donors according to an approved UNMC IRB exempt protocol.

6.5 Code of Ethics for Animals

Mice were maintained in a pathogen-free facility and treated humanely. All mouse studies were conducted in strict accordance with the Guide for the Care and Use of Laboratory Animals from University of Nebraska Medical Center (UNMC). All experimental protocols were approved by the Animal Care and Use Committee of UNMC.

6.6 Generation of A Humanized Liver TK-NOG Mouse Model

TK-NOG mice (NOD/Shi-scid IL-2 $R\gamma_c^{null}$) (5 – 6 months of age) expressing a herpes simplex virus type 1 thymidine kinase transgene under regulation of the albumin gene promoter were intra-splenically infused with 2 million human hepatocytes from the Lonza (lot#4145) [317, 321].

6.7 Efficacy Study in HBV Infected Humanized Liver TK-NOG Mice

Humanized liver TK-NOG mice were infected with 10^6 genome equivalents (GE) HBV [318, 322]. After a duration of 2 months post infection, these mice were given a single intramuscular injection of NM1NIT and NM1TFV each at 75 mg/kg of TIZ/TFV equivalents. Various levels of HBV DNA, and human serum albumin (Alb) were then monitored for 48 h and 10 weeks in animals respectively (**Figure 6.1**) (*P values obtained by t-test).
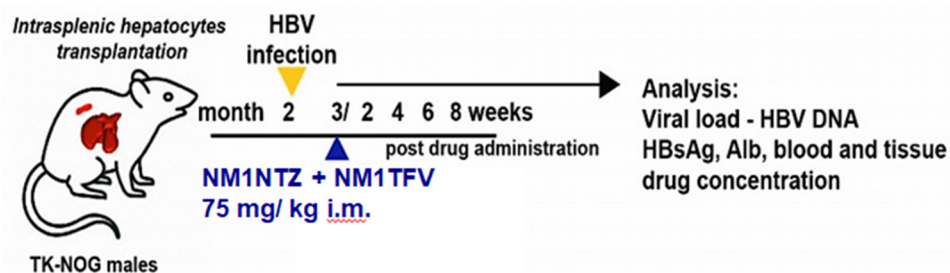
Figure 6.1. *Evaluation of anti-HBV efficacy of combination of NM1NIT and NM1TFV at 75 mg /kg of TIZ/TFV equivalents in humanized liver TK-NOG mice (timeline and quantitation biomarkers).*

6.8 Measurement of Blood HBV DNA, HBsAg levels and Human Serum Albumin

HBV DNA levels were measured using the COBAS TaqMan HBV Test (Roche Diagnostics, Switzerland). The samples were diluted approximately 20-fold and detection limits were 2240-3360 DNA copies/ml. Plasma HBsAg levels were measured by ELISA using the QuickTiter Hepatitis B Surface Antigen ELISA Kit (Cell Biolabs, Inc, VPK-5004, San Diego, CA) according to assay protocol.

6.9 Results

6.9.1 Efficacy of Compounds Against HBV Infections In-vitro

The anti-HBV activity of tizoxanide, and nitazoxanide were determined in infected Hep G2.2.15 cells after treatment at various concentrations ranging from 10 – 100 µM for 8 hours. Clear evidence of anti-HBV efficacy in terms of reduction in HBV cccDNA/ ng DNA was observed for tizoxanide (TIZ) at concentrations of 10 and 25 µM. Nitazoxanide (NTZ) showed dose dependent reduction in HBV cccDNA/ ng DNA in these treated cells and demonstrated highest efficacy at a dose of 100 µM **(Figure 6.2).**
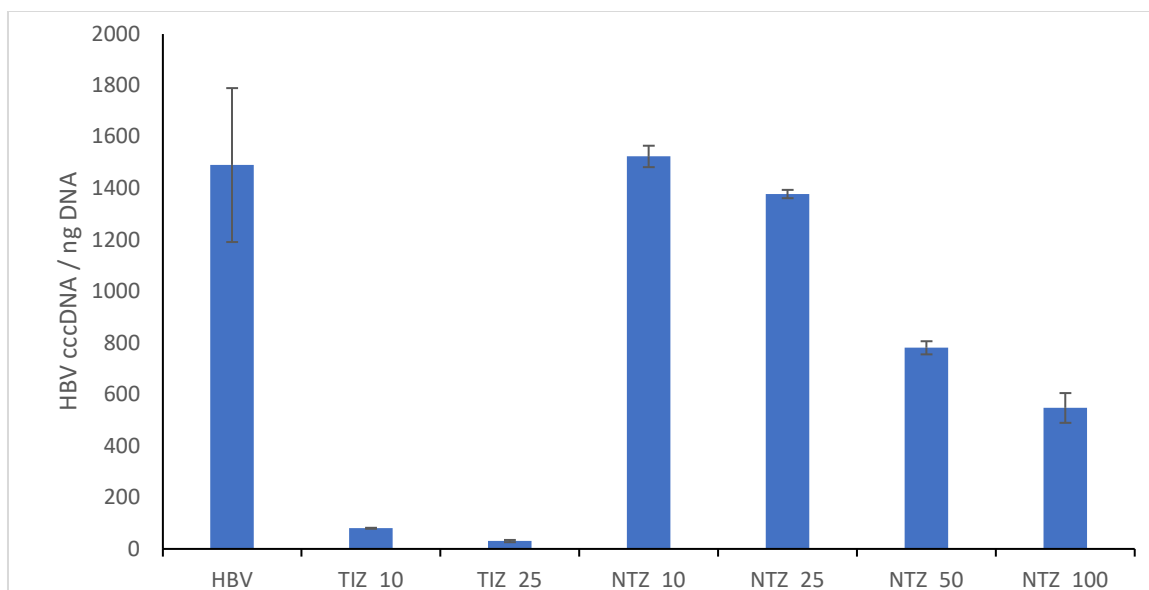
Figure 6.2 *Anti-HBV efficacy of TIZ, and NTZ in Hep G2.2.15 cells. Initially, cells were treated for 8 hours and then washed with PBS followed by maintaining cultures for 72 hours after which cells were pelleted in PBS and stored until further quantitation for HBV cccDNA following HBV DNA isolation.*

6.9.2 Synthesis and Characterization of M1NIT

A fatty acid esterification reaction was employed for the synthesis of M1NIT. Initially, stearyl chloride was reacted with tizoxanide in the presence of DIEA (**Figure 6.3)** and then purified by silica gel column chromatography and hexane washing leading to the formation M1NIT with 50 % yield. ^{1}H and ^{13}C nuclear magnetic resonance, Fourier transform infrared spectroscopy and mass spectrometry (NMR, FTIR and MS) confirmed the formation of the M1NIT prodrug. The M1NIT characterization in terms of ^{1}H NMR spectrum (blue) consisted of a triplet at 0.8 – 1.2 ppm, and a broad singlet between 1.4 – 1.6 ppm and a multiplet at 1.8 ppm representing terminal methyl, and symmetrical methylene protons of the fatty acid conjugation in M1NIT prodrug. Additionally, the multiplet signals at 7.09-7.7 ppm correspond to the aromatic protons representing aryl promoiety in M1NIT (**Fig. 6.4.A**). ^{13}C NMR spectrum of NM1NIT showed peaks at 171.2

and 163.3 ppm which correspond to the carbonyl moieties, peaks at 148.8, 143.6, 140.34, 134.37, 130.35, 125.5 and 124.7 ppm represent aromatic carbon atoms and peaks at 34.39, 29.70, 24.67, 22.66 and 14.12 correspond to aliphatic carbons representing fatty acid conjugation in the synthesized M1NIT (**Fig. 6.4.B**). Formation of hydrophobic and lipophilic M1NIT prodrug was demonstrated by its lower aqueous solubility ($0.151 \pm 0.0315\,\mu g/mL$) and relatively higher octanol solubility ($1.255 \pm 0.0125\,\mu g/mL$) (**Fig. 6.4.C**). FTIR spectra of M1NIT showed absorption bands in the regions of $2900 - 2800\,cm^{-1}$ and $1800 - 1700\,cm^{-1}$ representing the C-H and C=0 stretching vibrations originating from fatty acid conjugation and carbonyl ester bond respectively in M1NIT which was absent in NTZ (**Fig. 6.4.D**). Differential scanning calorimetric analysis of TIZ, NIT and M1NIT identified phase transitions generated by heat capacity changes with simultaneous variation in temperature conditions. Notable melting endothermic peaks were observed for TIZ, NIT and M1NIT at 220, 250 and 275 ^{0}C confirming distinct phase transitions at these temperatures. Additionally, exothermic peaks were observed for NIT and M1NIT at 200 and 145 ^{0}C likely due to polymorphic changes observed during heating process in these compounds [323, 324] (**Fig. 6.4.E**). Mass spectrometric infusion of M1NIT into Waters TQD mass spectrometer confirmed a M1NIT molecular ion peak at m/z of 531 confirming formation of M1NIT **(Fig. 6.4.F)**.
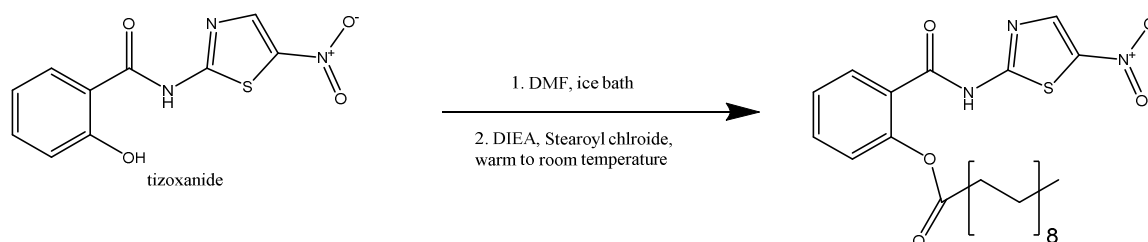
Figure 6.3. *Synthesis of M1NIT*
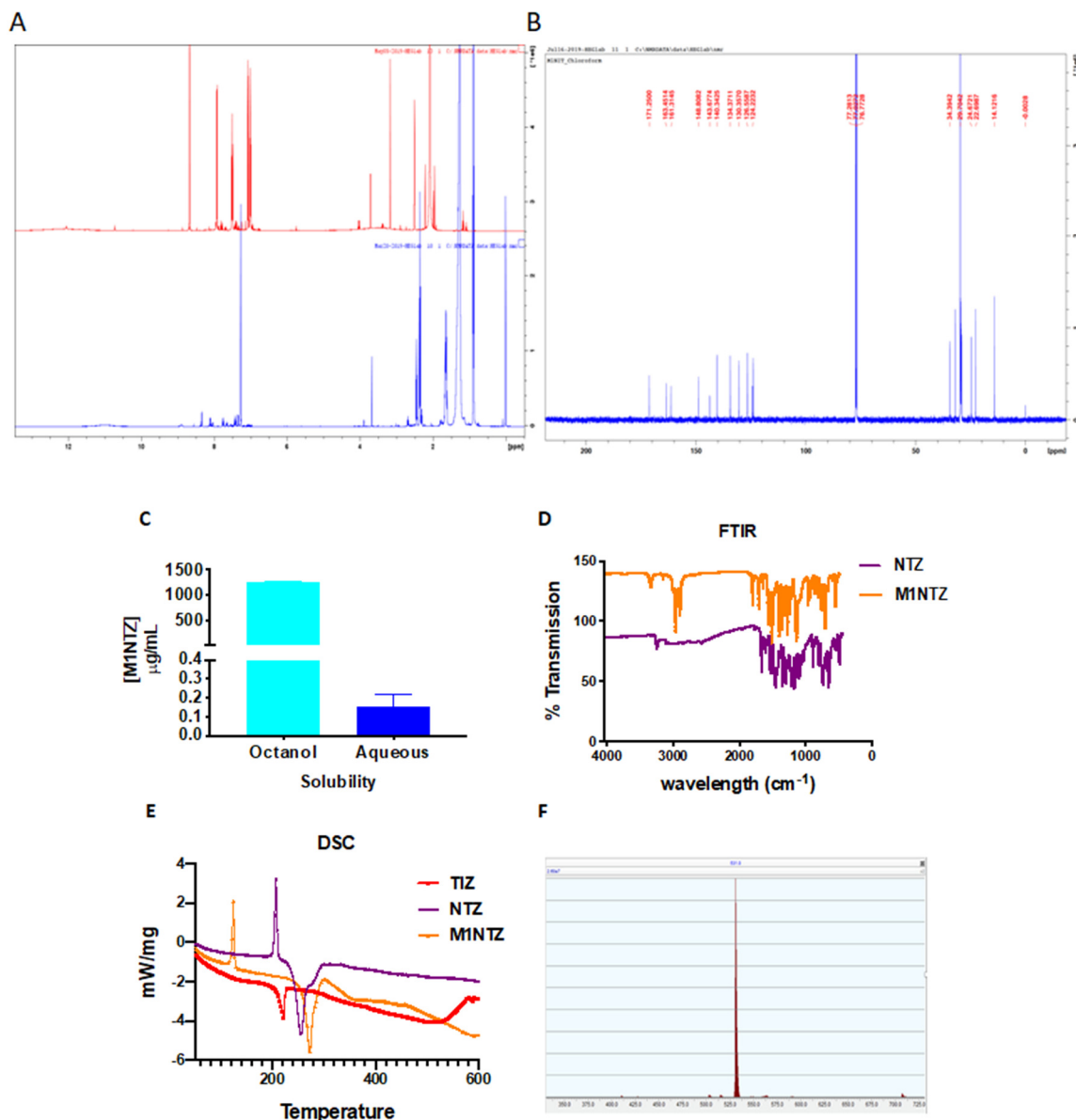
Fig. 6.4. M1NIT physicochemical characterization. (A) ^1H NMR spectra of NTZ (red) and M1NIT (blue) confirmed chemical modification of the parent drug. **(B)** ^{13}C NMR spectra of demonstrating the presence of functional carbons in the modified M1NIT prodrug. **(C)** Solubility of M1NIT in 1-octanol and water was measured at 37 ℃. Data are expressed as mean ± SEM for n = 2 samples evaluated. **(D)** Fourier transformed infra-red spectroscopic (FT-IR) analysis showed the presence of C=0, aromatic and aliphatic C-H stretching vibrations in the synthesized M1NIT prodrug. **(E)** DSC analysis of TIZ, NTZ and M1NIT supporting presence of phase transitions by varying temperature conditions in these compounds. **(F)** Waters Acquity TQD MS infusion showing molecular ion peak at m/z of 531.

6.9.3 Physico-chemical Characterization of NM1NIT

A scalable preparation process for nanoformulation was employed for developing NM1NIT nanosuspension using high pressure homogenization technique [277, 279, 325]. Poloxamer P407 used as stabilizer for the M1NIT formulation provided drug encapsulation efficiency of 47%. Particle size, polydispersity index (PDI), and zeta potential were determined by DLS and were tabulated in **Table 6.1**.

Formulation	NM1NIT
Stabilizer	Poloxamer P407
Prodrug : P407	2:1
Dispersion medium	PBS
Size (nm)	264 ± 2.0
Zeta potential (mV)	- 16.5 ± 0.31
Percent encasement	47 ± 0.47

***Table 6.1.** Nanoformulation of M1NIT using poloxamer P407 as stabilizer and high-pressure homogenization used as top-down technique for nanosizing.*

NM1NIT remained stable at 25 ^{0}C for up to 70 days (**Figure 6.5.A**). Improved physico-chemical stability of nanoformulation could be due to negative surface zeta potential of these nanoparticles thereby causing electrostatic repulsion and prevention of agglomeration in nanosuspension over longer duration of time [326]. Evaluation of nanoparticle morphologies by TEM demonstrated cuboidal shaped particles with sizes between 138 - 262 nm (**Figure 6.5.B**). Additionally, chemical stability evaluations of NM1NIT over 30 days showed maintenance of 80% of M1NIT in the nanoformulation as quantitated by validated UPLC-U.V. Vis method for M1NIT (**Figure 6.5.C**). Thus, together with smaller particle size and use of biocompatible excipients in NM1NIT formulation could eventually lead to enhance safety and efficacy of nanoparticle formulation post in-vivo administration. We further carried out MTT assay [278] on MDM to evaluate

cytoxicity of TIZ, NIT, M1NIT and NM1NIT treatments over 24 hours at various concentrations. DMSO (0.1% v/v) was used as vehicle control. No negative effects on mitochondrial reductase activity correlating to cell vitality was observed post treatments at all the concentrations tested. Thus, these treatments were non-cytotoxic in MDM demonstrating its safety and non-toxicity profile in MDM (**Figure 6.5.D**). Similarly, NM1TFV was characterized for percent encapsulation, particle size, zeta and polydispersity index (PDI) measurements. NM1TFV was found to have size in the range of 250 – 350 nm, a negative zeta potential, PDI < 0.2, drug encapsulation efficiency of >70 % thereby demonstrating suitable size and loading capacities of the formulation for further in-vivo evaluation.
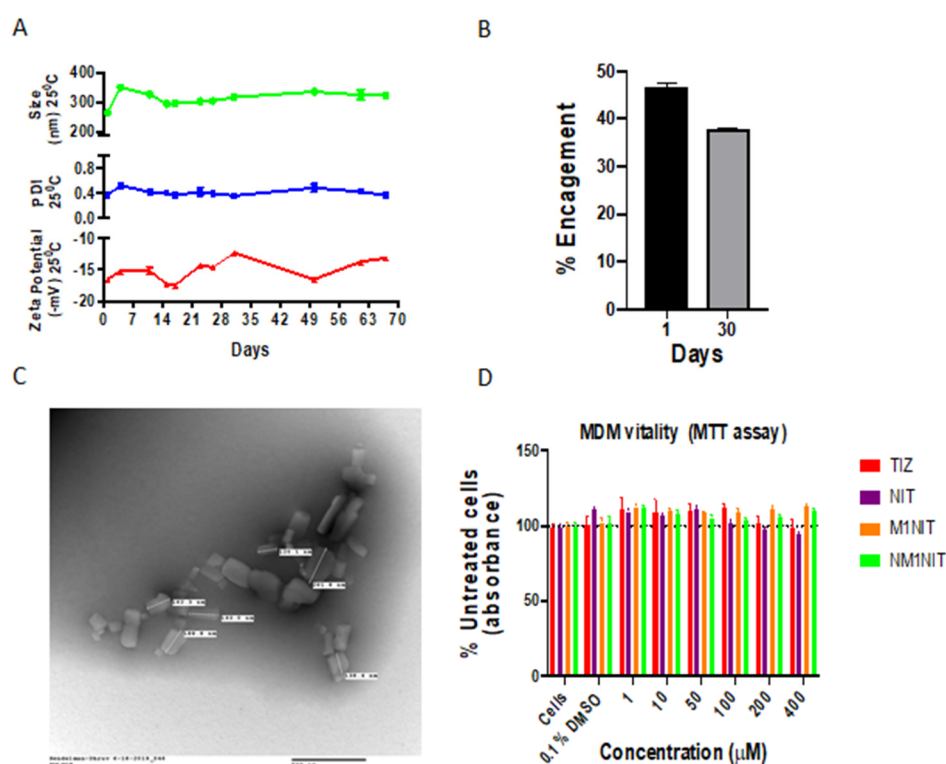
Figure 6.5. NM1NIT characterizations. (A) *Physico-chemical stability evaluation of NM1NIT at 25 ℃ in terms of particle size, zeta potential and polydispersity index over 70 days.* ***(B)*** *Chemical stability of M1NIT in NM1NIT over 30 days. M1NIT maintained its chemical stability over 80 % as evidence by its marginal reduction in % encagement on Day 30.* ***(C)*** *TEM of NM1NIT showed presence of cuboidal shaped*

*nanoparticles in the size range of 130-270 nm. **(D)** Cell vitality was assessed in MDM by MTT assay 24 h after TIZ, NIT, M1NIT or NM1NIT treatments over a range of concentrations (1 – 400 µM). Results were normalized to untreated control cells. All the treatments i.e. TIZ, NTZ, M1NIT and NM1NIT were found to be non-cytotoxic at the range of concentrations tested for the study. Data are represented as mean ± SEM for n = 4 samples per group.*

6.9.4 In-vivo Efficacy Against HBV Infection

Humanized liver TK NOG mice were used to evaluate anti-HBV activity of developed formulations. After confirmation of human albumin in peripheral blood post transplantation of human hepatocytes, mice were infected with patient derived sera containing 10^6 GE HBV DNA. These mice were then treated with the combination of NM1NIT and NM1TFV at 2 months post infection of HBV DNA. We evaluated the combination of NM1NIT with our tenofovir ProTide i.e. NM1TFV since tenofovir represents a vital treatment regimen for HBV infections [327]. Administration of M1NIT and NM1TFV each at 75 mg/kg of TIZ/TFV equivalents intramuscularly in combination suppressed HBV replication and viral load (measuring HBV DNA) in peripheral blood of all the treated liver TK NOG mice for up to 8 weeks. These mice showed >1 $\log_{10}$ reduction in HBV DNA levels 8 weeks post treatment as shown in **Figure 6.6.A** Interestingly, two out of four treated mice showed HBV DNA levels below LoD. These mice had human albumin levels in the range 0.5 – 2.5 mg/ml throughout the duration of study (**Figure 6.6.B**) which demonstrated absence of drastic adverse effects related to drug treatments.
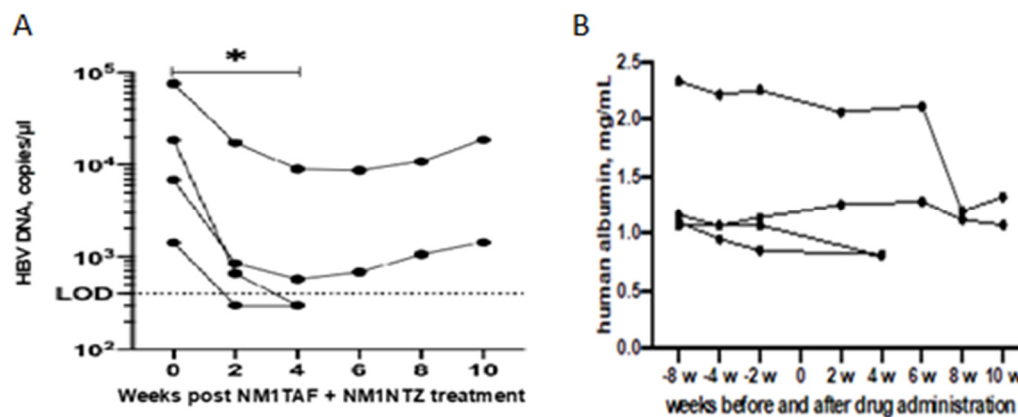
Figure 6.6. *Evaluation of NM1NIT (NM1NTZ) and NM1TFV (NM1TAF) nanoformulations' efficacy in combination treatment against HBV in human liver TK NOG mice. **(A)** Peripheral blood viral load levels in terms of HBV DNA (IU/mL) after NM1NIT and NM1TFV treatments up to 10 weeks post treatment. Dotted lines represent LoD. Bold lines represent mean & SEM. P values were obtained by t-tests. **(B)** Human albumin levels in peripheral blood of these mice over the duration of 10 weeks.*

6.10 Discussion

Given the probability of severe adverse reactions with HBV vaccines such as multiple sclerosis, rheumatoid arthritis [328], there is a great need of developing highly effective and safe LA anti-HBV injectables with cost effective measures [329]. Patient adherence issues with oral formulations of anti-HBV drugs and emergence of viral resistance to the treatments are the major issues towards developing effective HBV medications [330]. The applications of LASER formulations of anti-HBV drugs with their advantages of improved patient adherence and compliance forms a great promise in enhancing the probability of success in treating patients with HBV infection [331].

Chapter 7

Summary, Conclusions, Future Directions,

and Applications

7.1. Summary

The development of long acting (LA) antiretroviral therapy (ART) with dosing intervals from monthly to yearly could not only improve adhehrence to treatment regimen but also improve treatment outcomes. We have shown that prodrug approaches facilitate conversion of hydrophilic and hydrophobic antiretroviral drugs (ARVs) with short half-lives into LASER ART. These formulations demonstrate increased potency and bioavailability and have the potential to improve regimen adherence and facilitate reductions in viral transmission and mutation rates. These formulations facilitate drug entry into HIV-1 infected CD4+ T cells and mononuclear phagocytes (MP; monocytes, macrophages, microglia, and dendritic cells) within reservoirs that include gut associated lymphoid tissue, lymph nodes, spleen, and brain. And as a starting point for hydrophilic compounds, my work is focused on the design and production of phosphorylated ProTide prodrugs of FTC (referred as M2FTC). M2FTC chemical structure was affirmed by mass spectrometry, nuclear magnetic resonance, Fourier transform infrared spectroscopy, and aqueous solubility tests. Conversion of FTC and lipophilic and hydrophobic ProTides facilitated the production of aqueous poloxamer 407 stabilized nanocrystals (NM2FTC) by high-pressure homogenization. Uptake, release, retention, and drug potency was tested in human monocyte derived macrophages (MDM). The latter was confirmed by measuring inhibition of RT activity and HIV-1p24 immunostaining after challenge by a macrophage tropic CCR5 using viral strain (named, HIV-1$_{ADA}$) at a MoI of 0.1. NM2FTC particles were approximately 300 nm in size and negatively charged. These particles demonstrated a narrow polydispersity index, a loading capacity of 80% and a spherical morphology. NM2FTC nanocrystals were stable for > 1 month with drug uptake improved by > 30-fold when compared to native FTC. Drug retention of 10 µg/10^6 cells was recorded during a 30-day observation for NM2FTC. Single treatments of NM2FTC to MDM resulted in sustained intracellular FTP for one month and mirrored sustained and

potent antiretroviral activities. M2FTC and NM2FTC were non-cytotoxic at all tested drug concentrations. Thus, a LASER FTC formulation was developed, demonstrating sustained LA ART activity. NM2FTC can be developed as a LA parenteral (LAP) formulation for HIV-1 prevention and treatment. To further enhance intracellular and tissue active triphosphate metabolites delivery, two second-generation lipophilic FTC ProTides (M3- and M4-FTC) were synthesized then stabilized into poloxamer coated LASER aqueous nanosuspensions (NM3- and NM4-FTC). ProTide chemical structures were confirmed by MS, NMR and FTIR analyses. Poloxamer 407 stabilized nanoparticles were prepared by high-pressure homogenization and characterized for drug loading and crystallinity. Viability tests, cellular drug uptake, and IC_{50} studies were performed in human MDM and CD4+ T-cells. The synthesized ProTides showed characteristic C=0 stretching vibrations at 2800 cm^{-1} representing carbonyl ester bonds and N-H bending vibrations at 1600 cm^{-1} representing phosphoramide bonds. A reduction in aqueous solubility of 30 and 0.5 µg/mL was observed for M3 and M4- FTC, respectively, compared to FTC (150 mg/mL) confirming increased hydrophobicity of the synthesized FTC ProTides. Both formulations were characterized by particle sizes of 150-250 nm, polydispersity index (PDI) of 0.2-0.3, negative zeta potentials and high drug loading capacity of 85%. The formulations were stable at 25°C for at least 2 months without particle agglomeration. NM3- and NM4-FTC were found to be safe in MDM at 100 µM using MTT assay and demonstrated intracellular drug levels of 15-20 µg/10^6 compared to undetectable levels for the native drug, an enhancement in NM3FTC (IC_{50}=2.63 nM) and NM4FTC potency (IC_{50}=1.33 nM) in MDM compared to FTC (IC_{50}=19.56 nM). Consequently, both NM3- and NM4-FTC treatments demonstrated sustained antiretroviral activities in CD4+ T-cells compared to viral breakthrough for FTC. NM4FTC LASER ART formulation with improved antiretroviral activity is a promising lead candidate towards further pre-clinical development for HIV-1 prevention and treatment.

PrEP is the preventive measure for halting viral transmission of HIV-1 infection in those susceptible to viral infection. PrEP treatment strategies include combination of FTC and TDF given daily as single tablet combination. Truvada has shown greater promise in reducing the rate of transmission of HIV infection in cases of accidental exposure to needle stick contaminated with HIV or having sex with viral seropositive individuals. A combination PrEP regimen of FTC/TAF (Descovy) was recently approved by the US FDA as an alternative PrEP regimen to Truvada. Also, recent studies have shown superiority of LA CAB over FTC/TAF regimens [332]. This underscores the importance of single potent long acting drug regimens and adherence in preventing HIV-1 transmission. Indeed, the success of PrEP treatment in preventing HIV-1 infection is dependent on the level of patient adherence. With the goal of enhancing patient adherence and improving compliance, we evaluated combination of NM4FTC and NM2TFV at 75 mg/kg FTC and TFV dose equivalents as PrEP treatment regimen against HIV-1 infection in humanized mice model of infection. In our study of evaluating the optimum viral inoculum dose, a single I.M. injection of NM4FTC and NM2TFV in distinct thigh muscle of humanized mice showed 75 – 80% protection up to 8 weeks post HIV-1 challenge with 10^4 TCID$_{50}$ inoculum dose. These mice were treated with the combination formulations for 2 weeks and then challenged with HIV-1 and plasma viral loads were monitored 4 - 8 weeks post challenge. Thus, combination of NM4FTC and NM2TFV showed PrEP efficacy against HIV-1 infection in humanized mice. Further evaluations of single regimen for NM4FTC or NM2TFV is needed. Additionally, these treated humanized mice should be challenged multiple times through different route of challenge for eg. vaginal to further explore the efficacy of these formulations in infected animal models.

Furthermore, we applied our LASER technology to nitazoxanide (a broadly active antiviral) which has reported to have anti-HBV activities. We synthesized

hydrophobic and lipophilic prodrug of nitazoxanide named as M1NIT using fatty acid esterification reaction. M1NIT was characterized by NMR, FTIR and Mass spectrometric evaluations followed by its formulation into a poloxamer stabilized NM1NIT nanosuspension. NM1NIT was further evaluated for its encapsulation efficiency, physical/ chemical stability evaluations and MDM cytotoxicity by MTT assay. NM1NIT demonstrated particle size of less than 250 nm, had narrow PDI and a negative zeta potential. NM1NIT was found to be non-cytotoxic in MDM.

7.1 Conclusions, Future Directions and Application

LA nanomedicines developed for HIV treatment and prevention extend drug half-lives, improve biodistribution and facilitate therapeutic outcomes. The limitations of existing LA ARV parenteral include requirement for frequent dosing, injection site reactions and high injection volumes. Limited distribution of ART within tissue and cellular reservoirs of infection further limits their efficacy. Therefore, new treatment and prevention strategies that permit less frequent dosing, with abilities to sustain therapeutic concentrations of drug at sites of action could potentially improve adherence and reduce transmission of infection. The FTC ProTide formulations described in this work represent a promising approach towards development of a LA sustained release formulation with improved antiretroviral activity. Single treatment of MDM with NM2FTC demonstrated sustained intracellular FTP levels and antiretroviral activities. PK tests in Sprague Dawley rats demonstrate sustained high drug levels in blood and tissues in NM2FTC treated animals compared to rapid one day drug clearance after native drug treatment. Future studies will evaluate pharmacodynamic profiles of NM2FTC in rhesus macaques and inevitably to evaluation in humans infected or at risk of infection.

Second generation FTC ProTide, M4FTC demonstrated superior in-vitro and in-vivo characteristics. However, further ProTide developments would be aimed at increasing the FTP levels attained after ProTide hydrolysis. Introducing a methylene

functionality between 3' hydroxyl in the sugar moiety of nucleoside analog active compound and the phosphorus functional group could further increase the stability of monophosphate formed and thereby lead to enhancement in the amount of FTP generated inside the target cells. This would provide a robust ProTide hydrolysis profiles that could be further monitored and optimized based on intracellular FTP levels observed in comparison studies.

Additionally, the phenoxy moiety attached to the chiral phosphorus could be removed. This could further aid in enhancing the hydrolysis rates in wider subset of cells in-vitro. Formulations of dephenoxylated ProTides could be evaluated via oral route of administration as proper balance of lipophilicity and hydrophilicity is needed for efficient intestinal absorption and permeation into the systemic circulation.

Further efforts will be focused on developing formulations with improved scalability and physical stability for future studies in non-human primates. A robust screening of surfactants, optimization of formulation manufacture processes and lyophilization parameters are needed to be explored to develop an optimum ProTide formulation with desirable characteristics directed towards once a month injectable formulation for its pre-clinical evaluations.

References

1. Boasso, A., G.M. Shearer, and C. Chougnet, *Immune dysregulation in human immunodeficiency virus infection: know it, fix it, prevent it?* J Intern Med, 2009. **265**(1): p. 78-96.
2. Bowers, N.L., et al., *Immune suppression by neutrophils in HIV-1 infection: role of PD-L1/PD-1 pathway.* PLoS Pathog, 2014. **10**(3): p. e1003993.
3. Nyamweya, S., et al., *Comparing HIV-1 and HIV-2 infection: Lessons for viral immunopathogenesis.* Rev Med Virol, 2013. **23**(4): p. 221-40.
4. Williams, K.C. and T.H. Burdo, *HIV and SIV infection: the role of cellular restriction and immune responses in viral replication and pathogenesis.* APMIS, 2009. **117**(5-6): p. 400-12.
5. Choudhary, S.K. and D.M. Margolis, *Curing HIV: Pharmacologic approaches to target HIV-1 latency.* Annu Rev Pharmacol Toxicol, 2011. **51**: p. 397-418.
6. Xiao, Q., D. Guo, and S. Chen, *Application of CRISPR/Cas9-Based Gene Editing in HIV-1/AIDS Therapy.* Front Cell Infect Microbiol, 2019. **9**: p. 69.
7. Cassan, E., et al., *Concomitant emergence of the antisense protein gene of HIV-1 and of the pandemic.* Proc Natl Acad Sci U S A, 2016. **113**(41): p. 11537-11542.
8. Liu, Z., et al., *HIV-1 Antisense Protein of Different Clades Induces Autophagy and Associates with the Autophagy Factor p62.* J Virol, 2019. **93**(2).
9. HIVinfo.NIH.gov, *The HIV life cycle.* 2020.
10. Hladik, F. and M.J. McElrath, *Setting the stage: host invasion by HIV.* Nat Rev Immunol, 2008. **8**(6): p. 447-57.
11. Cohen, M.S., et al., *Acute HIV-1 Infection.* N Engl J Med, 2011. **364**(20): p. 1943-54.
12. Sharp, P.M. and B.H. Hahn, *Origins of HIV and the AIDS pandemic.* Cold Spring Harb Perspect Med, 2011. **1**(1): p. a006841.
13. Joseph, S.B., et al., *HIV-1 target cells in the CNS.* J Neurovirol, 2015. **21**(3): p. 276-89.
14. UNAIDS, *Global HIV & AIDS statistics 2020 factsheet.* 2020.
15. Organization, W.H., *HIV/AIDS.* 2020.
16. thewellproject, *HIV Drug Chart (Overview).* 2020.
17. Foundation, H.B., *Hepatitis B Facts and Figures* 2020.
18. Klevens, R.M., et al., *Estimating acute viral hepatitis infections from nationally reported cases.* Am J Public Health, 2014. **104**(3): p. 482-7.
19. US Department of Health and Human Services, C.f.D.C.a.P., *Centers for Disease Control and Prevention. Viral Hepatitis Surveillance—United States, 2018. Atlanta.* 2020.
20. *Viral Hepatitis, National Progress Report 2025 Goal: Reduce estimated* new hepatitis B virus infections by ≥20%.* Centers for Disease Control and Prevention, 2020.
21. Hyun Kim, B. and W. Ray Kim, *Epidemiology of Hepatitis B Virus Infection in the United States.* Clin Liver Dis (Hoboken), 2018. **12**(1): p. 1-4.
22. Organization, W.H., *Hepatitis B: Key facts.* 2020.
23. (CDC), C.f.D.C.a.P., *Perinatal Transmission.* 2020.
24. Chang, M.H. and D.S. Chen, *Prevention of hepatitis B.* Cold Spring Harb Perspect Med, 2015. **5**(3): p. a021493.

25. De Clercq, E., et al., *Antiviral treatment of chronic hepatitis B virus (HBV) infections.* Viruses, 2010. **2**(6): p. 1279-305.
26. Inoue, T. and Y. Tanaka, *Hepatitis B virus and its sexually transmitted infection - an update.* Microb Cell, 2016. **3**(9): p. 420-437.
27. Zoulim, F., *Emerging drugs for hepatitis B.* Expert Opin Emerg Drugs, 2007. **12**(2): p. 199-217.
28. Singh, L., et al., *Drug Delivery Strategies for Antivirals against Hepatitis B Virus.* Viruses, 2018. **10**(5).
29. Loglio, A. and P. Lampertico, *How Durable Is Functional Cure (Hepatitis B Surface Antigen Loss) in Patients With Chronic Hepatitis B Treated With Current Antivirals?* Hepatol Commun, 2020. **4**(1): p. 5-7.
30. Liang, T.J., *Hepatitis B: the virus and disease.* Hepatology, 2009. **49**(5 Suppl): p. S13-21.
31. Gao, W. and J. Hu, *Formation of hepatitis B virus covalently closed circular DNA: removal of genome-linked protein.* J Virol, 2007. **81**(12): p. 6164-74.
32. Allweiss, L. and M. Dandri, *The Role of cccDNA in HBV Maintenance.* Viruses, 2017. **9**(6).
33. Kostyusheva, A., et al., *Clinical Implications of Hepatitis B Virus RNA and Covalently Closed Circular DNA in Monitoring Patients with Chronic Hepatitis B Today with a Gaze into the Future: The Field Is Unprepared for a Sterilizing Cure.* Genes (Basel), 2018. **9**(10).
34. Wang, B., G. Mufti, and K. Agarwal, *Reactivation of hepatitis B virus infection in patients with hematologic disorders.* Haematologica, 2019. **104**(3): p. 435-443.
35. Suk-Fong Lok, A., *Hepatitis B Treatment: What We Know Now and What Remains to Be Researched.* Hepatol Commun, 2019. **3**(1): p. 8-19.
36. The Pharmaceutical Journal, t.R.P.S.P., *An update on the management of chronic hepatitis B and C infection.* 08/9/2017.
37. Yan, H., et al., *Sodium taurocholate cotransporting polypeptide is a functional receptor for human hepatitis B and D virus.* Elife, 2012. **1**: p. e00049.
38. Bogomolov, P., et al., *Treatment of chronic hepatitis D with the entry inhibitor myrcludex B: First results of a phase Ib/IIa study.* J Hepatol, 2016. **65**(3): p. 490-8.
39. Seto, W.K. and M.F. Yuen, *New pharmacological approaches to a functional cure of hepatitis B.* Clin Liver Dis (Hoboken), 2016. **8**(4): p. 83-88.
40. Lempp, F.A. and S. Urban, *Inhibitors of hepatitis B virus attachment and entry.* Intervirology, 2014. **57**(3-4): p. 151-7.
41. Katen, S.P., et al., *Assembly-directed antivirals differentially bind quasiequivalent pockets to modify hepatitis B virus capsid tertiary and quaternary structure.* Structure, 2013. **21**(8): p. 1406-16.
42. Brezillon, N., et al., *Antiviral activity of Bay 41-4109 on hepatitis B virus in humanized Alb-uPA/SCID mice.* PLoS One, 2011. **6**(12): p. e25096.
43. Alba, R., A. Bosch, and M. Chillon, *Gutless adenovirus: last-generation adenovirus for gene therapy.* Gene Ther, 2005. **12 Suppl 1**: p. S18-27.
44. Alonso-Padilla, J., et al., *Development of Novel Adenoviral Vectors to Overcome Challenges Observed With HAdV-5-based Constructs.* Mol Ther, 2016. **24**(1): p. 6-16.
45. Schiwon, M., et al., *One-Vector System for Multiplexed CRISPR/Cas9 against Hepatitis B Virus cccDNA Utilizing High-Capacity Adenoviral Vectors.* Mol Ther Nucleic Acids, 2018. **12**: p. 242-253.

46. Yang, H.C. and J.H. Kao, *Persistence of hepatitis B virus covalently closed circular DNA in hepatocytes: molecular mechanisms and clinical significance.* Emerg Microbes Infect, 2014. **3**(9): p. e64.

47. Ramanan, V., et al., *CRISPR/Cas9 cleavage of viral DNA efficiently suppresses hepatitis B virus.* Sci Rep, 2015. **5**: p. 10833.

48. Zhu, W., et al., *CRISPR/Cas9 produces anti-hepatitis B virus effect in hepatoma cells and transgenic mouse.* Virus Res, 2016. **217**: p. 125-32.

49. Moyo, B., et al., *Advances with using CRISPR/Cas-mediated gene editing to treat infections with hepatitis B virus and hepatitis C virus.* Virus Res, 2018. **244**: p. 311-320.

50. Wilson, E.M., L. Tang, and S. Kottilil, *Eradication Strategies for Chronic Hepatitis B Infection.* Clin Infect Dis, 2016. **62 Suppl 4**: p. S318-25.

51. Al-Mahtab, M., M. Bazinet, and A. Vaillant, *Safety and Efficacy of Nucleic Acid Polymers in Monotherapy and Combined with Immunotherapy in Treatment-Naive Bangladeshi Patients with HBeAg+ Chronic Hepatitis B Infection.* PLoS One, 2016. **11**(6): p. e0156667.

52. McCaffrey, A.P., et al., *Inhibition of hepatitis B virus in mice by RNA interference.* Nat Biotechnol, 2003. **21**(6): p. 639-44.

53. Gish, R.G., et al., *Synthetic RNAi triggers and their use in chronic hepatitis B therapies with curative intent.* Antiviral Res, 2015. **121**: p. 97-108.

54. Ezzikouri, S., et al., *Targeting Host Innate and Adaptive Immunity to Achieve the Functional Cure of Chronic Hepatitis B.* Vaccines (Basel), 2020. **8**(2).

55. Busca, A. and A. Kumar, *Innate immune responses in hepatitis B virus (HBV) infection.* Virol J, 2014. **11**: p. 22.

56. Stasi, C., C. Silvestri, and F. Voller, *Hepatitis B vaccination and immunotherapies: an update.* Clin Exp Vaccine Res, 2020. **9**(1): p. 1-7.

57. Ward, H., et al., *Treatment of hepatitis B virus: an update.* Future Microbiol, 2016. **11**: p. 1581-1597.

58. Lanford, R.E., et al., *GS-9620, an oral agonist of Toll-like receptor-7, induces prolonged suppression of hepatitis B virus in chronically infected chimpanzees.* Gastroenterology, 2013. **144**(7): p. 1508-17, 1517 e1-10.

59. Rossignol, J.F. and E.B. Keeffe, *Thiazolides: a new class of drugs for the treatment of chronic hepatitis B and C.* Future Microbiol, 2008. **3**(5): p. 539-45.

60. Rossignol, J.F., *Thiazolides: a new class of antiviral drugs.* Expert Opin Drug Metab Toxicol, 2009. **5**(6): p. 667-74.

61. Trabattoni, D., et al., *Thiazolides Elicit Anti-Viral Innate Immunity and Reduce HIV Replication.* Sci Rep, 2016. **6**: p. 27148.

62. Rossignol, J.F., *Nitazoxanide: a first-in-class broad-spectrum antiviral agent.* Antiviral Res, 2014. **110**: p. 94-103.

63. Korba, B.E., et al., *Nitazoxanide, tizoxanide and other thiazolides are potent inhibitors of hepatitis B virus and hepatitis C virus replication.* Antiviral Res, 2008. **77**(1): p. 56-63.

64. Sekiba, K., et al., *Inhibition of HBV Transcription From cccDNA With Nitazoxanide by Targeting the HBx-DDB1 Interaction.* Cell Mol Gastroenterol Hepatol, 2019. **7**(2): p. 297-312.

65. Keeffe, E.B. and J.F. Rossignol, *Treatment of chronic viral hepatitis with nitazoxanide and second generation thiazolides.* World J Gastroenterol, 2009. **15**(15): p. 1805-8.

66. U.S. National Library of Medicine, C.g., *Study of Nitazoxanide Compared to Placebo in Subjects With HBeAG-Negative Chronic Hepatitis B.* 2020.

67. Dawood, A., et al., *Drugs in Development for Hepatitis B.* Drugs, 2017. **77**(12): p. 1263-1280.

68. Rossignol, J.F. and C. Brechot, *A Pilot Clinical Trial of Nitazoxanide in the Treatment of Chronic Hepatitis B.* Hepatol Commun, 2019. **3**(6): p. 744-747.

69. Markham, A., *Bictegravir: First Global Approval.* Drugs, 2018. **78**(5): p. 601-606.

70. Rock, A.E., J. Lerner, and M.E. Badowski, *Doravirine and Its Potential in the Treatment of HIV: An Evidence-Based Review of the Emerging Data.* HIV AIDS (Auckl), 2020. **12**: p. 201-210.

71. U.S. National Library of Medicine, C.g., *Islatravir (MK-8591) With Doravirine and Lamivudine in Participants Infected With Human Immunodeficiency Virus Type 1 (MK-8591-011) (NCT03272347).* 2020.

72. U.S. National Library of Medicine, C.g., *Randomized, Double-blind, Efficacy, and Safety Study of Doravirine/Islatravir (DOR/ISL) in Treatment-naïve Participants With Human Immunodeficiency Virus Type 1 (HIV-1) Infection (MK-8591A-020).*

73. Cevik, M. and C. Orkin, *Insights into HIV-1 capsid inhibitors in preclinical and early clinical development as antiretroviral agents.* Expert Opin Investig Drugs, 2019. **28**(12): p. 1021-1024.

74. Link, J.O., et al., *Clinical targeting of HIV capsid protein with a long-acting small molecule.* Nature, 2020. **584**(7822): p. 614-618.

75. Eisele, E. and R.F. Siliciano, *Redefining the viral reservoirs that prevent HIV-1 eradication.* Immunity, 2012. **37**(3): p. 377-88.

76. Blankson, J.N., D. Persaud, and R.F. Siliciano, *The challenge of viral reservoirs in HIV-1 infection.* Annu Rev Med, 2002. **53**: p. 557-93.

77. Hong, F.F. and J.W. Mellors, *Changes in HIV reservoirs during long-term antiretroviral therapy.* Curr Opin HIV AIDS, 2015. **10**(1): p. 43-8.

78. Vanhamel, J., A. Bruggemans, and Z. Debyser, *Establishment of latent HIV-1 reservoirs: what do we really know?* J Virus Erad, 2019. **5**(1): p. 3-9.

79. Sengupta, S. and R.F. Siliciano, *Targeting the Latent Reservoir for HIV-1.* Immunity, 2018. **48**(5): p. 872-895.

80. Archin, N.M., et al., *Eradicating HIV-1 infection: seeking to clear a persistent pathogen.* Nat Rev Microbiol, 2014. **12**(11): p. 750-64.

81. Castro-Gonzalez, S., M. Colomer-Lluch, and R. Serra-Moreno, *Barriers for HIV Cure: The Latent Reservoir.* AIDS Res Hum Retroviruses, 2018. **34**(9): p. 739-759.

82. Cohn, L.B., N. Chomont, and S.G. Deeks, *The Biology of the HIV-1 Latent Reservoir and Implications for Cure Strategies.* Cell Host Microbe, 2020. **27**(4): p. 519-530.

83. Ananworanich, J., K. Dube, and N. Chomont, *How does the timing of antiretroviral therapy initiation in acute infection affect HIV reservoirs?* Curr Opin HIV AIDS, 2015. **10**(1): p. 18-28.

84. Battistini, A. and M. Sgarbanti, *HIV-1 latency: an update of molecular mechanisms and therapeutic strategies.* Viruses, 2014. **6**(4): p. 1715-58.

85. Van Lint, C., S. Bouchat, and A. Marcello, *HIV-1 transcription and latency: an update.* Retrovirology, 2013. **10**: p. 67.

86. Choudhary, S.K., et al., *Latent HIV-1 infection of resting CD4(+) T cells in the humanized Rag2(-)/(-) gammac(-)/(-) mouse.* J Virol, 2012. **86**(1): p. 114-20.

87. Kulpa, D.A. and N. Chomont, *HIV persistence in the setting of antiretroviral therapy: when, where and how does HIV hide?* J Virus Erad, 2015. **1**(2): p. 59-66.

88. Mzingwane, M.L. and C.T. Tiemessen, *Mechanisms of HIV persistence in HIV reservoirs.* Rev Med Virol, 2017. **27**(2).

89. Coffin, J. and R. Swanstrom, *HIV pathogenesis: dynamics and genetics of viral populations and infected cells.* Cold Spring Harb Perspect Med, 2013. **3**(1): p. a012526.

90. Chomont, N., et al., *HIV reservoir size and persistence are driven by T cell survival and homeostatic proliferation.* Nat Med, 2009. **15**(8): p. 893-900.

91. Barton, K., A. Winckelmann, and S. Palmer, *HIV-1 Reservoirs During Suppressive Therapy.* Trends Microbiol, 2016. **24**(5): p. 345-355.

92. Brenchley, J.M., et al., *T-cell subsets that harbor human immunodeficiency virus (HIV) in vivo: implications for HIV pathogenesis.* J Virol, 2004. **78**(3): p. 1160-8.

93. Meltzer, M.S., et al., *Macrophages as susceptible targets for HIV infection, persistent viral reservoirs in tissue, and key immunoregulatory cells that control levels of virus replication and extent of disease.* AIDS Res Hum Retroviruses, 1990. **6**(8): p. 967-71.

94. Herskovitz, J. and H.E. Gendelman, *HIV and the Macrophage: From Cell Reservoirs to Drug Delivery to Viral Eradication.* J Neuroimmune Pharmacol, 2019. **14**(1): p. 52-67.

95. McDonald, D., et al., *Recruitment of HIV and its receptors to dendritic cell-T cell junctions.* Science, 2003. **300**(5623): p. 1295-7.

96. Wong, J.K. and S.A. Yukl, *Tissue reservoirs of HIV.* Curr Opin HIV AIDS, 2016. **11**(4): p. 362-70.

97. Kahn, J.O. and B.D. Walker, *Acute human immunodeficiency virus type 1 infection.* N Engl J Med, 1998. **339**(1): p. 33-9.

98. Margolis, D.A. and M. Boffito, *Long-acting antiviral agents for HIV treatment.* Curr Opin HIV AIDS, 2015. **10**(4): p. 246-52.

99. Nachman, S., et al., *Long-acting or extended-release antiretroviral products for HIV treatment and prevention in infants, children, adolescents, and pregnant and breastfeeding women: knowledge gaps and research priorities.* Lancet HIV, 2019. **6**(8): p. e552-e558.

100. Kuritzkes, D.R., *Why cure, why now?* J Med Ethics, 2017. **43**(2): p. 67-70.

101. Jimmy, B. and J. Jose, *Patient medication adherence: measures in daily practice.* Oman Med J, 2011. **26**(3): p. 155-9.

102. Jin, J., et al., *Factors affecting therapeutic compliance: A review from the patient's perspective.* Ther Clin Risk Manag, 2008. **4**(1): p. 269-86.

103. Nachega, J.B., et al., *HIV treatment adherence, drug resistance, virologic failure: evolving concepts.* Infect Disord Drug Targets, 2011. **11**(2): p. 167-74.

104. Earnshaw, V.A., et al., *HIV stigma mechanisms and well-being among PLWH: a test of the HIV stigma framework.* AIDS Behav, 2013. **17**(5): p. 1785-95.

105. Waaijenborg, S., et al., *Waning of maternal antibodies against measles, mumps, rubella, and varicella in communities with contrasting vaccination coverage.* J Infect Dis, 2013. **208**(1): p. 10-6.

106. Simoni, J.M., et al., *Racial/Ethnic disparities in ART adherence in the United States: findings from the MACH14 study.* J Acquir Immune Defic Syndr, 2012. **60**(5): p. 466-72.

107. Kong, M.C., et al., *Association between race, depression, and antiretroviral therapy adherence in a low-income population with HIV infection.* J Gen Intern Med, 2012. **27**(9): p. 1159-64.

108. Hong, Y. and X. Li, *HIV/AIDS behavioral interventions in China: a literature review and recommendation for future research.* AIDS Behav, 2009. **13**(3): p. 603-13.

109. Langebeek, N., et al., *Predictors and correlates of adherence to combination antiretroviral therapy (ART) for chronic HIV infection: a meta-analysis.* BMC Med, 2014. **12**: p. 142.

110. Mannheimer, S., et al., *The consistency of adherence to antiretroviral therapy predicts biologic outcomes for human immunodeficiency virus-infected persons in clinical trials.* Clin Infect Dis, 2002. **34**(8): p. 1115-21.

111. Uthman, O.A., et al., *Depression and adherence to antiretroviral therapy in low-, middle- and high-income countries: a systematic review and meta-analysis.* Curr HIV/AIDS Rep, 2014. **11**(3): p. 291-307.

112. Al-Dakkak, I., et al., *The impact of specific HIV treatment-related adverse events on adherence to antiretroviral therapy: a systematic review and meta-analysis.* AIDS Care, 2013. **25**(4): p. 400-14.

113. Bachman Desilva, M., et al., *Feasibility and Acceptability of a Real-Time Adherence Device among HIV-Positive IDU Patients in China.* AIDS Res Treat, 2013. **2013**: p. 957862.

114. Haberer, J.E., et al., *Realtime adherence monitoring of antiretroviral therapy among HIV-infected adults and children in rural Uganda.* AIDS, 2013. **27**(13): p. 2166-8.

115. Safi, S., T. Thiessen, and K.J. Schmailzl, *Acceptance and Resistance of New Digital Technologies in Medicine: Qualitative Study.* JMIR Res Protoc, 2018. **7**(12): p. e11072.

116. Havlir, D. and M. Gandhi, *Implementation challenges for long-acting antivirals as treatment.* Curr Opin HIV AIDS, 2015. **10**(4): p. 282-9.

117. Siegel, S.J., *Extended release drug delivery strategies in psychiatry: theory to practice.* Psychiatry (Edgmont), 2005. **2**(6): p. 22-31.

118. Rana, A.I., et al., *Advances in Long-Acting Agents for the Treatment of HIV Infection.* Drugs, 2020. **80**(6): p. 535-545.

119. Wen, H., H. Jung, and X. Li, *Drug Delivery Approaches in Addressing Clinical Pharmacology-Related Issues: Opportunities and Challenges.* AAPS J, 2015. **17**(6): p. 1327-40.

120. Puri, A., et al., *Development of a Transdermal Delivery System for Tenofovir Alafenamide, a Prodrug of Tenofovir with Potent Antiviral Activity Against HIV and HBV.* Pharmaceutics, 2019. **11**(4).

121. Haddad, P.M., C. Brain, and J. Scott, *Nonadherence with antipsychotic medication in schizophrenia: challenges and management strategies.* Patient Relat Outcome Meas, 2014. **5**: p. 43-62.

122. Williams, J., et al., *Long-acting parenteral nanoformulated antiretroviral therapy: interest and attitudes of HIV-infected patients.* Nanomedicine (Lond), 2013. **8**(11): p. 1807-13.

123. Jacobson, J.M. and C.W. Flexner, *Universal antiretroviral regimens: thinking beyond one-pill-once-a-day.* Curr Opin HIV AIDS, 2017. **12**(4): p. 343-350.

124. Winston, D.J., et al., *Recombinant interferon alpha-2a for treatment of herpes zoster in immunosuppressed patients with cancer.* Am J Med, 1988. **85**(2): p. 147-51.

125. Kane, J.M., et al., *Patients With Early-Phase Schizophrenia Will Accept Treatment With Sustained-Release Medication (Long-Acting Injectable Antipsychotics): Results From the Recruitment Phase of the PRELAPSE Trial.* J Clin Psychiatry, 2019. **80**(3).

126. Crandall, C.J., et al., *Comparative effectiveness of pharmacologic treatments to prevent fractures: an updated systematic review.* Ann Intern Med, 2014. **161**(10): p. 711-23.

127. Sheikh, V., J.S. Murray, and A. Sherwat, *Ibalizumab in Multidrug-Resistant HIV - Accepting Uncertainty.* N Engl J Med, 2018. **379**(7): p. 605-607.

128. U.S. Food and Drug Administration, H.D.o.H.a.H.S., *Edurant (Rilpivirine) Tablets, Drug Approval Package.* 2013.

129. Molina, J.M., et al., *Rilpivirine versus efavirenz with tenofovir and emtricitabine in treatment-naive adults infected with HIV-1 (ECHO): a phase 3 randomised double-blind active-controlled trial.* Lancet, 2011. **378**(9787): p. 238-46.

130. Verloes, R., et al., *Safety, tolerability and pharmacokinetics of rilpivirine following administration of a long-acting formulation in healthy volunteers.* HIV Med, 2015. **16**(8): p. 477-84.

131. Yoshinaga, T., et al., *Antiviral characteristics of GSK1265744, an HIV integrase inhibitor dosed orally or by long-acting injection.* Antimicrob Agents Chemother, 2015. **59**(1): p. 397-406.

132. Hassounah, S.A., et al., *Antiviral Activity of Bictegravir and Cabotegravir against Integrase Inhibitor-Resistant SIVmac239 and HIV-1.* Antimicrob Agents Chemother, 2017. **61**(12).

133. Spreen, W., et al., *GSK1265744 pharmacokinetics in plasma and tissue after single-dose long-acting injectable administration in healthy subjects.* J Acquir Immune Defic Syndr, 2014. **67**(5): p. 481-6.

134. Fernandez, C. and C.L. van Halsema, *Evaluating cabotegravir/rilpivirine long-acting, injectable in the treatment of HIV infection: emerging data and therapeutic potential.* HIV AIDS (Auckl), 2019. **11**: p. 179-192.

135. U.S. National Library of Medicine, C.g., *Study to Evaluate the Efficacy, Safety, and Tolerability of Long-acting Intramuscular Cabotegravir and Rilpivirine for Maintenance of Virologic Suppression Following Switch From an Integrase Inhibitor in HIV-1 Infected Therapy Naive Participants (NCT02938520).* 2020.

136. U.S. National Library of Medicine, C.g., *Study Evaluating the Efficacy, Safety, and Tolerability of Switching to Long-acting Cabotegravir Plus Long-acting Rilpivirine From Current Antiretroviral Regimen in Virologically Suppressed HIV-1-infected Adults.* 2020.

137. Organization, W.H., *Trial results reveal that long-acting injectable cabotegravir as PrEP is highly effective in preventing HIV acquisition in women.* 2020.

138. Healthcare, V., *ViiV Healthcare receives complete response letter from US FDA for use of investigational cabotegravir and rilpivirine long-acting regimen in the treatment of HIV.* 2020.

139. Healthcare, V., *ViiV Healthcare announces first global regulatory approval of CABENUVA; the first complete, long-acting, regimen for the treatment of HIV.* 2020.

140. Zhang, H., et al., *Combination of long-acting HIV fusion inhibitor albuvirtide and LPV/r showed potent efficacy in HIV-1 patients.* AIDS Res Ther, 2016. **13**: p. 8.

141. Schurmann, D., et al., *Safety, pharmacokinetics, and antiretroviral activity of islatravir (ISL, MK-8591), a novel nucleoside reverse transcriptase translocation inhibitor, following single-dose administration to treatment-naive adults infected with HIV-1: an open-label, phase 1b, consecutive-panel trial.* Lancet HIV, 2020. **7**(3): p. e164-e172.

142. *Merck Advances Phase 3 Trial to Evaluate Investigational Islatravir as Once-Monthly Oral PrEP for Women at High Risk for Acquiring HIV-1.* Merck.

143. Schoen, J.C., K.M. Erlandson, and P.L. Anderson, *Clinical pharmacokinetics of antiretroviral drugs in older persons.* Expert Opin Drug Metab Toxicol, 2013. **9**(5): p. 573-88.

144. Edagwa, B., et al., *Long-acting slow effective release antiretroviral therapy.* Expert Opin Drug Deliv, 2017. **14**(11): p. 1281-1291.

145. Rautio, J., et al., *The expanding role of prodrugs in contemporary drug design and development.* Nat Rev Drug Discov, 2018. **17**(8): p. 559-587.

146. Huttunen, K.M. and J. Rautio, *Prodrugs - an efficient way to breach delivery and targeting barriers.* Curr Top Med Chem, 2011. **11**(18): p. 2265-87.

147. Alexaki, A., Y. Liu, and B. Wigdahl, *Cellular reservoirs of HIV-1 and their role in viral persistence.* Curr HIV Res, 2008. **6**(5): p. 388-400.

148. Nowacek, A.S., et al., *Nanoformulated antiretroviral drug combinations extend drug release and antiretroviral responses in HIV-1-infected macrophages: implications for neuroAIDS therapeutics.* J Neuroimmune Pharmacol, 2010. **5**(4): p. 592-601.

149. Puligujja, P., et al., *Macrophage folate receptor-targeted antiretroviral therapy facilitates drug entry, retention, antiretroviral activities and biodistribution for reduction of human immunodeficiency virus infections.* Nanomedicine, 2013. **9**(8): p. 1263-73.

150. Puligujja, P., et al., *Pharmacodynamics of long-acting folic acid-receptor targeted ritonavir-boosted atazanavir nanoformulations.* Biomaterials, 2015. **41**: p. 141-50.

151. Ramana, L.N., et al., *Stealth anti-CD4 conjugated immunoliposomes with dual antiretroviral drugs--modern Trojan horses to combat HIV.* Eur J Pharm Biopharm, 2015. **89**: p. 300-11.

152. Gautam, N., et al., *Pharmacokinetics, biodistribution, and toxicity of folic acid-coated antiretroviral nanoformulations.* Antimicrob Agents Chemother, 2014. **58**(12): p. 7510-9.

153. Mofenson, L.M., et al., *Guidelines for the Prevention and Treatment of Opportunistic Infections among HIV-exposed and HIV-infected children: recommendations from CDC, the National Institutes of Health, the HIV Medicine Association of the Infectious Diseases Society of America, the Pediatric Infectious Diseases Society, and the American Academy of Pediatrics.* MMWR Recomm Rep, 2009. **58**(RR-11): p. 1-166.

154. Weld, E.D. and C. Flexner, *Long-acting implants to treat and prevent HIV infection.* Curr Opin HIV AIDS, 2020. **15**(1): p. 33-41.

155. Stewart, S.A., et al., *Implantable Polymeric Drug Delivery Devices: Classification, Manufacture, Materials, and Clinical Applications.* Polymers (Basel), 2018. **10**(12).

156. Gunawardana, M., et al., *Pharmacokinetics of long-acting tenofovir alafenamide (GS-7340) subdermal implant for HIV prophylaxis.* Antimicrob Agents Chemother, 2015. **59**(7): p. 3913-9.

157. Anderson, P.L., et al., *Emtricitabine-tenofovir concentrations and pre-exposure prophylaxis efficacy in men who have sex with men.* Sci Transl Med, 2012. **4**(151): p. 151ra125.

158. Chua, C.Y.X., et al., *Transcutaneously refillable nanofluidic implant achieves sustained level of tenofovir diphosphate for HIV pre-exposure prophylaxis.* J Control Release, 2018. **286**: p. 315-325.

159. Markowitz, M. and S.G. Sarafianos, *4'-Ethynyl-2-fluoro-2'-deoxyadenosine, MK-8591: a novel HIV-1 reverse transcriptase translocation inhibitor.* Curr Opin HIV AIDS, 2018. **13**(4): p. 294-299.

160. Kovarova, M., et al., *Ultra-long-acting removable drug delivery system for HIV treatment and prevention.* Nat Commun, 2018. **9**(1): p. 4156.

161. Baum, M.M., et al., *An intravaginal ring for the simultaneous delivery of multiple drugs.* J Pharm Sci, 2012. **101**(8): p. 2833-43.

162.   Jacobstein, R. and H. Stanley, *Contraceptive implants: providing better choice to meet growing family planning demand.* Glob Health Sci Pract, 2013. **1**(1): p. 11-7.

163.   Caskey, M., F. Klein, and M.C. Nussenzweig, *Broadly Neutralizing Antibodies for HIV-1 Prevention or Immunotherapy.* N Engl J Med, 2016. **375**(21): p. 2019-2021.

164.   Caskey, M., F. Klein, and M.C. Nussenzweig, *Broadly neutralizing anti-HIV-1 monoclonal antibodies in the clinic.* Nat Med, 2019. **25**(4): p. 547-553.

165.   Miller, M.S., et al., *Neutralizing antibodies against previously encountered influenza virus strains increase over time: a longitudinal analysis.* Sci Transl Med, 2013. **5**(198): p. 198ra107.

166.   Mehandru, S., et al., *Adjunctive passive immunotherapy in human immunodeficiency virus type 1-infected individuals treated with antiviral therapy during acute and early infection.* J Virol, 2007. **81**(20): p. 11016-31.

167.   Chen, W. and D.S. Dimitrov, *Human monoclonal antibodies and engineered antibody domains as HIV-1 entry inhibitors.* Curr Opin HIV AIDS, 2009. **4**(2): p. 112-7.

168.   Halper-Stromberg, A. and M.C. Nussenzweig, *Towards HIV-1 remission: potential roles for broadly neutralizing antibodies.* J Clin Invest, 2016. **126**(2): p. 415-23.

169.   Klein, F., et al., *HIV therapy by a combination of broadly neutralizing antibodies in humanized mice.* Nature, 2012. **492**(7427): p. 118-22.

170.   Liu, Y., et al., *Broadly neutralizing antibodies for HIV-1: efficacies, challenges and opportunities.* Emerg Microbes Infect, 2020. **9**(1): p. 194-206.

171.   Hendriks, J. and S. Blume, *Measles vaccination before the measles-mumps-rubella vaccine.* Am J Public Health, 2013. **103**(8): p. 1393-401.

172.   Montefiori, D.C., *Bispecific Antibodies Against HIV.* Cell, 2016. **165**(7): p. 1563-1564.

173.   Robbie, G.J., et al., *A novel investigational Fc-modified humanized monoclonal antibody, motavizumab-YTE, has an extended half-life in healthy adults.* Antimicrob Agents Chemother, 2013. **57**(12): p. 6147-53.

174.   Ko, S.Y., et al., *Enhanced neonatal Fc receptor function improves protection against primate SHIV infection.* Nature, 2014. **514**(7524): p. 642-5.

175.   Nguyen, T.T., et al., *Progress in microneedle array patch (MAP) for vaccine delivery.* Hum Vaccin Immunother, 2020: p. 1-12.

176.   Vora, L.K., et al., *Novel bilayer dissolving microneedle arrays with concentrated PLGA nano-microparticles for targeted intradermal delivery: Proof of concept.* J Control Release, 2017. **265**: p. 93-101.

177.   Kennedy, J., et al., *In vivo studies investigating biodistribution of nanoparticle-encapsulated rhodamine B delivered via dissolving microneedles.* J Control Release, 2017. **265**: p. 57-65.

178.   Golla, S., et al., *Virtual design of chemical penetration enhancers for transdermal drug delivery.* Chem Biol Drug Des, 2012. **79**(4): p. 478-87.

179.   Nguyen, T.T. and J.H. Park, *Human studies with microneedles for evaluation of their efficacy and safety.* Expert Opin Drug Deliv, 2018. **15**(3): p. 235-245.

180.   Mc Crudden, M.T.C., et al., *Design, formulation and evaluation of novel dissolving microarray patches containing a long-acting rilpivirine nanosuspension.* J Control Release, 2018. **292**: p. 119-129.

181.   Sun, B. and Y. Yeo, *Nanocrystals for the parenteral delivery of poorly water-soluble drugs.* Curr Opin Solid State Mater Sci, 2012. **16**(6): p. 295-301.

182.   Fletcher, C.V., et al., *Persistent HIV-1 replication is associated with lower antiretroviral drug concentrations in lymphatic tissues.* Proc Natl Acad Sci U S A, 2014. **111**(6): p. 2307-12.

183. Organization, W.H., *European Medicines Agency (EMA) approval of the dapivirine ring for HIV prevention for women in high HIV burden settings.* 2020.

184. Montgomery, E.T., et al., *Acceptability and use of a dapivirine vaginal ring in a phase III trial.* AIDS, 2017. **31**(8): p. 1159-1167.

185. Nel, A., et al., *Safety and Efficacy of a Dapivirine Vaginal Ring for HIV Prevention in Women.* N Engl J Med, 2016. **375**(22): p. 2133-2143.

186. Baeten, J.M., et al., *Use of a Vaginal Ring Containing Dapivirine for HIV-1 Prevention in Women.* N Engl J Med, 2016. **375**(22): p. 2121-2132.

187. Binford, M.C., S.Y. Kahana, and F.L. Altice, *A systematic review of antiretroviral adherence interventions for HIV-infected people who use drugs.* Curr HIV/AIDS Rep, 2012. **9**(4): p. 287-312.

188. sure., D.c.K.m.B., *HIV & AIDS Update: New Treatments, Easier Options.* 2020.

189. Nachega, J.B., et al., *Treatment simplification in HIV-infected adults as a strategy to prevent toxicity, improve adherence, quality of life and decrease healthcare costs.* Patient Prefer Adherence, 2011. **5**: p. 357-67.

190. Tripathi, K. and J.D. Feuerstein, *New developments in ulcerative colitis: latest evidence on management, treatment, and maintenance.* Drugs Context, 2019. **8**: p. 212572.

191. Kirtane, A.R., et al., *Development of an oral once-weekly drug delivery system for HIV antiretroviral therapy.* Nat Commun, 2018. **9**(1): p. 2.

192. Kermanizadeh, A., et al., *Nanodelivery systems and stabilized solid-drug nanoparticles for orally administered medicine: current landscape.* Int J Nanomedicine, 2018. **13**: p. 7575-7605.

193. Sun, Y. and S. Soh, *Printing Tablets with Fully Customizable Release Profiles for Personalized Medicine.* Adv Mater, 2015. **27**(47): p. 7847-53.

194. Khaled, S.A., et al., *Desktop 3D printing of controlled release pharmaceutical bilayer tablets.* Int J Pharm, 2014. **461**(1-2): p. 105-11.

195. Sacks, S.L., et al., *Clinical efficacy of topical docosanol 10% cream for herpes simplex labialis: A multicenter, randomized, placebo-controlled trial.* J Am Acad Dermatol, 2001. **45**(2): p. 222-30.

196. Leung, D.T. and S.L. Sacks, *Docosanol: a topical antiviral for herpes labialis.* Expert Opin Pharmacother, 2004. **5**(12): p. 2567-71.

197. Barnhart, M., *Long-Acting HIV Treatment and Prevention: Closer to the Threshold.* Glob Health Sci Pract, 2017. **5**(2): p. 182-187.

198. Andrews, C.D. and W. Heneine, *Cabotegravir long-acting for HIV-1 prevention.* Curr Opin HIV AIDS, 2015. **10**(4): p. 258-63.

199. Benitez-Gutierrez, L., et al., *Treatment and prevention of HIV infection with long-acting antiretrovirals.* Expert Rev Clin Pharmacol, 2018. **11**(5): p. 507-517.

200. Landovitz, R.J., R. Kofron, and M. McCauley, *The promise and pitfalls of long-acting injectable agents for HIV prevention.* Curr Opin HIV AIDS, 2016. **11**(1): p. 122-8.

201. Citrome, L., *New second-generation long-acting injectable antipsychotics for the treatment of schizophrenia.* Expert Rev Neurother, 2013. **13**(7): p. 767-83.

202. Vyas, T.K., L. Shah, and M.M. Amiji, *Nanoparticulate drug carriers for delivery of HIV/AIDS therapy to viral reservoir sites.* Expert Opin Drug Deliv, 2006. **3**(5): p. 613-28.

203. Tagar, E., et al., *Multi-country analysis of treatment costs for HIV/AIDS (MATCH): facility-level ART unit cost analysis in Ethiopia, Malawi, Rwanda, South Africa and Zambia.* PLoS One, 2014. **9**(11): p. e108304.

204. Sosnik, A., D.A. Chiappetta, and A.M. Carcaboso, *Drug delivery systems in HIV pharmacotherapy: what has been done and the challenges standing ahead.* J Control Release, 2009. **138**(1): p. 2-15.

205. Kirtane, A.R., R. Langer, and G. Traverso, *Past, Present, and Future Drug Delivery Systems for Antiretrovirals.* J Pharm Sci, 2016. **105**(12): p. 3471-3482.

206. Zhou, T., et al., *Creation of a nanoformulated cabotegravir prodrug with improved antiretroviral profiles.* Biomaterials, 2018. **151**: p. 53-65.

207. Sillman, B., et al., *Creation of a long-acting nanoformulated dolutegravir.* Nat Commun, 2018. **9**(1): p. 443.

208. Rautio, J., et al., *Prodrug approaches for CNS delivery.* AAPS J, 2008. **10**(1): p. 92-102.

209. Sozio, P., et al., *Designing prodrugs for the treatment of Parkinson's disease.* Expert Opin Drug Discov, 2012. **7**(5): p. 385-406.

210. Lee, J.B., et al., *Lipophilic activated ester prodrug approach for drug delivery to the intestinal lymphatic system.* J Control Release, 2018. **286**: p. 10-19.

211. Stella, V.J. and K.W. Nti-Addae, *Prodrug strategies to overcome poor water solubility.* Adv Drug Deliv Rev, 2007. **59**(7): p. 677-94.

212. Ettmayer, P., et al., *Lessons learned from marketed and investigational prodrugs.* J Med Chem, 2004. **47**(10): p. 2393-404.

213. Albert, A., *Chemical aspects of selective toxicity.* Nature, 1958. **182**(4633): p. 421-2.

214. Stella, V.J., W.N. Charman, and V.H. Naringrekar, *Prodrugs. Do they have advantages in clinical practice?* Drugs, 1985. **29**(5): p. 455-73.

215. Jana, S., S. Mandlekar, and P. Marathe, *Prodrug design to improve pharmacokinetic and drug delivery properties: challenges to the discovery scientists.* Curr Med Chem, 2010. **17**(32): p. 3874-908.

216. Clas, S.D., R.I. Sanchez, and R. Nofsinger, *Chemistry-enabled drug delivery (prodrugs): recent progress and challenges.* Drug Discov Today, 2014. **19**(1): p. 79-87.

217. Andrews, C.D., et al., *Long-acting integrase inhibitor protects macaques from intrarectal simian/human immunodeficiency virus.* Science, 2014. **343**(6175): p. 1151-4.

218. Kadiu, I., et al., *Macrophage endocytic trafficking of antiretroviral nanoparticles.* Nanomedicine (Lond), 2011. **6**(6): p. 975-94.

219. Barnhart, M. and J.D. Shelton, *ARVs: the next generation. Going boldly together to new frontiers of HIV treatment.* Glob Health Sci Pract, 2015. **3**(1): p. 1-11.

220. Kudalkar, S.N., et al., *From in silico hit to long-acting late-stage preclinical candidate to combat HIV-1 infection.* Proc Natl Acad Sci U S A, 2018. **115**(4): p. E802-E811.

221. Singh, D., et al., *Development and characterization of a long-acting nanoformulated abacavir prodrug.* Nanomedicine (Lond), 2016. **11**(15): p. 1913-27.

222. Guo, D., et al., *Creation of a Long-Acting Nanoformulated 2',3'-Dideoxy-3'-Thiacytidine.* J Acquir Immune Defic Syndr, 2017. **74**(3): p. e75-e83.

223. Lin, Z., et al., *ProTide generated long-acting abacavir nanoformulations.* Chem Commun (Camb), 2018. **54**(60): p. 8371-8374.

224. Piantadosi, C., et al., *Synthesis and evaluation of novel ether lipid nucleoside conjugates for anti-HIV-1 activity.* J Med Chem, 1991. **34**(4): p. 1408-14.

225. Marcelletti, J.F., *Synergistic inhibition of herpesvirus replication by docosanol and antiviral nucleoside analogs.* Antiviral Res, 2002. **56**(2): p. 153-66.

226. Katz, D.H., et al., *n-docosanol: broad spectrum anti-viral activity against lipid-enveloped viruses.* Ann N Y Acad Sci, 1994. **724**: p. 472-88.

227. Gupta, D., et al., *Chemical and enzymatic stability of amino acid prodrugs containing methoxy, ethoxy and propylene glycol linkers.* Mol Pharm, 2009. **6**(5): p. 1604-11.

228. Gendelman, H.E., et al., *Efficient isolation and propagation of human immunodeficiency virus on recombinant colony-stimulating factor 1-treated monocytes.* J Exp Med, 1988. **167**(4): p. 1428-41.

229. Mosmann, T., *Rapid colorimetric assay for cellular growth and survival: application to proliferation and cytotoxicity assays.* J Immunol Methods, 1983. **65**(1-2): p. 55-63.

230. Balkundi, S., et al., *Comparative manufacture and cell-based delivery of antiretroviral nanoformulations.* Int J Nanomedicine, 2011. **6**: p. 3393-404.

231. Kalter, D.C., et al., *Enhanced HIV replication in macrophage colony-stimulating factor-treated monocytes.* J Immunol, 1991. **146**(1): p. 298-306.

232. McGuigan, C., et al., *Application of phosphoramidate pronucleotide technology to abacavir leads to a significant enhancement of antiviral potency.* J Med Chem, 2005. **48**(10): p. 3504-15.

233. Irby, D., C. Du, and F. Li, *Lipid-Drug Conjugate for Enhancing Drug Delivery.* Mol Pharm, 2017. **14**(5): p. 1325-1338.

234. Banerjee, S. and A. Kundu, *Lipid-drug conjugates: a potential nanocarrier system for oral drug delivery applications.* Daru, 2018. **26**(1): p. 65-75.

235. Bahar, F.G., et al., *Species difference of esterase expression and hydrolase activity in plasma.* J Pharm Sci, 2012. **101**(10): p. 3979-88.

236. Zhou, T., et al., *Optimizing the preparation and stability of decorated antiretroviral drug nanocrystals.* Nanomedicine (Lond), 2018. **13**(8): p. 871-885.

237. Kakuda, T.N., *Pharmacology of nucleoside and nucleotide reverse transcriptase inhibitor-induced mitochondrial toxicity.* Clin Ther, 2000. **22**(6): p. 685-708.

238. Edagwa, B.J., et al., *Development of HIV reservoir targeted long acting nanoformulated antiretroviral therapies.* Curr Med Chem, 2014. **21**(36): p. 4186-98.

239. Molina, J.M. and S.L. Cox, *Emtricitabine: a novel nucleoside reverse transcriptase inhibitor.* Drugs Today (Barc), 2005. **41**(4): p. 241-52.

240. Masho, S.W., C.L. Wang, and D.E. Nixon, *Review of tenofovir-emtricitabine.* Ther Clin Risk Manag, 2007. **3**(6): p. 1097-104.

241. *Drug and Device News.* P T, 2018. **43**(4): p. 194-246.

242. McMillan, J., et al., *Pharmacokinetics of a Long-Acting Nanoformulated Dolutegravir Prodrug in Rhesus Macaques.* Antimicrob Agents Chemother, 2018. **62**(1).

243. Edagwa, B., et al., *Long-acting slow effective release antiretroviral therapy.* Expert Opin Drug Deliv, 2017: p. 1-11.

244. Singh, L., et al., *The role of nanotechnology in the treatment of viral infections.* Ther Adv Infect Dis, 2017. **4**(4): p. 105-131.

245. Sinokrot, H., et al., *Advanced Prodrug Strategies in Nucleoside and Non-Nucleoside Antiviral Agents: A Review of the Recent Five Years.* Molecules, 2017. **22**(10).

246. Gautam, N., et al., *Preclinical pharmacokinetics and tissue distribution of long-acting nanoformulated antiretroviral therapy.* Antimicrob Agents Chemother, 2013. **57**(7): p. 3110-20.

247. Trezza, C., et al., *Formulation and pharmacology of long-acting cabotegravir.* Curr Opin HIV AIDS, 2015. **10**(4): p. 239-45.

248. Jackson, A. and I. McGowan, *Long-acting rilpivirine for HIV prevention.* Curr Opin HIV AIDS, 2015. **10**(4): p. 253-7.

249. van 't Klooster, G., et al., *Pharmacokinetics and disposition of rilpivirine (TMC278) nanosuspension as a long-acting injectable antiretroviral formulation.* Antimicrob Agents Chemother, 2010. **54**(5): p. 2042-50.

250. Williams, P.E., H.M. Crauwels, and E.D. Basstanie, *Formulation and pharmacology of long-acting rilpivirine.* Curr Opin HIV AIDS, 2015. **10**(4): p. 233-8.

251. Rabinow, B.E., *Nanosuspensions in drug delivery.* Nat Rev Drug Discov, 2004. **3**(9): p. 785-96.

252. Arainga, M., et al., *A mature macrophage is a principal HIV-1 cellular reservoir in humanized mice after treatment with long acting antiretroviral therapy.* Retrovirology, 2017. **14**(1): p. 17.

253. Gnanadhas, D.P., et al., *Autophagy facilitates macrophage depots of sustained-release nanoformulated antiretroviral drugs.* J Clin Invest, 2017. **127**(3): p. 857-873.

254. Thomas, M.B., et al., *Modulating cellular autophagy for controlled antiretroviral drug release.* Nanomedicine (Lond), 2018.

255. Birkus, G., et al., *Activation of 9-[(R)-2-[[(S)-[[(S)-1-(Isopropoxycarbonyl)ethyl]amino] phenoxyphosphinyl]-methoxy]propyl]adenine (GS-7340) and other tenofovir phosphonoamidate prodrugs by human proteases.* Mol Pharmacol, 2008. **74**(1): p. 92-100.

256. Birkus, G., et al., *Cathepsin A is the major hydrolase catalyzing the intracellular hydrolysis of the antiretroviral nucleotide phosphonoamidate prodrugs GS-7340 and GS-9131.* Antimicrob Agents Chemother, 2007. **51**(2): p. 543-50.

257. Jarvis, M., V. Krishnan, and S. Mitragotri, *Nanocrystals: A perspective on translational research and clinical studies.* Bioeng Transl Med, 2019. **4**(1): p. 5-16.

258. Gigliobianco, M.R., et al., *Nanocrystals of Poorly Soluble Drugs: Drug Bioavailability and Physicochemical Stability.* Pharmaceutics, 2018. **10**(3).

259. Gao, W., et al., *Exploring intracellular fate of drug nanocrystals with crystal-integrated and environment-sensitive fluorophores.* J Control Release, 2017. **267**: p. 214-222.

260. Elazzouzi-Hafraoui, S., et al., *The shape and size distribution of crystalline nanoparticles prepared by acid hydrolysis of native cellulose.* Biomacromolecules, 2008. **9**(1): p. 57-65.

261. Slusarczyk, M., M. Serpi, and F. Pertusati, *Phosphoramidates and phosphonamidates (ProTides) with antiviral activity.* Antivir Chem Chemother, 2018. **26**: p. 2040206618775243.

262. Mehellou, Y., H.S. Rattan, and J. Balzarini, *The ProTide Prodrug Technology: From the Concept to the Clinic.* J Med Chem, 2018. **61**(6): p. 2211-2226.

263. Prochazkova, E., et al., *Reactive cyclic intermediates in the ProTide prodrugs activation: trapping the elusive pentavalent phosphorane.* Org Biomol Chem, 2019. **17**(2): p. 315-320.

264. Okon, A., et al., *Anchimerically Activated ProTides as Inhibitors of Cap-Dependent Translation and Inducers of Chemosensitization in Mantle Cell Lymphoma.* J Med Chem, 2017. **60**(19): p. 8131-8144.

265. Pantaleo, G., et al., *HIV infection is active and progressive in lymphoid tissue during the clinically latent stage of disease.* Nature, 1993. **362**(6418): p. 355-8.

266. Embretson, J., et al., *Massive covert infection of helper T lymphocytes and macrophages by HIV during the incubation period of AIDS.* Nature, 1993. **362**(6418): p. 359-62.

267. McGuigan, C., et al., *Phosphoramidate ProTides of 2'-C-methylguanosine as highly potent inhibitors of hepatitis C virus. Study of their in vitro and in vivo properties.* J Med Chem, 2010. **53**(13): p. 4949-57.

268. Song, H., et al., *Pharmacokinetics of amino acid phosphoramidate monoesters of zidovudine in rats.* Antimicrob Agents Chemother, 2002. **46**(5): p. 1357-63.

269. Grande, F., et al., *Reverse Transcriptase Inhibitors Nanosystems Designed for Drug Stability and Controlled Delivery.* Pharmaceutics, 2019. **11**(5).

270. Holec, A.D., et al., *Nucleotide Reverse Transcriptase Inhibitors: A Thorough Review, Present Status and Future Perspective as HIV Therapeutics.* Curr HIV Res, 2017. **15**(6): p. 411-421.

271. Halling Folkmar Andersen, A. and M. Tolstrup, *The Potential of Long-Acting, Tissue-Targeted Synthetic Nanotherapy for Delivery of Antiviral Therapy Against HIV Infection.* Viruses, 2020. **12**(4).

272. Aquaro, S., et al., *Mechanisms underlying of antiretroviral drugs in different cellular reservoirs with a focus on macrophages.* Virulence, 2020. **11**(1): p. 400-413.

273. Eastman, R.T., et al., *Remdesivir: A Review of Its Discovery and Development Leading to Emergency Use Authorization for Treatment of COVID-19.* ACS Cent Sci, 2020. **6**(5): p. 672-683.

274. Pruijssers, A.J. and M.R. Denison, *Nucleoside analogues for the treatment of coronavirus infections.* Curr Opin Virol, 2019. **35**: p. 57-62.

275. Tamargo, J., J.Y. Le Heuzey, and P. Mabo, *Narrow therapeutic index drugs: a clinical pharmacological consideration to flecainide.* Eur J Clin Pharmacol, 2015. **71**(5): p. 549-67.

276. Chaudhuri, S., J.A. Symons, and J. Deval, *Innovation and trends in the development and approval of antiviral medicines: 1987-2017 and beyond.* Antiviral Res, 2018. **155**: p. 76-88.

277. Soni, D., et al., *Synthesis of a long acting nanoformulated emtricitabine ProTide.* Biomaterials, 2019. **222**: p. 119441.

278. Smith, N., et al., *A long acting nanoformulated lamivudine ProTide.* Biomaterials, 2019. **223**: p. 119476.

279. Ibrahim, I.M., et al., *Synthesis and characterization of a long-acting emtricitabine prodrug nanoformulation.* Int J Nanomedicine, 2019. **14**: p. 6231-6247.

280. Din, F.U., et al., *Effective use of nanocarriers as drug delivery systems for the treatment of selected tumors.* Int J Nanomedicine, 2017. **12**: p. 7291-7309.

281. Permana, A.D., et al., *Solid lipid nanoparticle-based dissolving microneedles: A promising intradermal lymph targeting drug delivery system with potential for enhanced treatment of lymphatic filariasis.* J Control Release, 2019. **316**: p. 34-52.

282. Savla, R., et al., *Review and analysis of FDA approved drugs using lipid-based formulations.* Drug Dev Ind Pharm, 2017. **43**(11): p. 1743-1758.

283. Nowacek, A. and H.E. Gendelman, *NanoART, neuroAIDS and CNS drug delivery.* Nanomedicine (Lond), 2009. **4**(5): p. 557-74.

284. Cao, S. and K.A. Woodrow, *Nanotechnology approaches to eradicating HIV reservoirs.* Eur J Pharm Biopharm, 2019. **138**: p. 48-63.

285. Danaei, M., et al., *Impact of Particle Size and Polydispersity Index on the Clinical Applications of Lipidic Nanocarrier Systems.* Pharmaceutics, 2018. **10**(2).

286. Sadeghi, A., et al., *Rapid expansion of T cells: Effects of culture and cryopreservation and importance of short-term cell recovery.* Acta Oncol, 2013. **52**(5): p. 978-86.

287. Mallone, R., et al., *Isolation and preservation of peripheral blood mononuclear cells for analysis of islet antigen-reactive T cell responses: position statement of the T-Cell Workshop Committee of the Immunology of Diabetes Society.* Clin Exp Immunol, 2011. **163**(1): p. 33-49.

288. Zhang, X., et al., *Peripheral blood mononuclear cells show prominent gene expression by erythroid progenitors in diseases characterized by heightened erythropoiesis.* Br J Haematol, 2020. **190**(1): p. e42-e45.

289. Warren, R.L., et al., *Exhaustive T-cell repertoire sequencing of human peripheral blood samples reveals signatures of antigen selection and a directly measured repertoire size of at least 1 million clonotypes.* Genome Res, 2011. **21**(5): p. 790-7.

290. Hanamsagar, R., et al., *An optimized workflow for single-cell transcriptomics and repertoire profiling of purified lymphocytes from clinical samples.* Sci Rep, 2020. **10**(1): p. 2219.

291. Coelho, L.E., et al., *Pre-exposure prophylaxis 2.0: new drugs and technologies in the pipeline.* Lancet HIV, 2019. **6**(11): p. e788-e799.

292. Matos de Souza, M.R., et al., *In Vitro and In Vivo Characterization of the Anti-Zika Virus Activity of ProTides of 2'-C-beta-Methylguanosine.* ACS Infect Dis, 2020. **6**(7): p. 1650-1658.

293. Choy, C.J., et al., *Second-Generation Tunable pH-Sensitive Phosphoramidate-Based Linkers for Controlled Release.* Bioconjug Chem, 2016. **27**(9): p. 2206-13.

294. Dash, P.K., et al., *Sequential LASER ART and CRISPR Treatments Eliminate HIV-1 in a Subset of Infected Humanized Mice.* Nat Commun, 2019. **10**(1): p. 2753.

295. Mehellou, Y., *The ProTides Boom.* ChemMedChem, 2016. **11**(11): p. 1114-6.

296. McGuigan, C., et al., *Synthesis and anti-HIV activity of some haloalkyl phosphoramidate derivatives of 3'-azido-3'-deoxythymidine (AZT): potent activity of the trichloroethyl methoxyalaninyl compound.* Antiviral Res, 1991. **15**(3): p. 255-63.

297. Nikitina, E., et al., *Monocytes and Macrophages as Viral Targets and Reservoirs.* Int J Mol Sci, 2018. **19**(9).

298. Ahire, E., et al., *Parenteral nanosuspensions: a brief review from solubility enhancement to more novel and specific applications.* Acta Pharm Sin B, 2018. **8**(5): p. 733-755.

299. Mozafari, M.R., *Liposomes: an overview of manufacturing techniques.* Cell Mol Biol Lett, 2005. **10**(4): p. 711-9.

300. Pattanapanyasat, K., *Immune status monitoring of HIV/AIDS patients in resource-limited settings: a review with an emphasis on CD4+ T-lymphocyte determination.* Asian Pac J Allergy Immunol, 2012. **30**(1): p. 11-25.

301. Purswani, M., et al., *The effect of three broad-spectrum antimicrobials on mononuclear cell responses to encapsulated bacteria: evidence for down-regulation of cytokine mRNA transcription by trovafloxacin.* J Antimicrob Chemother, 2000. **46**(6): p. 921-9.

302. Haaland, R.E., et al., *Levels of Intracellular Phosphorylated Tenofovir and Emtricitabine Correlate With Natural Substrate Concentrations in Peripheral Blood Mononuclear Cells of Persons Prescribed Daily Oral Truvada for HIV Pre-exposure Prophylaxis.* J Acquir Immune Defic Syndr, 2017. **75**(3): p. e86-e88.

303. Saade, F., S.A. Gorski, and N. Petrovsky, *Pushing the frontiers of T-cell vaccines: accurate measurement of human T-cell responses.* Expert Rev Vaccines, 2012. **11**(12): p. 1459-70.

304. Hendrix, C.W., et al., *Dose Frequency Ranging Pharmacokinetic Study of Tenofovir-Emtricitabine After Directly Observed Dosing in Healthy Volunteers to Establish Adherence Benchmarks (HPTN 066).* AIDS Res Hum Retroviruses, 2016. **32**(1): p. 32-43.

305. Baum, M.M., et al., *Highly synergistic drug combination prevents vaginal HIV infection in humanized mice.* Sci Rep, 2020. **10**(1): p. 12995.

306. Gao, Y., et al., *Recent developments of nanotherapeutics for targeted and long-acting, combination HIV chemotherapy.* Eur J Pharm Biopharm, 2019. **138**: p. 75-91.

307. Ford, N. and E.J. Mills, *Simplified ART delivery models are needed for the next phase of scale up.* PLoS Med, 2011. **8**(7): p. e1001060.

308. Gorantla, S., et al., *Human immunodeficiency virus type 1 pathobiology studied in humanized BALB/c-Rag2-/-gammac-/- mice.* J Virol, 2007. **81**(6): p. 2700-12.

309. MacLachlan, J.H. and B.C. Cowie, *Hepatitis B virus epidemiology.* Cold Spring Harb Perspect Med, 2015. **5**(5): p. a021410.

310. Nelson, N.P., P.J. Easterbrook, and B.J. McMahon, *Epidemiology of Hepatitis B Virus Infection and Impact of Vaccination on Disease.* Clin Liver Dis, 2016. **20**(4): p. 607-628.

311. Lim, J.K., et al., *Prevalence of Chronic Hepatitis B Virus Infection in the United States.* Official journal of the American College of Gastroenterology | ACG, 2020. **115**(9): p. 1429-1438.

312. Karnsakul, W. and K.B. Schwarz, *Hepatitis B and C.* Pediatr Clin North Am, 2017. **64**(3): p. 641-658.

313. Fox, L.M. and L.D. Saravolatz, *Nitazoxanide: a new thiazolide antiparasitic agent.* Clin Infect Dis, 2005. **40**(8): p. 1173-80.

314. Pankuch, G.A. and P.C. Appelbaum, *Activities of tizoxanide and nitazoxanide compared to those of five other thiazolides and three other agents against anaerobic species.* Antimicrob Agents Chemother, 2006. **50**(3): p. 1112-7.

315. Rossignol, J.F. and Y.M. El-Gohary, *Nitazoxanide in the treatment of viral gastroenteritis: a randomized double-blind placebo-controlled clinical trial.* Aliment Pharmacol Ther, 2006. **24**(10): p. 1423-30.

316. Korba, B.E., et al., *Potential for hepatitis C virus resistance to nitazoxanide or tizoxanide.* Antimicrob Agents Chemother, 2008. **52**(11): p. 4069-71.

317. Hasegawa, M., et al., *The reconstituted 'humanized liver' in TK-NOG mice is mature and functional.* Biochem Biophys Res Commun, 2011. **405**(3): p. 405-10.

318. Wang, W., et al., *A long-acting 3TC ProTide nanoformulation suppresses HBV replication in humanized mice.* Nanomedicine, 2020. **28**: p. 102185.

319. Akkina, R., et al., *Small Animal Models for Human Immunodeficiency Virus (HIV), Hepatitis B, and Tuberculosis: Proceedings of an NIAID Workshop.* Curr HIV Res, 2020. **18**(1): p. 19-28.

320. Zhao, R., et al., *Hepatoma cell line HepG2.2.15 demonstrates distinct biological features compared with parental HepG2.* World J Gastroenterol, 2011. **17**(9): p. 1152-9.

321. Kim, M., et al., *Generation of humanized liver mouse model by transplant of patient-derived fresh human hepatocytes.* Transplant Proc, 2014. **46**(4): p. 1186-90.

322. Ortega-Prieto, A.M., et al., *In Vivo Model Systems for Hepatitis B Virus Research.* ACS Infect Dis, 2019. **5**(5): p. 688-702.

323. Leyva-Porras, C., et al., *Application of Differential Scanning Calorimetry (DSC) and Modulated Differential Scanning Calorimetry (MDSC) in Food and Drug Industries.* Polymers (Basel), 2019. **12**(1).

324. Trasi, N.S. and S.R. Byrn, *Mechanically induced amorphization of drugs: a study of the thermal behavior of cryomilled compounds.* AAPS PharmSciTech, 2012. **13**(3): p. 772-84.

325. Kulkarni, T.A., et al., *A year-long extended release nanoformulated cabotegravir prodrug.* Nat Mater, 2020. **19**(8): p. 910-920.

326. Ahmadi Tehrani, A., et al., *Formation of nanosuspensions in bottom-up approach: theories and optimization.* Daru, 2019. **27**(1): p. 451-473.

327. Jenh, A.M., C.L. Thio, and P.A. Pham, *Tenofovir for the treatment of hepatitis B virus.* Pharmacotherapy, 2009. **29**(10): p. 1212-27.

328. Institute of Medicine (US) Vaccine Safety Committee, N.A.P.U., *adverse events associated with childhood vaccines: Evidence bearing on casuality.* 1994.

329. Flexner, C., D.L. Thomas, and S. Swindells, *Creating demand for long-acting formulations for the treatment and prevention of HIV, tuberculosis, and viral hepatitis.* Curr Opin HIV AIDS, 2019. **14**(1): p. 13-20.

330. Abu-Freha, N., et al., *Adherence to Anti-Viral Treatment for Chronic Hepatitis B.* J Clin Med, 2020. **9**(6).

331. Abreu, R.M., et al., *Assessment of Adherence to Prescribed Therapy in Patients with Chronic Hepatitis B.* Infect Dis Ther, 2016. **5**(1): p. 53-64.

332. The US Department of Health and Human Services, N.I.o.H., *Long-acting injectable form of HIV prevention outperforms daily pill in NIH study.* 2020.